DEVELOPMENT OF MICROBIAL ELECTROCHEMICAL SENSOR FOR TOXICITY SCREENING OF INFLUENT WASTEWATER

SHEN YUJIA

NATIONAL UNIVERSITY OF SINGAPORE
2013

DEVELOPMENT OF MICROBIAL ELECTROCHEMICAL SENSOR FOR TOXICITY SCREENING OF INFLUENT WASTEWATER

SHEN YUJIA

(B.Eng., Tsinghua University)

A THESIS SUBMITTED

FOR THE DEGREE OF DOCTOR OF PHILOSOPHY

DEPARTMENT OF CIVIL AND ENVIRONMENTAL ENGINEERING
NATIONAL UNIVERSITY OF SINGAPORE

2013

DECLARATION

I hereby declare that the thesis is my original work and it has been written by me in its entirety. I have duly acknowledged all the sources of information which have been used in the thesis.

This thesis has also not been submitted for any degree in any university previously.

SHEN YUJIA

30 September 2013

ACKNOWLEDGEMENTS

First, I would like to express my deep and sincere gratitude to my supervisor, Dr. Ng How Yong, an Associate Professor in the Department of Civil and Environmental Engineering at the National University of Singapore. He not only gives me constant advice and fully support throughout my Ph.D. study and research, but also advise me significantly in my personal development. He guided me in critical thinking, writing and communications skills, and encourages me to become an excellent researcher. I really appreciate his personal charisma, passion, scientific attitude and down-to-earth thinking, which have greatly inspired and influenced me.

Sincere thanks are extended to the members of the examination committee, as well as the external examiners for reviewing this thesis.

I want to express my deep appreciation to all the staff of the Water Science and Technology Laboratory in the Department of Civil and Environmental Engineering: Mr. Chandrasegaran, Ms. Lee Leng Leng, and Ms. Tan Xiaolan, for their assistance in experimental support and with lab equipment. Contributions by final year students, Ms. Lim Kah Huay, Ms. Wang Meng and Mr. Yu Ji are gratefully acknowledged. I also want to express my gratitude to all my labmates for their help, support and valuable suggestions, especially to Dr. Lefebvre Olivier, Mr. Arnaud Uzabiaga, Mr. Tan Zi, Dr. Jin le, Dr. Huang Zhi, Dr. Cai Bijing, Dr. Tan Chien Hsiang, Mr. Zhang Junyou, Mr. Shailesh Kharkwal, Mr. Shi Xue Qing, Dr. Ng Kok Kwang, Mr. Fu Chen, Ms. Wang Ying and so on.

I also appreciate the great chance I had to intern at UNESCAP, special thanks to Dr. Sangmin Nam, who is my mentor during my internship and helped me a lot with my confusions and concerns about the environment and development. I would also like to thank all the friends and colleagues there who give me a lot of valuable suggestions and make my thesis writing more enjoyable.

Finally, I truly appreciate my parents, for their love and constant support. Their love is the strong motivation and encouragement for me. I would also like to give my special thanks to all my friends, who have helped me a lot when I faced difficulties and also made my life more colorful and interesting. Without all of these, I could never achieve this honorable milestone in my life.

Yujia Shen

Aug, 2013

TABLE OF CONTENTS

SUMMARY

Wastewater may contain various potential toxicants, which could affect the activities and viability of microorganisms in the activated sludge process (ASP), leading to the upset of the biological treatment system. Therefore, a sensor is needed to screen the influent wastewater for toxicity to prevent the toxicant upset to the ASP. A microbial fuel cell (MFC) is a device in which bacteria convert the chemical energy into electricity. If a toxic event occurs, microbial activity shall be inhibited and the power output of the MFC shall decrease. To utilize this advantage, a real time biomonitoring system using MFCs, known as microbial electrochemical sensor (MES) hereafter, could be developed to detect the inflow of toxic substances into wastewater treatment systems.

According to the sensor criteria of high and stable baseline, fast response to a toxic event and good recovery, the MES was firstly optimized in terms of both sensing material (biofilm) and the transistor composed of different factors such as MES configuration, size, flow conditions, membrane, and external resistance. The optimal MES design was a single-chambered design, where the anode and cathode were separated by a Selemion proton exchange membrane and channels were drilled inside to make the flow followed a serpentine path through the system. Under an external resistance of 5 Ω, the maximum power averaged 0.33 ± 0.031 mW with domestic wastewater. Besides, the optimized MES showed high sensitivity and fast recovery when exposed to the acidic toxic event. When the hydraulic retention time was decreased from 22 to 3.5 min, the sensitivity further increased substantially.

The behavior of the electrochemically active biofilm is a key controlling factor of the MES. Research was also undertaken to increase MES sensitivity to toxicity by evaluating the impact of shear rate caused by mixing and intermittent nitrogen sparging on the biofilm structure. It was found that that MES enriched under low flow rate with intermittent nitrogen sparging could produce an anodic biofilm that was less dense, more porous, contained less EPS and ultimately, displayed higher sensitivity to toxicity.

The application of the optimized MES to different kinds of toxicants and their characteristics were studied. Toxic compounds that were tested included common individual heavy metal ions (Cu(II), Zn(II), Pb(II), Cd(II) and Ni(II)), binary mixtures of heavy metals, cyanide and organic chemicals that represented two different chemical structures - halogen substituted alkanes and aromatics. Heavy metals and cyanide at concentrations ranging from 2 to10 ppm were found to be toxic to the anodic biofilm as they were to microorganisms in the ASP, and the exposure of the anodic biofilm of the MES to those toxicants resulted in a reduction of the generated current - the signal of which was dependent on both the toxicant and concentration. Exponential decay regression was used to fit the current decrease profile versus time and the dose-response curve was determined through regression. The calibration curve was found linear over the range of heavy metal concentration tested and the MES was very sensitive, with detection limit of 1 to 2 ppm for all heavy metals tested except Pb(II). The sensitivity of the MES to different heavy metal ions were found to be: 9.5% inhibition/ppm for Zn(II), 11.3% inhibition/ppm for Ni(II), 7.2% inhibition/ppm for Cd(II), 7.6% inhibition/ppm for Cu(II) and 4.0% inhibition/ppm for Pb(II). The IC_{50} values (toxicant concentration eliciting a 50% inhibitory effect)

were determined to be 6 ppm for Zn(II), 4.9 ppm for Ni(II), 6.5 ppm for Cd (II) and 5.3 ppm for Cu(II), which are relevant to the toxicity information to the ASP. It was found that sensitivity, response time, IC_{50} and detection limit were the key parameters to affect the MES response profile curve and dose-response curve.

Under appropriate conditions, toxicity information could also be predicted through the specific response profiles. Specific information different from response to heavy metals could also be acquired for sensing cyanide. However, MES was found not suitable for detecting organic toxicants. Extreme change of normal wastewater characteristics were also considered as a kind of toxic event and the response to the pH, nitrate, ionic strength and COD were studied.

To get a better understanding of the mechanism of the MES, both the electrochemical and biological characteristics of the MES were studied. It was found that neither the viability of bacteria in the anodic biofilm nor the microbial communities was changed due to the short-term exposure to the toxicants. It was the inhibition of the electrochemical activity that led to the decrease of the MES current, which was proven by the electrochemical analysis. This also helped to explain the fast recovery and long-term stability of the MES.

The research undertaken within this thesis presented a MES that is capable to detect influent wastewater toxicity, having the characteristics of being quick, preventative, simple, inexpensive, on-line, and relevant to the ASP.

LIST OF TABLES

LIST OF FIGURES

ABBREVIATIONS

AS	--	Activated Sludge
ASP	--	Activated Sludge Process
BOD	--	Biochemical oxygen demand
CLSM	--	Confocal laser scanning microscopy
CFM	--	Chloroform
COD	--	Chemical oxygen demand
CE	--	Coulombic efficiency
CV	--	Cyclic voltammetry
DCM	--	Dichlomethane
DGGE	--	*Denaturing Gradient Gel Electrophoresis*
DTSS	--	Deep Tunnel Sewerage System
D_O	--	Diffusivities of oxygen
E^0_{cell}	--	Theoretical cell voltage
E_{an}	--	The maximum potential obtained at the anode
E_{cat}	--	The maximum potential obtained at the cathode
E_{emf}	--	Electromotive force
EAM	--	Electrochemically active microorganisms
EPS	--	Extracellular polymeric substances
EIS	--	Electrochemical impedance spectroscopy
F	--	Faraday's constant (96 485 $C.mol^{-1}$)
GC-MS	--	Gas chromatography–mass spectrometry
HPLC	--	High performance liquid chromatography
HRT	--	Hydraulic retention time
I	--	Inhibition (%)

i	--	Current
K_O	--	Mass transfer coefficients
MEA	--	Membrane Electrode Assembly
MEC	--	Microbial electrolysis cell
MES	--	Microbial electrochemical sensor
MFC	--	Microbial fuel cell
OCV	--	Open circuit voltage
P	--	Power
PC	--	Polarization Curve
P_{max}	--	Maximum power delivered by the cell
V_{cell}	--	Voltage output
PBS	--	Phosphate buffered saline
PCR	--	polymerase chain reaction
PEM	--	Proton Exchange Membrane
PTFE	--	Polytetrafluoroethylene
R	--	universal gas constant 8.314 J mol^{-1} K^{-1}
R_s	--	Ohmic resistance
R_p	--	Polarization resistance
R_m	--	Membranal contribution to the internal resistance
R_{int}	--	Internal Resistance
R_{ext}	--	External Resistance (load)
SCOD	--	Soluble chemical oxygen demand
SEM	--	Scanning electron microscope
T	--	Absolute temperature (K)
TSS	--	Total suspended solids

TDS	--	Total dissolved solids
VOCs	--	Volatile organic compounds
VSS	--	Volatile suspended solids
WRP	--	Water reclamation plant
η_{conc}	--	Concentration loss
η_{ohmic}	--	Ohmic loss
η_{act}	--	Activation loss
τ_{rec}	--	Recovery time
τ_{res}	--	Response time

PUBLICATIONS

Journal Articles

1. **Yujia Shen**, Olivier Lefebvre, Zi Tan, How Y. Ng "Microbial fuel-cell-based toxicity sensor for fast monitoring of acidic toxicity" Water Science & Technology, 2012; 65 (7)
2. **Yujia Shen**, Meng Wang, Chang I S, and How Y. Ng "Effect of Shear Rate on the Response of Microbial Fuel Cell Toxicity Sensor to Cu(II)" Bioresource Technology, 2013 136 (0), Pages 707–710
3. Olivier Lefebvre, **Yujia Shen**, Zi Tan, Arnaud Uzabiaga, In Seop Chang, How Y. Ng "A comparison of membranes and enrichment strategies for microbial fuel cells" Bioresource Technology, 2011; 102 (10)
4. Olivier Lefebvre, **Yujia Shen**, Zi Tan, Arnaud Uzabiaga, In Seop Chang, How Y. Ng"Full-loop operation and cathodic acidification of a microbial fuel cell operatedon domestic wastewater" Bioresource Technology, 2011; 102 (10)
5. Olivier Lefebvre, Zi Tan, **Yujia Shen**, How Y. Ng "Optimization of a microbial fuel cell for wastewater treatment using recycled scrap metals as a cost-effective cathode material" Bioresource Technology, 2012; 127

Conference presentations

1. **Yujia Shen,** Olivier Lefebvre, Zi Tan, How Y. Ng, "Microbial fuel-cell-based toxicity sensor for fast monitoring of acidic toxicity", presented *at 3rd IWA Asia Pacific Young Water Professionals Conference*, Singapore, Nov, 2010
2. **Yujia Shen,** Olivier Lefebvre, Zi Tan, How Y. Ng, "Response of MFC-based toxicity sensor to Cd(II)", presented at the *3rd International MFC Conference*, Leeuwarden, the Netherlands, Jun, 2011

3. **Yujia Shen,** Olivier Lefebvre, Zi Tan, How Y. Ng, "Response of MFC-based toxicity sensor to heavy metals", presented at the *20th Joint KAIST-KU-NTU-NUS Symposium on Environmental Engineering*, Taiwan, Jul, 2011
4. **Yujia Shen,** Olivier Lefebvre, Zi Tan, How Y. Ng, "Effect of the shear rate on the sensitivity of MFC toxicity sensors", presented at the *21st Joint KAIST-KU-NTU-NUS Symposium on Environmental Engineering,* Malaysia, Jul, 2012
5. **Yujia Shen,** Olivier Lefebvre, How Y. Ng, "Optimization of a microbial fuel cell–based toxicity sensor" presented at *IWA World Water Congress & Exhibition,* Busan, Korea, Sep, 2012
6. **Yujia Shen**, How Y. Ng, "Microbial Fuel Cell Based Biosensor for Heavy Metal Detection", presented at "*First Asia-Pacific International Society for Microbial Electrochemical Technologies Meeting*", Jan, 2013, Harbin, China
7. **Yujia Shen**, How Y. Ng, "Microbial Fuel Cell Based Biosensor for Zn(II) and Ni(II) Detection", presented at *10th IWA Leading Edge Conference on Water and Waste Water Technologies*, Bordeaux, France, June 2013

CHAPTER 1 Introduction

1.1 Background

1.1.1 The need to maintain good biological activity of the activated sludge process (ASP)

Rapid increase in development has placed Singapore in the frontier as one of the fastest growing Asian cities. In order to meet Singapore's growing needs, the Deep Tunnel Sewerage System (DTSS) project has been put in place. The system is used to direct about half of the Singapore wastewater to a centralized water reclamation plant (WRP) located at the Changi East, which collected wastewater from domestic households, educational institutions, health care facilities and industrial effluents from various sources as shown in Fig. 1.1. The centralized WRP have to be in proper operating condition in order to ensure that the desired effluent qualities are met at all times. Any unforeseen upsets in the WRP process may cause adverse effects to the downstream processes such as the NEWater plants, resulting in RO product water hacing high TOC values and more rapid membrane fouling, and may also violate the discharge limits at the outfall.

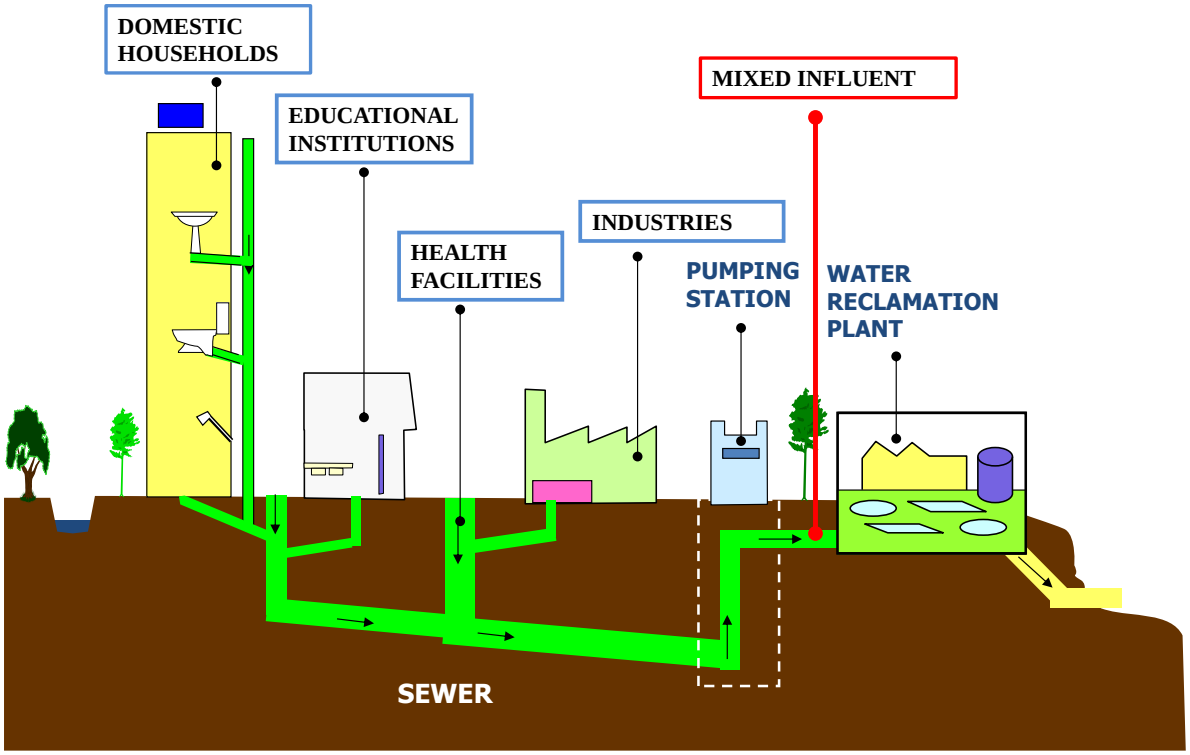

Figure 1.1. A schematic of the centralized treatment system.

The WRP include physical, chemical and biological processes to remove contaminants present in influent wastewater, making the treated effluent environmentally safe. The biological processes are the key to the successful treatment, and the ASP is the most widely used biological processes (Wong et al., 1997). A typical flow diagram of a biological wastewater treatment plant is shown in Fig. 1.2.

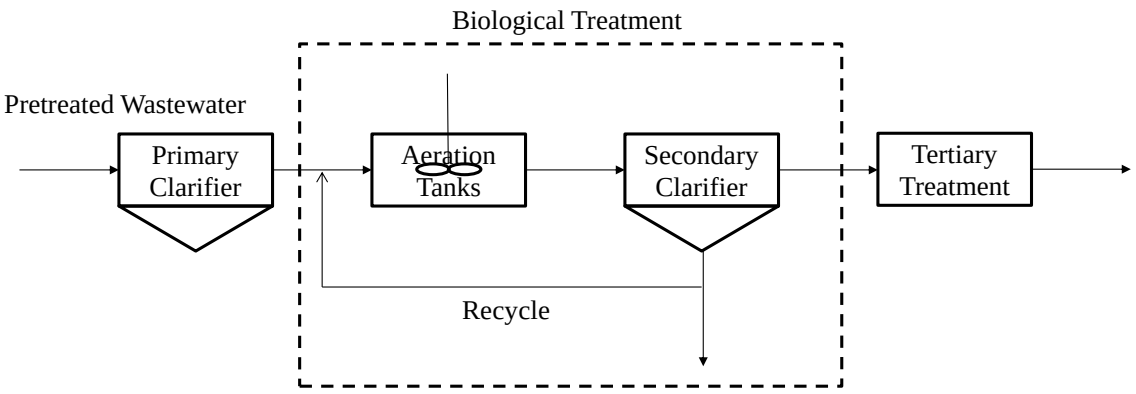

Figure 1.2. A typical flow diagram of a biological wastewater treatment plant.

After the primary treatment process for solids removal, wastewater enters the secondary treatment - the activated sludge process (ASP). The biomass present in the ASP process is a mixture of various aerobic microorganisms and is typically aerated with air. The microorganisms are biologically active and help to biodegrade most of the organic pollutants. Typically, 85-99% of the biochemical oxygen demand (BOD) is removed by the activated sludge process. Subsequently, the wastewater may enter the tertiary and advanced treatments if further purification is required.

The biological activity of the biomass in the ASP is crucial to the successful treatment of wastewater. Therefore, in-time toxicity screening of the influent wastewater entering the biological treatment will be advisable to prevent any upset of the biological process.

1.1.2 Toxicants present in wastewater

The composition in the influent wastewater is highly complex and could consist of a wide variety of potential toxicants. In some cases, effluents containing toxic components such as heavy metals, volatile organic compounds (VOCs), acids, alkalis and cyanide are discharged into a centralized wastewater treatment plant without pretreatment, both accidentally or illegally. They could affect the activity and viability of activated sludge, impeding the performance of the biological treatment process (Halling-Sørensen, 2001; Lin et al., 2003).

Heavy metals are identified as the transition and post-transition groups of elements in the periodic table that have been associated with contamination and potential toxicity.

They include copper, zinc, nickel, cobalt, silver, chromium, lead, cadmium and etc. The major industrial sources of heavy metals are electroplating, iron and steel, paper mills, metal-processing industries, leather tanning and so on (Çeçen et al., 2010). Many industrial uses of heavy metals often involve the discharge of metal laden effluents to the sewage system (Gil et al., 2003) and they often constitute the leading cause for disturbance of wastewater treatment processes (Altas, 2009).

Cyanide, widely used in industrial applications such as electroplating and mining process, is a deadly poison most likely to disrupt the secondary treatment process. Serious monitoring and pretreatment processes need to be established to prevent interference with the downstream biological treatment processes and to reduce impacts to waste sludge quality (Registry July 2006; Nakanishi et al., 1996; Torrens, 2000).

Organic chemicals are also another important cause for the disturbance of wastewater treatment process, broadly used both in industries, e.g., paper manufacturing, chemical processing, and production of domestic products such as detergents and insecticides (Ren and Frymier, 2002).

Hence, the development of upstream toxicity sensors before toxic compounds are released into ASP is of prime interest, which could avoid or minimize the adverse effects on the biological activity in an ASP caused by influent toxicity.

1.1.3 Existing methods for toxicity screening of influent wastewater

Many methods are available to monitor the chemical components crucial in determining water quality, which can generally be categorized into chemical analysis, bioassays and biosensors. Chemical methods like GC-MS and HPLC-MS (Batt et al., 2008), which usually need the treatment of the sample, are usually time consuming, irrelevant to the biological toxicity and may inevitably lead to a delay in the response time for detection. This limits their application for early warning and process control.

The most commonly used toxicity bioassays incorporate the higher organisms, including plants, invertebrates and fish (Gu and Choi, 2001), which need long detection time in the range of days to weeks, and the toxicity data is usually based on the accumulative effect that made it impossible to provide real-time information. Besides, it is also very difficult to convert directly biological data to electrical signal.

The same problem happens with the Activated Sludge Respirometry, which has been used to assess wastewater toxicity to both heterotrophic bacteria and nitrifying bacteria. The principle behind is that the presence of toxicants would lead to the decrease of the respiration rate of activated sludge or biomass, which is mostly measured by oxygen uptake rate. Although it is a more direct and related method for assessing biomass activity and thus toxicity to biomass (Riedel et al., 2002), the signal is not easily measured, which has to be inferred from the derivative of the oxygen concentration in the aqueous phase.

In contrast with conventional bioassays, biosensors give easy-to-measure signals as the interaction takes place and no auxiliary procedures are required. Thus the development of the toxicity biosensor using microorganisms, including bioluminescent bacteria, which offers high sensitivity, a rapid response and an easily measured signal, has received heavy attention from researches. However, some existing toxicity biosensors that employ luminescent bacteria are not suitable for screening the influent wastewater for toxicity because their sensitivity to toxicants is overly high compared to activated sludge microorganisms (Ren, 2001).

Therefore, in terms of toxicity screening of influent wastewater, an online real-time sensor that offers easy-to-measure signal, fast response, and relativity to the toxicant information on the activated sludge process is ideal to provide an early warning when there is a sudden surge in concentrations and/or the presence of a particular toxicant in the influent wastewater. MES is one candidate that can be developed as a sensor to serve this purpose.

1.1.4 Microbial Electrochemical Sensor for toxicity detection

A MFC is a device in which microorganisms convert chemical energy into electricity (Logan et al., 2006). Bacteria in the anode chamber oxidize organic matter and transfer the electrons to the anode, and these electrons pass through an external circuit producing current (Lovley, 2008). Electricity generation is the main focus and feature of the MFC technology. Besides of that, the transport of the electrons have been utilized in many other applications, including desalination (Cao et al., 2009; Jacobson

et al., 2011; Mehanna et al., 2010), recovery or removal of nutrients in wastewater (Cusick and Logan, 2012; He and Angenent, 2006; Clauwaert et al., 2007) , degradation of some pollutants such as pheonl (Luo et al., 2009) or production of valuable products like hydrogen gas and other chemicals (Angenent et al., 2004).

The electrons can also be utilized as a signal to indicate the existence of the toxicants inside wastewater. The incorporation of a toxic substance in the system shall inhibit the metabolic activity of electrochemically active bacteria and reduce the electron transfer rate and power output. This implies that the current generation can be used as a signal to detect the occurrence of a toxic event and consequently, MFC shows potential to be used as an online biosensor for the detection of toxic compounds in water (Kim et al., 2007).

However, only a few works have been presented on the application of the MES in toxicity screening and not much detailed description of the sensor characteristics and mechanisms were given. Some results were even controversial. For example, Kim et al. (2007) successfully used an MFC to detect Pb(II) and Hg(II) at a concentration of 1 ppm; however, Patil et al. (2010) showed that the electrochemically active biofilm was not affected in the presence of Pb(II) and Hg(II) at concentrations in the range of 0.41-12.48 ppm and 0.83-8.33 ppm, respectively. The contradiction between these two studies suggests that the behavior of the electrochemically active biofilm and thus the sensitivity of an MFC as a toxicity sensor can be influenced by several factors and the mechanism behind need more exploration. A broader screening of the toxicants is also necessary (Patil et al., 2010).

1.2 Research objectives

The present study on MES for the toxicity screening of the influent wastewater is undertaken with a broad objective of establishing the concept/fundamentals of rapid, in-situ sensing of toxic compounds that is detrimental to the ASP through direct current production and measurement. The results of this research can serve as the basis for the future developments and perfection of MES that could eventually be commercialized.

Research objectives in details are listed below:

(1) To develop a MES system suitable for the continuous monitoring of influent wastewater toxicity;

(2) To improve the MES stability, sensitivity through the optimization of the sensing materials (biofilm) and the signal transducer;

(3) To demonstrate the applicability and sensor characteristics of the MES in the application of sensing heavy metals, cyanide, organics and extreme variation of common wastewater characteristics (i.e., COD, pH, ionic strength and nitrate).

(4) To understand both the electrochemical and biological mechanism of the response of the MES to toxicants.

1.3 Organization of the dissertation

This dissertation is organized into six chapters following this introduction chapter, consisting of a literature review (chapter 2), materials and methods (chapter 3), three

chapters (Chapter 4, 5 and 6) that presented the results and discussion of the three phases of the study (i.e., optimization of the sensor, application of the sensor and the mechanism of the sensor) that address the stated objectives, and a final chapter summarizing the major findings of this research along with recommendations for future research. The logic of the thesis is shown in Fig. 1.3.

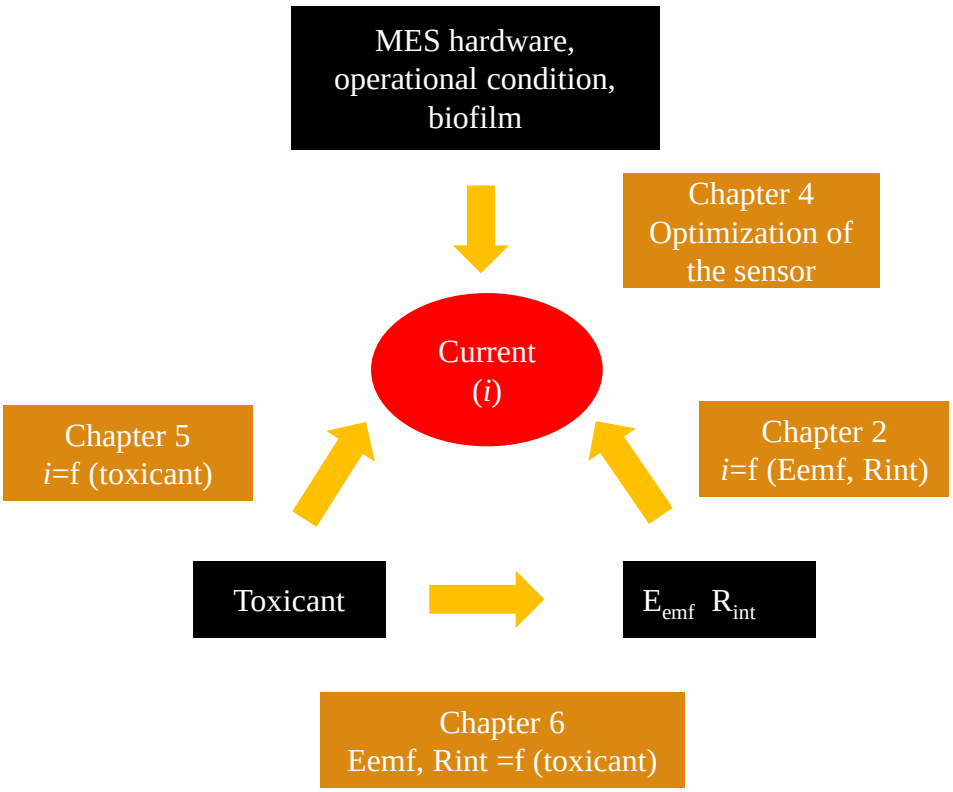

Figure 1.3. Organization of the thesis.

In Chapter 4, based on the sensor criteria of having stable baseline, fast response and good recovery, the optimization of the MES in terms of both the biological sensing element (i.e., biofilm in the anode compartment) and the transducer were conducted.

In Chapter 5, the application of the optimized MES in the toxicity screening of the influent wastewater was examined. Toxic compounds that were tested included individual heavy metals, binary mixtures of heavy metals, cyanide and organic

chemicals that represented two different chemical structures, halogen substituted alkanes and aromatics. Exponential decay regression was used to fit the current decrease profile versus time and dose-response curve was achieved through regression. The sensor characteristics (i.e., sensitivity, response time, IC_{50} values and detection limit) were obtained and their relativity with the toxicants effect to the ASP was investigated. It was found that sensitivity, response time, IC_{50} values and detection limit were the key parameters to affect the sensor response profile curve and dose-response relation. To further study the sensor specificity, one MES was continuously inoculated with wastwater containing Ni(II) to investigate its selectivity to metals.

In Chapter 6, both the electrochemical and biological characteristics of the MES were investigated to get a better understanding of the mechanism of the sensor. CV, EIS and polarization curves were used to study the electrochemical characteristics. Bacteria viability and community were investigated by DGGE and CLSM. It was found that neither the viability of bacteria in the anodic biofilm nor the microbial communities was changed due to the short term exposure to the toxicants. It was the inhibition of the electrochemical activity that led to the decrease of the sensor current, which was proven by the electrochemical analysis. This explained the fast recovery ability and long-term stability of the MFC-based biosensor.

CHAPTER 2 Literature Review

2.1 Introduction

This chapter first reviewed electron production process in MFCs with an emphasis on the detailed theoretical anode process and voltage loss in the MFC systems and give a theoretical basis of how the current generation could be affected by the toxicant. Heavy metal toxicology was also reviewed here to understand the interaction of metals with biofilm. After the theory framework, different biosensors applied for influent toxicity screening and existing MEC biosensors were reviewed to identify the achievements so far and problems which need to be focused on as well.

2.2 MFC principle

MFCs are devices that use bacteria as the catalyst to convert chemical energy to electrical energy via electrochemical reactions involving biochemical pathways (Logan et al., 2006; Rabaey and Verstraete, 2005; Potter, 1911; Lovley, 2006; Bennetto, 1990). The MFC system normally consists of an anode chamber and a cathode chamber separated by a proton exchange membrane (Fig. 2.1). At the anode, substrate (organic matter or biomass) is oxidized, producing electrons, protons and carbon dioxide. For example, when acetate is the fuel, its oxidation reaction is

$$\mathbf{CH_3COO^- + 2H_2O \rightarrow 2CO_2 + 8H^+ + 8e^-} \quad (2.1)$$

As Fig. 2.1 shows, the released protons migrate from the anode chamber to the cathode through the membrane which at the same time restricts the oxygen diffusion from the cathode chamber into the anode chamber. The produced electrons are

transferred to the anode electrode by the bacteria and then flow from the anode through an external circuit to the cathode. At the cathode, electrons, protons and the final electron acceptor (oxygen) combine to form water as follows:

$$4H^+ + O_2 + 4e^- \rightarrow 2H_2O \quad (2.2)$$

With these electrochemical reactions, electrical energy is obtained from biochemical energy via the catalytic activities of microorganisms.

$$CH_3COO^- + 2\,O_2 \rightarrow 2CO_2 + 2H_2O + \text{electrical energy} \quad (2.3)$$

The flow of electrons is measured as current and it is a direct measure of the activity of the microorganisms (Logan et al., 2006; Stein et al., 2011).

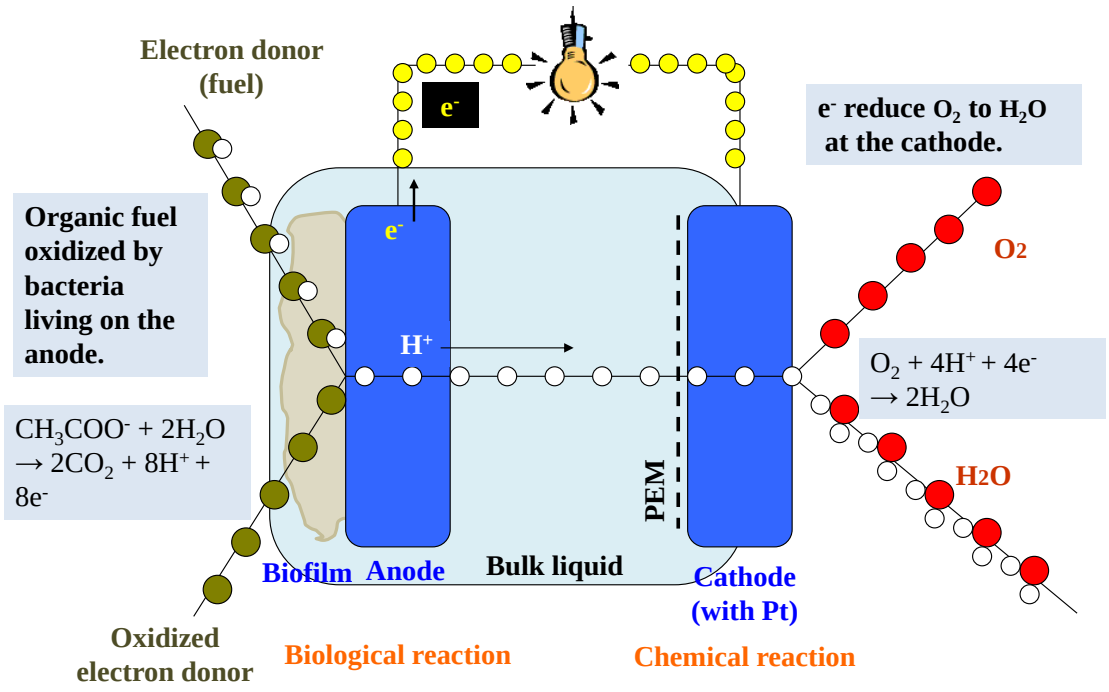

Figure 2.1. Schematic illustration of the working principle of a MFC. The fuel ( ) is oxidized producing H^+ ( ) and e^- ( ) in the anode, H^+ and e^- transport to the cathode through membrane and external circuit, respectively and reduce O_2 ( ) to H_2O ( ) in the cathode.

2.2.1 Electroactive microbial biofilms

The anodic microbial consortium of an MFC usually grows as biofilm structures on the anode as they adhere to the surface (Rabaey et al., 2007). Biofilm structures consist of aggregated microbial communities embedded with the extracellular polymeric substances (EPS), including complex mixtures of heteropolysaccharides, protein, and nucleic acids (Grady et al., 1999; Lazarova and Manem, 1995), separated by a network of open water channels (Stoodley et al., 2010). Liu et al. (2008) has proven that electroactive biofilms can be directly evolved from natural inoculums such as wastewater. This electroactive microbial biofilms that biologically oxidize organic matter and transfer electrons to the anode are the unique feature of the MFC (Logan, 2009). Both the biofilm structure and composition of the microbial communities are important to the performance of the MFC.

Reguera et al. (2006) has shown that biofilms performing extracellular electron transfer can reach considerable thickness and cells at a distance from the anode remained viable in MFC. Active biomass was found to persist up till tens of micrometers away from the anode as indicated by Marcus et al. (2007). Marcus et al. (2007) also suggested that increase in biofilm thickness and accumulation of inert biomass reduce the current density. However, in another study, a thicker and denser biofilm instead increased the current density and Pham et al. (2008) explained that the thicker and denser biofilm could not only improve the electron transfer via direct contacts, but also enhance the electron transfer via electron shuttles as more cells might be involved in electron transfer and more shuttles could be produced (Pham et al., 2008). This kind of contradiction was common in the researches of MFC and pointed out that many variables may influence the behavior of biofilms (Patil et al.,

2010). Logan (2009) also suggested that power densities produced by a bacterium in one study cannot be directly compared with another bacterium or a mixed culture unless the MFC architecture and chemical solution are the same.

The microbial ecology of anodic electroactive microbial biofilms is usually complex and diverse microbial communities develop in reactor type MFC (Rabaey et al., 2007). A number of species has shown ability to oxidize organic compounds with an electrode serving as the electron acceptor (Lovley, 2006), including *Geobacter sulfurreducens* (Bond and Lovley, 2003), *Geobacter* metallireducens (Bond et al., 2002), *Desulfuromonas acetoxidans* (Bond et al., 2002), *Shewanella oneidensis* (Ringeisen et al., 2007), etc.

2.2.2 Electricity generation process

The electricity generation of the MFC is a process combined of electrochemistry and biofilm kinetics. Rittmann et al. (2008) has summarized the key processes taking place inside the biofilm which determined the current density produced by the biofilm (Fig. 2.2): (i) mass transport: the substrates transport within the biofilm and reach the bacteria; (ii) microbial processes (cell growth and respiration): the electrochemically active microorganisms (EAMs) oxidize the substrates (electron donors) and electrons and protons are produced; (iii) the electrical potential gradient: the electrons produced transferred between the cell and from the cell to the electrode; and (iv) proton transport: the protons produced during the oxidation transported out of the biofilm .

Four primary electron-transferring mechanisms have been shown to explain the processes of transferring the electrons produced during the oxidation of the electron

donors to the electrode (Lovley, 2006; Pham et al., 2009) as shown in Fig. 2.2: (i) indirect electron transfer by externally added mediators like Phenazines, falvins and anthraquinone-2,6-disulfonate (Ringeisen et al., 2006; Sund et al., 2007); (ii) indirect electron transfer by self-produced mediators, which were proven in the studies where *Shewanella* species could reduce Fe^{3+} oxides at substantial distances from the cell surface (Lovley, 2006; Nevin and Lovley, 2002; Rosso et al., 2003). However, Nevin and Lovley (2000) showed that *Geobacter* species lack of production of these electron shuttles; (iii) direct electron transfer by the outer-membrane cytochrome (Bond and Lovley, 2003; Kim et al., 1999a; Lies et al., 2005) ; and (iv) direct electron transfer by 'nanowires' shown by *Geobacter sulfurreducens* (Reguera et al., 2005).

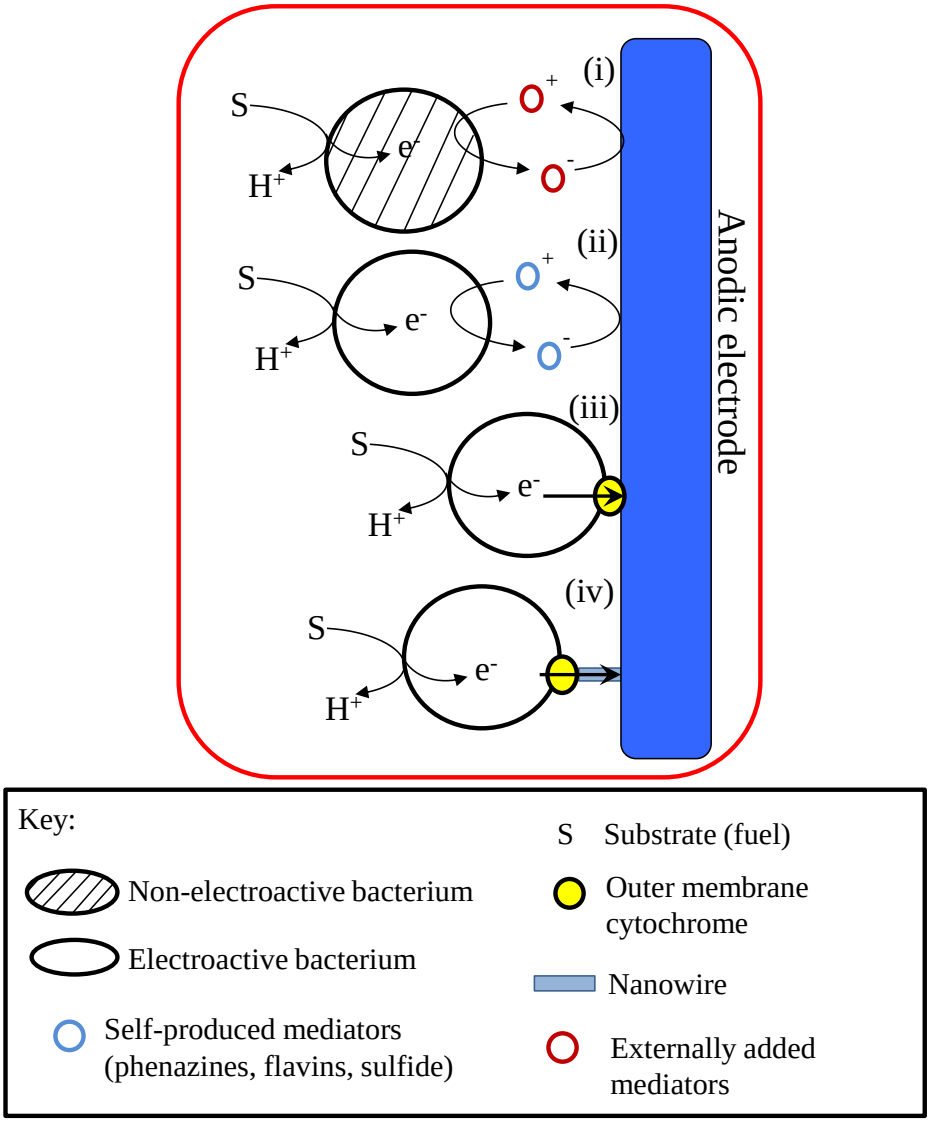

Figure 2.2. Established models for electron-transfer mechanisms occurring in bioanodes: (i) indirect electron transfer by externally added mediators; (ii) indirect electron transfer by self-produced mediators; (iii) direct electron transfer by (a single) outer membrane cytochrome; and (iv) direct electron transfer by 'nanowires' (Pham et al., 2009)

2.2.3 Factors affecting the electricity generation

According to the anode process discussed above, Pham et al. (2009) has summarized the factors affecting the current generation of the MFC into three categories: "hardware", biological and operation conditions.

The “hardware” factors include reactor design (Liu et al., 2005a; Fan et al., 2007), the properties of the proton exchange membrane (Oh and Logan, 2006), distance between the electrodes (Ghangrekar and Shinde, 2007; Cheng et al., 2006), electrode material (Park and Zeikus, 2003) and external resistance (Aelterman et al., 2008), etc. Logan (2009) has suggested that the power densities produced by mixed cultures are often similar when the specific architecture, electrode spacing and solution conductivity of the MFC are the same. Biological factors include the amount of biocatalyzing microorganisms in relation to the available surface area, the biological activity of the microbial consortium and the intrinsic electron transfer rate of the rate determining enzyme/redox system (Rabaey and Verstraete, 2005; Clauwaert et al., 2008). The performance of MFC is also affected by many operating conditions imposed on the reactor, such as wastewater strength (Min and Logan, 2004; Liu et al., 2004), substrate loading rate (Reddy et al., 2010; Mohan et al., 2007) , ionic strength (Liu et al., 2005a) and pH (Gil et al., 2003; He et al., 2008; Jadhav and Ghangrekar, 2009).

2.2.4 The voltage generation of the MFC

The voltage between the anode and the cathode, V_{cell} (V), is the useful energy that is actually harvested and is less than its predicted thermodynamic ideal value, the electromotive force (E_{emf}) (V) due to irreversible losses (i.e., overpotentials) caused by activation losses, ohmic losses and mass transport losses, respectively (Logan et al., 2006; Rittmann et al., 2008; Wen et al., 2009; O'Hayre et al., 2006). The real operational voltage output (V_{cell}) of an MFC can be determined by subtracting the voltage losses from the thermodynamically predicted voltage as follows:

$$\boldsymbol{V_{cell} = E_{emf} - (\eta_{act} + \eta_{conc} + \eta_{ohmic})} \quad (2.4)$$

where η_{act} is the activation loss due to reaction kinetics, η_{ohmic} is the ohmic loss from ionic and electronic resistances, and η_{conc} is the concentration loss due to mass transport limitations (Logan et al., 2006; Rittmann et al., 2008; Wen et al., 2009; O'Hayre et al., 2006; Rismani-Yazdi et al., 2008) .

Lefebvre et al. (2011a) has modeled the MFC by an ideal voltage source producing its electromotive force E_{emf} (V) in series with an ideal resistor representing its internal resistance R_{int} (Ω) (Fig. 2.3). The R_{int} consists of three components: activation (charge transfer) resistance, ohmic resistance (R_s, also called solution resistance, representing the resistance from solution, electrode materials and membrane) and concentration (diffusion) resistance.

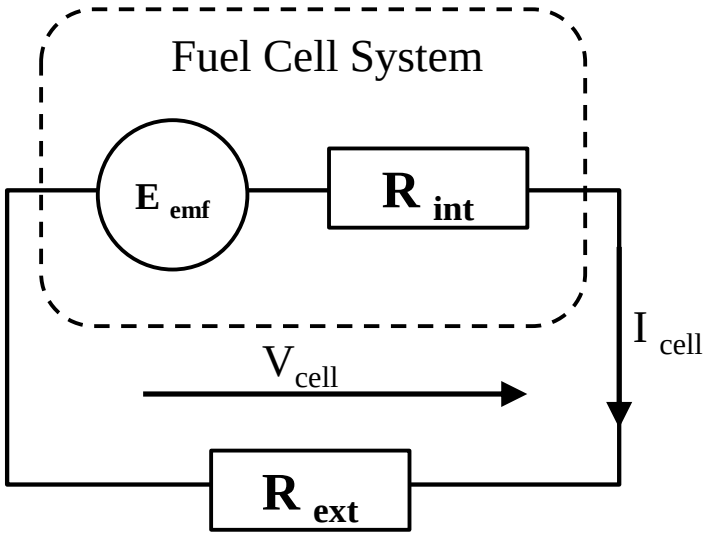

Figure 2.3. Simplified model showing a MFCsystem characterized by its E_{emf} and R_{int}, and generating a current of I cell at a voltage of V_{cell} through an external resistance of R_{ext} (Lefebvre et al. 2011a).

In MFC, the measured cell voltage (V_{cell}) (V) is usually a linear function of the electrical current (I) (A) , and can be described simply as

$$\boldsymbol{V_{cell} = E_{emf} - IR_{int}} \quad (2.5)$$

where IR_{int} is the sum of all internal losses of the MFC, including the voltage loses due to reaction kinetic, ohmic resistance and mass transport, respectively.

According to the ohm's law,

$$\boldsymbol{V_{cell} = IR_{ext}} \quad (2.6)$$

where R_{ext} (Ω) is the external circuit where current flow through.

Substituting Eq. 2.6 to Eq. 2.5, the current of the MFC monitored is decided by

$$\boldsymbol{I = \frac{E_{emf}}{R_{int}+R_{ext}}} \quad (2.7)$$

Thus E_{emf} and R_{int} are the two parameters that will, in turn, affect the I (A) monitored, which are discussed below.

2.2.4.1 Maximum Potential

The theoretical overall cell electromotive force (E_{emf}) of MFCs can be calculated from the Gibbs free energy of the corresponding biochemical reaction and is defined as the potential difference between the cathode and anode (Logan et al., 2006)

$$\boldsymbol{E_{emf} = E_{cat} - E_{an}} \quad (2.8)$$

Where E_{cat} and E_{an} are the maximum potential obtained at the anode and cathode, respectively, which are the potential difference between the half reactions of the electron donor and acceptor. They are usually determined by the Nernst equation (Rittmann et al., 2008):

$$\boldsymbol{E_{electrode} = E_{electrode}^{0} - \frac{RT}{nF}\ln(\frac{[red]^{\gamma}}{[ox]^{\beta}})} \quad (2.9)$$

where $E_{electrode}^{0}$ (V) is the standard free energy at pH = 7, R is the universal gas constant (8.314 J/mol K), T is the operation temperature (K), n is the number of electrons transferred, F is the Faraday constant (96,485 Coulombs/mol), [ox] and [red] are the concentrations of the oxidized and reduced compounds, respectively, and γ and β are their corresponding stoichiometric coefficients.

For example, if an MFC is using acetate as the electron donor in the anode, the E_{an} is determined as follows.

Anode half reaction:

$$\boldsymbol{CO_2 + HCO_3^- + 8H^+ + 8e^- = CH_3COO^- + 3H_2O\ E^{0'} = -0.285\ V} \quad (2.10)$$

Where $E^{0'}$ (V) is the standard free energy at pH =7.

The equilibrium anode potential is

$$\boldsymbol{E_{an} = -0.285\ V - \frac{RT}{8F}\ln\left(\frac{[CH_3COO^-][10^{-7}]}{[HCO_3^-][CO_2][H^+]}\right)} \quad (2.11)$$

It could be seen that E_{an} is a thermodynamic value that does not take into account internal losses and is controlled by temperature, pH, and the concentrations of reactants and products.

The open circuit voltage (OCV) is the cell voltage that can be measured after the MFCs are kept open circuit for some time. It should be equal to the E_{emf} theoretically. However, OCV is substantially lower than E_{emf} in practice due to various potential losses (Logan et al., 2006; Wen et al. 2009).

2.2.4.2 Voltage losses of the bioanode

Electron-quenching reactions

Processes such as fermentation, methanogenesis or respiration will consume the substrate as well and result in losses of electrons. In addition, a fraction of the substrate is also used for the growth of the microorganisms. All these processes lower the conversion of substrates into current (Pham et al., 2009).

Activation losses

An energy barrier needs to be overcome for the onset of electron transfer from the electroactive microorganisms towards the electrode, resulting in a voltage loss or activation overpotential (Clauwaert et al., 2008). The interactions between EAMs and the electrode, which are related to the electrode surface properties, is another determinant for the activation losses (Pham et al., 2009).

Ohmic losses

Ohmic losses in an MFC are resulted from the resistance to the electrons flow through the electrodes and interconnections, and the ions flow through the membrane and the electrolytes (Logan et al., 2006).

Mass transfer losses

The transport of substrate to the anodic biofilm and the transfer of products outside of the biofilm will result in concentration or mass transfer losses. Inefficient mass transfer through diffusion and convection of substrate or removal of products may limit the maximal current production at an electrode (Clauwaert et al., 2008).

2.2.5 Abiotic cathode process

Two cathode processes were employed in MFC and can be classified into biocathode and abiotic cathode depending on the source of the final electron acceptor available

(He and Angenent, 2006). In this thesis, only abiotic cathode process that uses oxygen as the terminal electron acceptor is discussed. The reduction of oxygen is the most dominant electrochemical reaction at the surface of cathode electrodes. As the same in the anode process, the potential of the cathode is also dependent on the activation loss, the ohmic loss and the transport loss. However, the difference from the anode is that it is a chemical process and is more related with the "hardware" factors (Rismani-Yazdi et al., 2008). For example, activation losses are affected by the cathode materials (catalytic activity). Transport losses depend on the oxygen transport to the cathode. The ohmic losses are resulted from the conductivity of the electrode (Rismani-Yazdi et al., 2008).

2.3 Electrochemical techniques

An MFC performance can be assessed in terms of OCV and internal losses, based on various techniques like Polarization Curves (CV), Cyclic Voltammetry (CV), Electrochemical Impedance Spectroscopy (EIS).

2.3.1 PC

A polarization curve is a powerful tool commonly used to rapidly evaluate the activity of electrochemically active microorganisms and performance of a MFC (Logan et al., 2006; Aelterman et al., 2006). Both of the OCV and R_{int} can be easily obtained from Polarization Curves (Fig. 2.4). It usually includes three regions related with different dominant losses: (i) the activation region where the activation losses are dominant and the drop of current is slow and near-linear; (ii) the ohmic region where the ohmic losses are dominant and the voltage falls more slowly and fairly linearly with current;

and (iii) the concentration polarization region where the concentration losses (mass transport effects) are dominant and the voltage falls rapidly at higher currents.

The R_{int} is calculated from the slope of the linear curve and is referred to as internal resistance rather than ohmic resistance since activation loss and concentration polarization affect the slope of the polarization curve, and the influence has been considered in the calculation (Fan et al., 2008). The maximum power output is obtained when R_{ext} was equivalent to R_{int}, and is calculated as

$$\boldsymbol{P_{max} = \frac{OCV^2}{4R_{int}}} \tag{2.12}$$

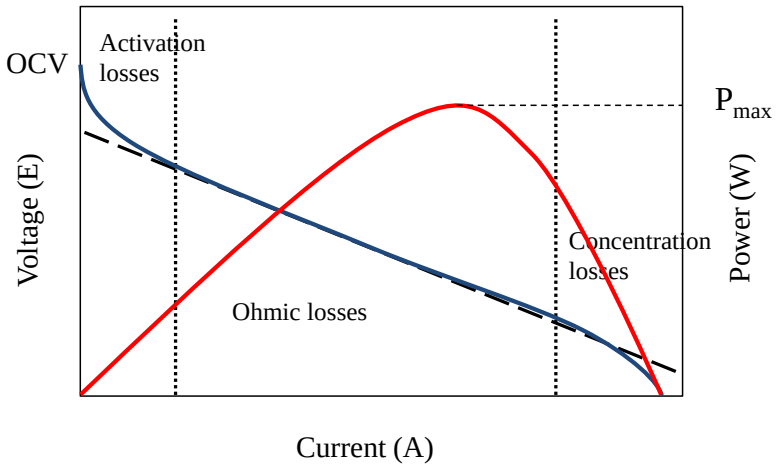

Figure 2.4. The polarization curve (blue), with the respective open circuit voltage (OCV) and the power performance curve (red), with the maximum power (P_{max}) (Clauwaert et al., 2008).

2.3.2 CV

CV is one of the most common and straight-forward technique to determine the mechanisms of electrode reactions underlying oxidation or reduction reactions and is used for assessing the electrochemical activity of microbial biofilm of MFCs (Logan et al., 2006; Kim et al., 2002; He et al., 2005; Liu et al., 2005b).

In CV, when the applied potential changes from low to high, the rate of the degradation of organic substrate catalyzed by bacteria will gradually increase and the current also increase at the same time. When the current reaches a certain value, the supply of sufficient substrate to the anodic biofilm becomes the limiting factor and cannot sustain the current generation anymore. Thus further increase of the current becomes impossible, and the oxidation peaks thus appears in the CV curve. When the bacteria do not have any electrochemical activity or when the electrochemical activity is too low such that the mass transfer would not become a limiting factor, no oxidation peak would appear in the CV curve (Fricke et al., 2008; Nicholson, 1965; Marsili et al., 2008). If the component could be reversibly oxidized or reduced, peaks appeared on both the upper and lower curves, namely the reduction/oxidation peak (Rabaey et al., 2004a). The size of the peak indicates the quantity of the component involved (Allen and Larry, 2001).

2.3.3 EIS analysis

EIS analysis provide information on the ohmic resistance (R_s) as well as polarization resistance (R_p) (or charge transfer resistance), which is affected by the kinetics of the electrode reaction. He and Mansfeld (2009) suggested that a MFC can be connected to a potentiostat in either a three-electrode mode or a two-electrode mode, in which the three-electrode mode is used to analyze an individual electrode and the two-electrode mode is used to measure R_{int} of the whole cell.

The Bode plot (Fig. 2.5) shows the impedance at different frequencies, and the low- and high-frequency data can be easily determined from the Bode plot, representing R_p+R_s and R_s, respectively (He and Mansfeld, 2009).

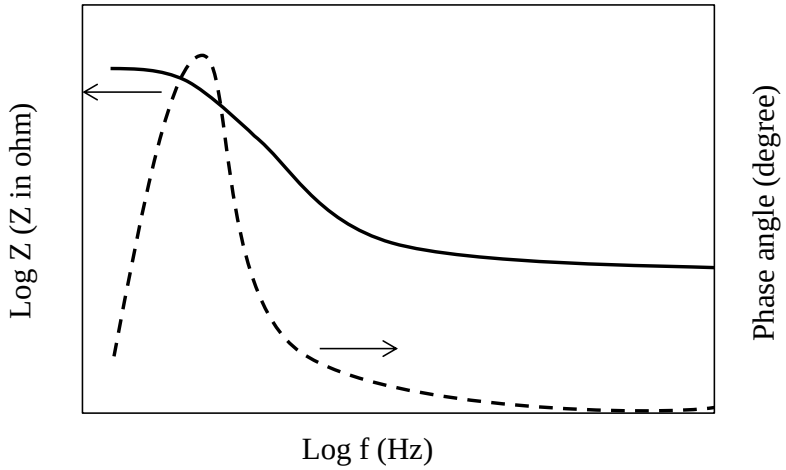

Figure 2.5. A schematic of the Bode plot of the MFC impedance (He and Mansfeld 2009).

2.4 Toxicants principles

2.4.1 Toxicants inside wastewater affecting the ASP

Biological wastewater treatment systems are susceptible to shock loads of toxic chemicals such as heavy metals (Battistoni et al., 1993; Cabrero et al.. 1998; Cecen et al., 2010)), organic compounds (Boon et al., 2003; Schwartz-Mittelmann and Galil, 2000; Bott and Love, 2002), cyanide (Henriques and Love, 2007) and extreme pH levels. Copper, zinc, lead, cadmium and nickel are the most frequently found heavy metals in industrial wastewaters.

According to Altas (2009), heavy metals often constitute the leading cause for disturbance of wastewater treatment processes. Heavy metal ion concentrations at

ppm (mg/L) level are known to be toxic to most microorganisms due to the inhibition of many enzymes by the heavy metal ions (Pamukoglu and Kargi, 2007). The biological wasteater treatment process efficiency will be adversely affected (Love and Bott, 2000) in terms of COD removal, nitrification, respiration rates or settleability of the biomass. Table 2.1 summarized the concentration of heavy metals and cyanide affecting the activated sludge process in terms of the activated sludge treatment efficiency.

Table 2.1. List of inorganic compounds affecting ASP.

Inorganics	Concentration	Effects on activated sludge	Reference
CN^-	3 mg/L	~75% sOUR inhibition	(Henriques and Love, 2007a)
Ni(II)	> 20 mg/L > 80 mg/L	Growth inhibition Almost no growth	(Gikas, 2007; Yetis and Gokcay, 1989)
	5 mg/L	22% reduction of TOC removal	(Ong et al., 2004)
	10 mg/L	5% reduction in COD removal	(Moore et al., 1961)
	25 mg/L	serious upsets of the activated sludge system	(Yetis and Gokcay, 1989)
Cd(II)	3 mg/L	20% sOUR inhibition after 1 h exposure	(Zarnovsky et al., 1994)
	10 mg/L	4% reduction in COD removal efficiency	(Neufeld and Hermann, 1975)
	5.15 mg/L	100% inhibition of nitrifying bacteria	(Bagby and Sherrard, 1981a)
Cu(II)	5 mg/L	Sharp decreases in the maximum growth rate and biomass yield parameters were observed	(Cabrero et al., 1998)
	10 mg/L	5% reduction in COD removal	(Moore et al., 1961)
Pb(II)	17 mg/L	67% inhibition on sOUR	(Madoni et al., 1999)
Zn(II)	2.1 mg/L	11% mortality in the whole protozoan community after 24 h exposure	(Madoni et al. 1996)
	10 mg/L	5% reduction in COD removal	(Moore et al., 1961)
	3 mg/L	100% inhibition to nitrifying bacteria	(Benmoussa et al., 1986)
	> 10 mg/L (at 10 mg/L)	Growth Inhibition (15% growth inhibition)	(Cabrero et al., 1998)

2.4.2 The mechanisms of toxic effects

The mechanisms of toxic effects of different groups of toxicants such as heavy metals and organic chemicals are different. The mechanisms of action for organics are generally more complicated, which will not be discussed here.

No defined mechanisms of heavy metal toxic action have been reported and only in rare cases has an important single mechanism been found. Nies (1999) has summarized two general known mechanisms of heavy metal toxicity: inducing oxidative stress and interfering with protein function, which include "thiol-binding and protein denaturation", "interaction with calcium metabolism and membrane damage", "interaction with zinc metabolism" and loss of a protective function. Bagby and Sherrard (1981) also mentioned that cation may react with active cellular components such as respiratory enzymes to form stable inactive complexes, leading to inhibitory effect to biological organisms. The inactive enzymes and other cellular components that are complexed by heavy metals may be reinstated to an active form if the reaction between these constituents can be reversed (Bagby and Sherrard, 1981). The toxicity of heavy metals depends mainly upon two factors, namely, metal species and concentration (Madoni et al., 1996). Other factors such as pH, sludge concentration and influent strength in activated sludge mixed liquor are also reported to affect the toxicity of metals, though to a lesser degree. (Yetis and Gokcay, 1989; Dilek and Yetis, 1992).

2.4.3 Biofilm resistance to heavy metal toxicity

Biofilm bacteria are usually embedded in an extracellular polymeric substance (EPS) matrix composed of polysaccharides, proteins, and nucleic acids that have negatively charged phosphate, sulfate, and carboxylic acid groups. They can protect the biofilm from the toxicants by biosorption of metal ions or complexation. This increases the biofilm resistance to antimicrobial agents compared to the resistance of free-swimming organisms. The biosorption of metal ions is proportional to the kinetics of the biosorption-reaction equilibriums, which restrict diffusion and alter the biological availability of the toxic metals (Harrison et al., 2007). Another proposed mechanism that contributes to the resistance of biofilms is that many antimicrobial agents target metabolically active cells, and the resistance of biofilms to antimicrobial agents can be primarily attributed to the stationary phase or slow growth of the biofilms (Harrison et al., 2007).

2.5 Bioassays for toxicity screening of influent wastewater

2.5.1 Principle and biosensor types

A biosensor is composed of two elements: a biological recognition unit able to interact specifically with a target, and a transducer able to convert a change in property of the solution or surface, due to complex formation, into a recordable signal (Scheller et al., 2001). In contrast with conventional bioassays, the molecular interactions and the detection of it take place at the same time in a biosensor (Fig. 2.6), without requiring auxiliary procedures, making them highly attractive for assessing wastewater toxicity to biological treatment systems.

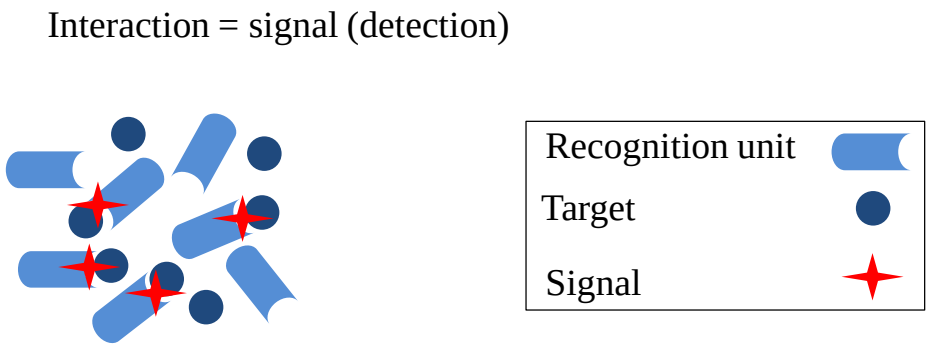

Figure 2.6. A schematic explanation of biosensor.

Different sensor types have been used for assessing wastewater toxicity to activated sludge and the most common ones were categorized as respirometry, molecular-based biosensors and bioluminescence methods (Ren, 2004) according to their difference in the recognition unit and output. Available methods are summarized in Table 2.2.

Table 2.2 A summary of the common sensor types used for assessing wastewater toxicity to activated sludge.

Biosensing elements	Output	Advantage	Disadvantage	References
Molecular-based methods				
DNA	Electrochemical signal	Fast response (min)	The result was not directly used to infer toxicity.	(Lucarelli et al., 2002a; Lucarelli et al., 2002b)
Bioluminescence Methods				
Microorganisms (including genetically engineered microorganisms)	Bioluminescence	Easy measured signal and very quick responses (min)	low specificity, Expensive and unstable, excessively sensitive compared to AS respirmetry	(Ren and Frymier, 2002; Gu and Choi, 2001; Ren, 2001; Steinberg et al., 1995; Ren and Frymier, 2005)
Respirometry methods				
Activated sludge	Respiration rate (oxygen uptake rate)	More direct method for assessing sludge activity	Relatively slow and the results depend on the source of the sludge	(Riedel et al., 2002; Spanjers and Vanrolleghem, 1995)

2.5.2 Sensor characteristics

To meet the basic criteria of the application and make the comparison of the sensors possible, the sensor characteristics on the same basis should be described and Table 2.3 shows the summary of the characteristics of the sensor reviewed.

Table 2.3 Summary of the definition of the sensor characteristics.

Characteristics	Definition	Reference
Signal To Noise Ratio (SNR)	The ratio of a signal power to the noise power corrupting the signal.	
Limit of Detection	The lowest concentration value measured with biosensor for a signal to noise ratio of 3:1.	(Ram ŕez et al., 2011)
Sensitivity	The sensitivity is determined by the decrease of electrical current per amount of chemical.	(Stein et al., 2012)
EC_{50}	Effective concentration reducing signal by 50%.	
Response Time	The time required for the signal to reach a given percentage of the difference between the two steady states after switching from one concentration to the other.	(Menil et al., 2005)
Repeatability	Difference in value between two successive measurements under the same operating environment.	
Stability (Lifetime)	The degree to which sensor characteristics remain constant over time.	
Robustness	low sensitivity to environmental parameters	
Output signal	Electrical signal is preferred because microcontrollers and computers are being used to automatically gather the data.	

2.6 MES

2.6.1 MES BOD sensor

MES biosensors have been developed for assaying BOD, a value related to total content of organic materials in wastewater. Ever since the first effort of such a

microbial sensor by Kim et al. (1999b) was made, a large number of researches have been conducted in this field because its advantages include direct output signal, long-term stability and high repeatability.

The first application of a direct electrochemical reaction by an intact bacteria cell for the construction of a biosensor was done by Kim et al. (1999b), which was a two chamber MFC with cation exchange membrane and Potassium Ferricyanide as the cathode electrolyte. No external mediator was added and the anode volume was 19 mL. Bacterial suspension of *Shewanella putrefaciens IR-1* was used as the sensing material to measure the lactate concentration due to its lactate oxidizing activity. The current was proportional to the lactate concentration over the range of 2-25 mM with the correlation coefficient factor of 0.84, and the sensor gave unstable results when the lactate concentrations were lower than 1 mM due to the increased noise in the electrochemical signal. It was shown that the current increased dramatically during the first 150 s and reached a plateau after 600 s.

A MES BOD sensor measuring BOD in the wastewater had been operated for over 5 years in a stable manner without any servicing by Kim et al. (2003). Naturally enriched and electrochemically active microbial consortium was employed in this device that could metabolize a wide range of organic contaminants and measures BOD more accurately than BOD sensors based on a pure culture. Coulomb instead of current was used as a signal in their study since the maximum current did not increase further when the sample BOD concentrations were higher than 25 ppm, while the coulomb generated from the MES BOD sensor was directly proportional to the strength of the wastewater up to 206 ppm. However, it took about 10 h to test the

sample with a BOD value higher than 200 ppm, which was a disadvantage despite of its good linearity up to this high concentration. High strength samples may therefore have to be diluted to be analyzed within a reasonable time. Another disadvantage was that phosphate buffer was used to maintain the stable coulomb generation.

The 5-year operation life of this MES BOD sensor (Kim et al., 2003) proved the big advantage of the MES as a real time on-line sensor that has long-term stability (Finkelstein et al., 2006). Bullen et al. (2006) have also operated an MFC continuously and no depletion in power was observed for at least a year. Possible reasons were discussed as follows: one was the continual replenishment of the electrode reactants and second was the lack of reliance on added redox mediators (Tender et al., 2002; Reimers et al., 2006). It may also result from anode microbial catalysts that appeared to conserve a significant portion of energy liberated from the oxidation of fuel for self-maintenance (Finkelstein et al., 2006).

Low BOD concentration can be measured by mediator-less MES enriched with oligotrophic microbes (Kang et al., 2003). Moon et al. (2005) also utilized it as a microbial sensor for continuous and on-line monitoring of low BOD below 20 mg/l. The sensitivity was 0.43 μA/(mg BOD/l), which could be increased by increasing the feeding rate. The dynamic linear range of the calibration curve was between 2.0 and 10.0 mg BOD/l, and the response time to the change of 2 mg BOD/l was about 60 min. However, phosphate buffer was also used to eliminate the interference of the current signal by the salts concentration.

The oxygen diffusion into the anode compartment is one problem for the MES since it consumed the electrons and affects the current signal due to its higher redox potential. Chang et al. (2005) used respiratory inhibitors such as azide and cyanide to eliminate the inhibitory effects of the electron acceptors on the current generation from MFCs. In their study, the addition of azide and cyanide did not change the signal in the absence of the electron acceptors.

Other studies have also been made to improve the performance of a microbial fuel cell (MFC) as a BOD sensor (Tront et al., 2008; Di Lorenzo et al., 2009a; Di Lorenzo et al., 2009b).

In summary, MES showed good ability to be used as a BOD sensor for real-time wastewater monitoring. The BOD range that could be measured was 10- 400 ppm and dilution was needed if the concentration was higher than 400 ppm. Oligotrophic type MES was used low BOD sensor. The response time was between 5 to 600 min, and the operational stability could be up to 5 years.

2.6.2 MES as toxicity sensor

Compared to the MES BOD biosensor, the application of the sensor to monitor the toxicity was studied less and most of them were like pre-trial to prove the idea instead of in-depth investigation.

Kim et al. (2004) investigated the effect of inhibitory toxicants such as rotenone, 2-heptyl-4-hydroxyquinolone-N-oxide (HQNO), p-chloromercuriphenylsulfonate (p-CMPS), 2-4-dinitrophenol (DNP) and dicyclohexylcarbodiimide (DCCD) on the

current generation of MFC. The current showed fast drop once the toxicants were dosed, and the level of inhibition varied depending on the type of inhibitors used, showing that MFC has great potential to be used to monitor the toxicants.

A MES was then developed that was able to detect the inflow of toxicants in real wastewater entering into a WWTP (Kim et al., 2007) such as organophosphorus (OP) compound, heavy metals like Hg(II) and Pb(II) and polychlorinated biphenyl (PCBs). Pb(II) and Hg(II) at a concentration of 1 ppm were successfully detected. Fast response and recovery was shown in the study. However, Patil et al. (2010) showed that the electrochemically active biofilm was not affected in the presence of Pb(II) and Hg(II) at concentrations in the range of 0.41-12.48 ppm and 0.83-8.33 ppm, respectively, where planktonic cells were inhibited. This study demonstrated that one of the disadvantages of the MES was that the electrochemically active biofilm would be more resistant towards toxicants as compared to planktonic cells. Besides, this contradiction showed again that many factors affected current generation of the MES as mentioned in the section 2.2.3.

Therefore, those factors would affect both of the sensor baseline stability and sensor sensitivity. Stein et al. (2010) showed the effect of anodic overpotential control for detection of toxic compounds. They suggested a MES to be operated at controlled anode potential, pH and saturated substrate concentrations to reach a stable baseline current under nontoxic conditions. Stein et al. (2012) also studied the influence of membrane type, current and potential on the response to Ni(II) of a MES. No delay was found in the response of the sensor to Ni(II) and the sensitivity was 0.0027 A/m^2/mg Ni/L at an anode potential of −0.4 V. The sensitivity was higher at higher

overpotential (higher current density); however, the difference between four types of cation exchange membranes was not significant.

A microfabricated toxicity sensor based on MEC process was firstly developed by Dávila et al. (2011) that was simple, compact and planar. The current decreased remarkably when toxic materials were present in the anodic compartment. However, the lower power generation ability of the microfabricated MESs was a problem to give broader testing range and higher sensitivity, and thus the study only focused on the detection of toxic compounds by applying the operation principle of a miniaturized MEC cell to the development of a silicon-based toxicity biosensor.

CHAPTER 3 Materials and Methods

3.1 Introduction

This study was divided into three phases. Phase 1 was designed to optimize the MES in terms of baseline, sensitivity and recovery, and it was divided into two sub-sections: Phase 1-1 focused on the "hardware", operational factors; and Phase 1-2 targeted at the biofilm. Phase 2 focused on the application of the MES by investigating its operational stability and sensitivity in response to various toxicants. Phase 3 studied the mechanism of the MES in terms of the fate of heavy metal, electrochemical and microbial characteristics affected by the toxicant. In each phase, three steps were involved, first MESs were constructed and then the MES were subject to inoculation and toxicity testing. Experimentation and analysis were conducted both during and after the second step. Table 3.1 gives a short summary of the construction, operational condition, measurement and analysis of each phase, which would be discussed in detail in the following sections in this Chapter.

Table 3.1 Summary of the construction, operational condition, measurement and analysis of each phase.

Phases	MFC construction	Operational condition				Measurement and analysis		
		Inoculation period		Toxicity testing		Electrochemical testing	Biofilm analysis	Other analysis
		Shear Stress	Electrolyte and inoculum	Toxicant HRT	Toxicant dosed			
1-1 (Chapter 4.2.1)	Different 'hardware' (Table 3.2)	1.3 mL/min	wastewater	Different toxicant HRT	Acidic toxicity	PC	/	/
1-2 (Chapter 4.2.2)	Fig. 3.4c	Different shear stress (Table 3.4)	wastewater	2 min	Cu	PC	SEM, VSS, EPS,	/
	Optimal condition (Fig. 3.5)	1.3 mL/min	wastewater contain Ni	2 min	Ni, Zn	/	/	/
2 (Chapter 5)	Optimal condition (Fig. 3.5)	1.3 mL/min	wastewater	2 min	Different toxicant(Table 3.6)	PC	/	Modeling
3 (Chapter 6)	Optimal condition (Fig. 3.5)	1.3 mL/min	wastewater	2 min	Cd	EIS,CV,PC	CLSM, SEM, DGGE	Metal fate study

3.2 Online biomonitoring system set up

The sensing system consisted of a wastewater feeding pump, a toxicity injection pump (Masterflex 07523-70, Spectra-Teknik Pte Ltd., Singapore), an MEC cell and a digital multimeter connected to a desktop computer (Fig. 3.1). The voltage (V) generated by the MES across an external resistance (R_{ext}) connected between the anode and cathode of the MES was recorded by the desktop computer using a data acquisition system (M3500A, Array Electronic, Taiwan). Current (i) was calculated using the ohm's law. The inhibition ratio (I) induced by toxicant was calculated as I (%) = 100 × (i_{nor} – i_{tox})/ i_{nor} according to Kim et al. (2007), where i_{nor} (mA) is the baseline current generated by the MES in the absence of toxicant and i_{tox} (mA) is the generated current in the presence of toxicant.

a)

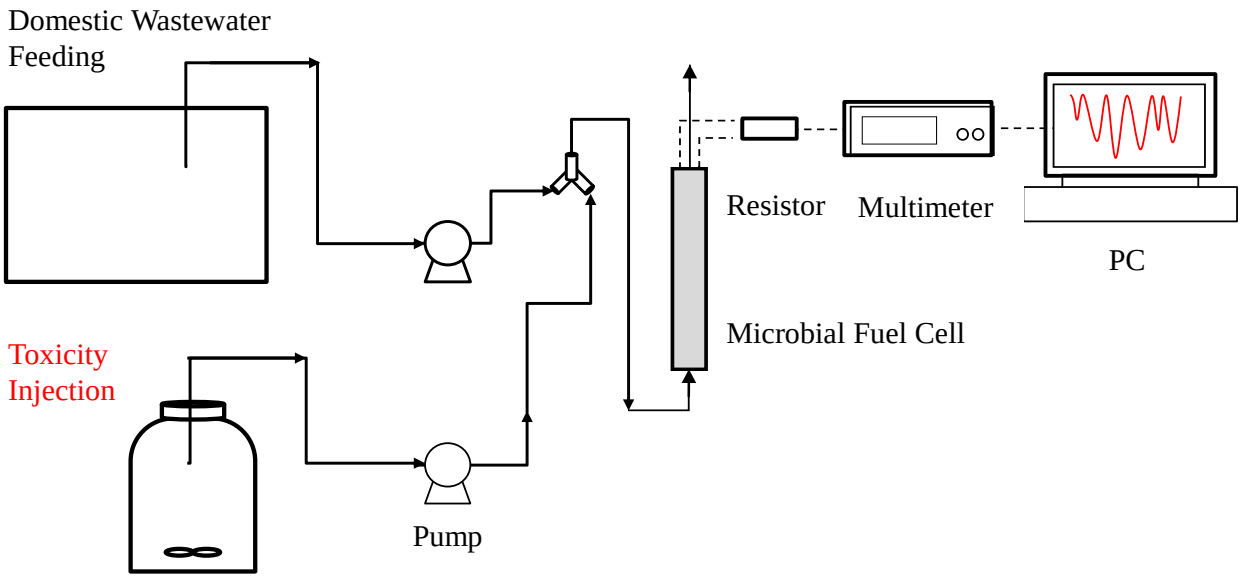

Figure 3.1. a) Schematic diagram of the sensing system using MES (size not to scale) b) A photo of the laboratory-scale MES. c) A photo of the group of MES.

In Chapter 4, one set of MES was switched to MEC mode by replacing the reactor circuit with a potentiostat (VersaSTAT 3, Princeton Applied Research, US) at an applied voltage of -0.6 V as shown in Fig. 3.2. The positive lead of the power source was connected to the anode, and the negative lead was connected to the resistor in the circuit connecting the electrodes.

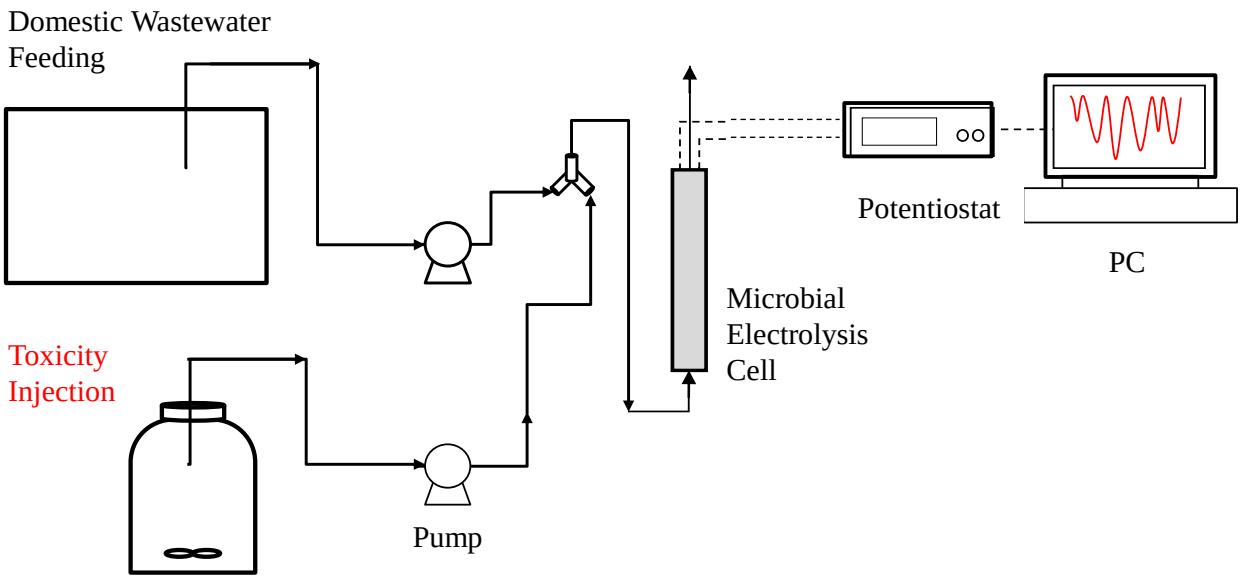

Figure 3.2. Schematic diagram of the sensing system using MEC-MES (size not to scale).

3.3 MES construction

3.3.1 MES reactor construction

Two different types of MES reactors were used in study, both of them were single-chambered air-cathode designs (Liu and Logan, 2004) (Fig. 3.3). Oxygen in the air in contact with the cathode was used as the electron acceptor. The difference between the two type of MES was the flow condition - the first type is a cylindrical reactor without channels (Figs. 3.3a and b) (denoted as "MES without channels") and the second type was a rectangular channel flow reactor (Fig. 3.3c and d) (denoted as "MES with channels"). The first reactor type consisted of a cylindrical chamber 1 cm wide by 6 cm diameter, resulting in an empty volume of 28 cm^3 (unless indicated otherwise). In one set of tests to optimize the reactor size, the electrode spacing was changed from 1 to 0.5 cm, resulting in a decrease of reactor size from 28 to 14 cm^3. The second reactor type was single-chamber flat plate reactors with channels as

shown in Figs 3.3c and d based on the prototype single chamber MFC described by (Min and Logan, 2004). The anode chamber was 8 cm long, 1 cm wide and 6 cm high. Channels were constructed to make the flow follow a serpentine path of 1 cm wide and 0.6 cm deep, having a total volume of 41.4 cm^3. Both the anode and the cathode were made of carbon cloth (E-Tek, USA) and the cathode was coated with platinum catalyst on one side at a load of 0.5 mg cm^{-2}.

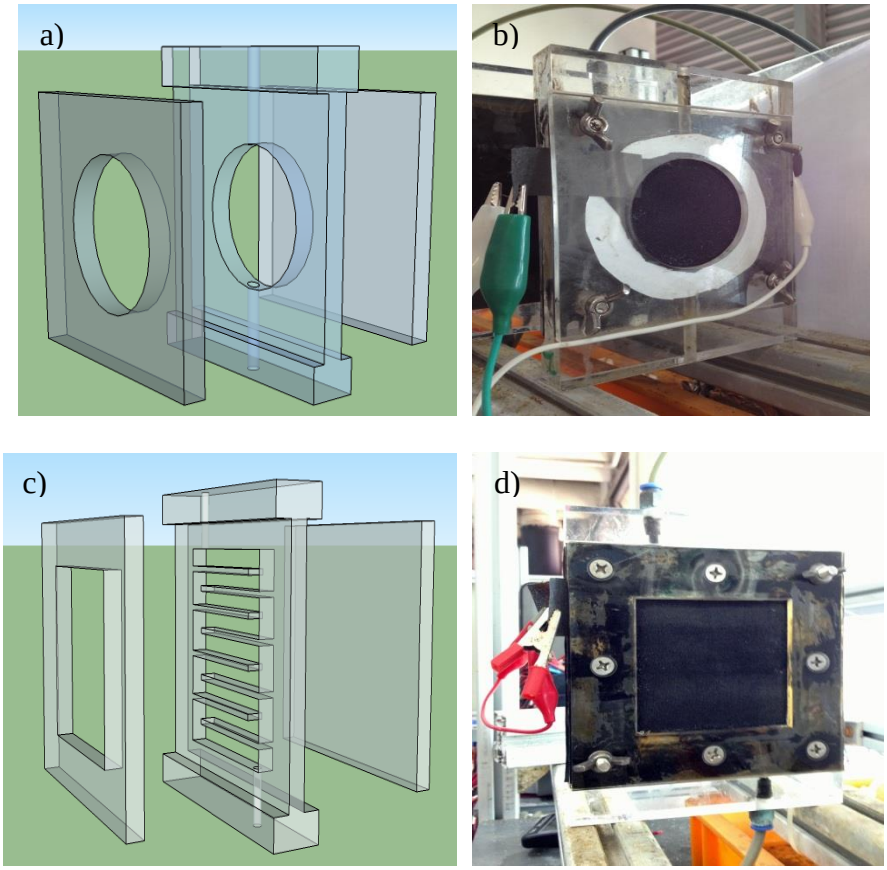

Figure 3.3. (a) A 3-D schematic and (b) a photograph of a single-chamber cylindrical MES without channels (MES without channels). (c) A 3-D schematic and (d) a photograph of a single-chamber flat plate MES with channels (MES with channels).

3.3.2 MES configuration

Three different configurations were tested on the MES without channels: (i) a membrane electrode assembly (MEA, Fig 3.4a, Type A); (ii) separated anode and cathode with a polytetrafluoroethylene (PTFE) layer on the air-side of the cathode (Fig. 3.4b, Type B) as suggested by (Cheng et al., 2006) (referred as "SAC-P") and (iii) separated anode and cathode with a membrane adjunct to the cathode (Fig. 3.4c, Type C) (referred as "SAC-M").

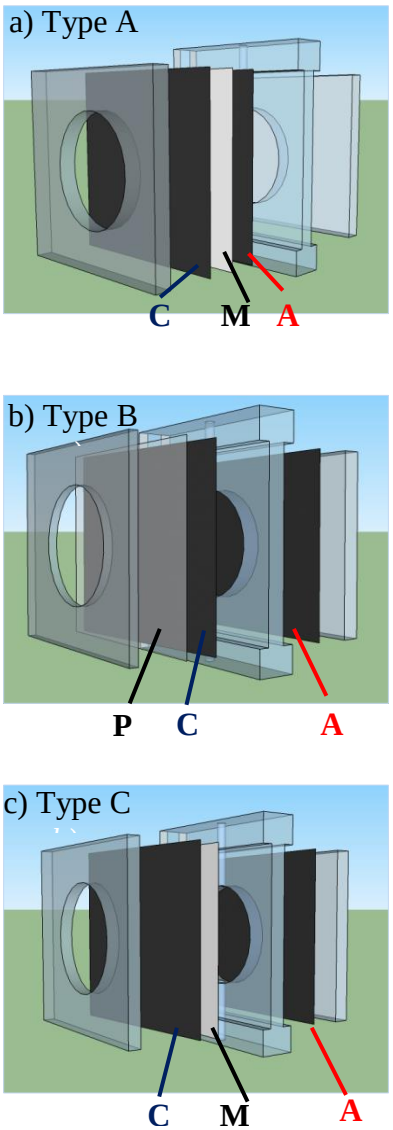

Figure 3.4. Details of the electrode configuration used. (a) Type A: MEA-MES in which the anode, membrane and cathode were pressed together; (b) Type B: Separated anode and cathode configuration with PTFE coated on cathode; and (c) Type C: Separated anode and cathode configuration with a membrane adjunct to the cathode. (A-Anode, C-Cathode, M-Membrane, P-PTFE)

For the MES with channels, only the type C configuration was used as shown in Fig. 3.5.

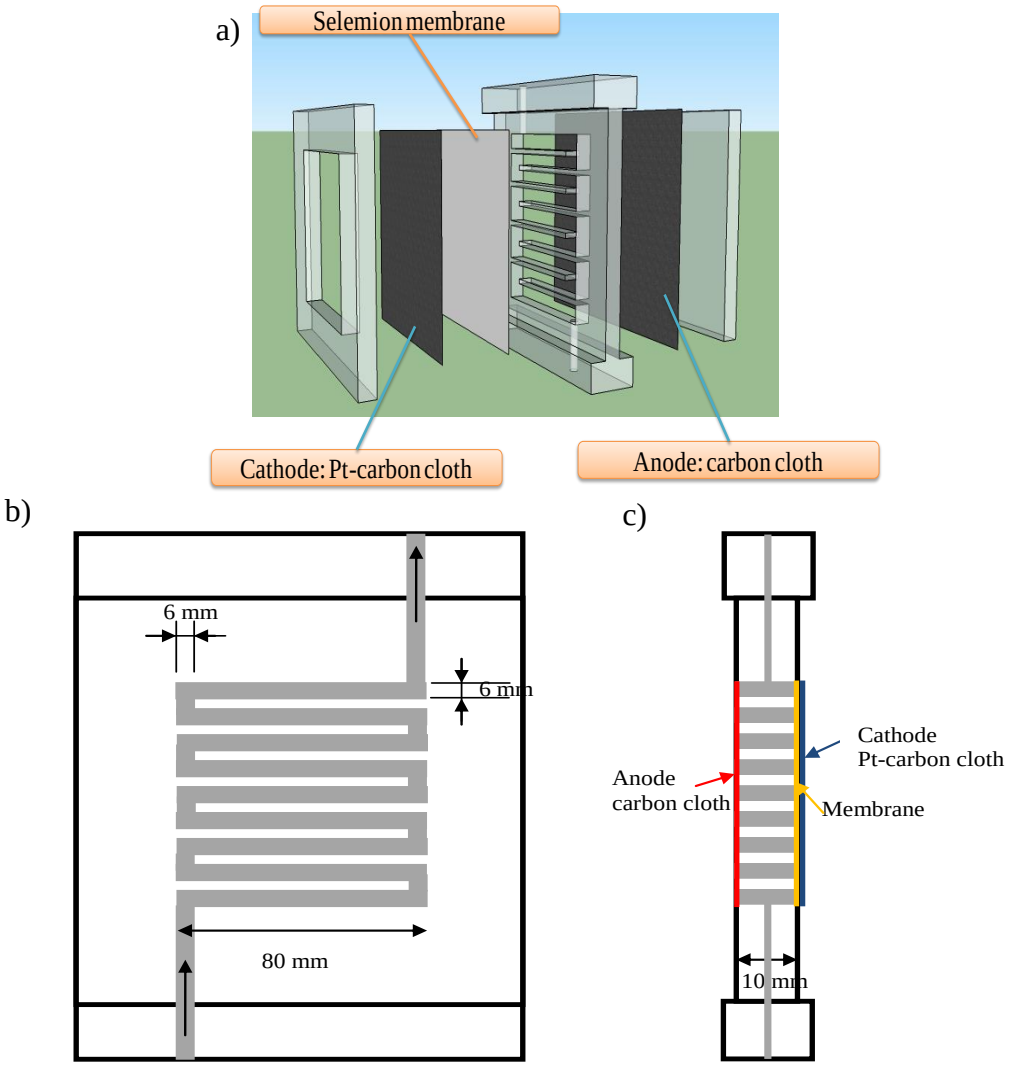

Figure 3.5. Details of the MES with channels with type C configuration (separate anode and cathode with membrane close to the cathode) a) 3-D image, b) Front view and c) Side view.

3.3.3 Membranes

Five different membranes were tested in the MEA-MES configuration to assess their suitability for sensor application: (i) Nafion 117 (DuPont Co., USA); (ii) Selemion HSF (Asahi Glass Co., Japan); (iii) (PTFE) membrane (Sartorius Stedim, Germany); (iv) Isopore membrane filter (Millipore, USA); and (v) Biomax ultrafiltration disc (Millipore, USA). These will be hereafter referred as Nafion, Selemion, PTFE, Isopore and Biomax.

3.3.4 External resistances

To evaluate the effect of external resistance, R_{ext} (i.e., the electrical load applied to the MESs), three different resistors (5, 430 and 5,000 Ω) were individually connected between the anode and the cathode of the MEA-MES at any one time. 5 Ω was chosen to generate the maximum current for the MESs; 430 Ω was chosen because it was close to the internal resistance of the MESs that would allow them to generate the maximum power; 5000 Ω was chosen to allow the MESs to generate the maximum voltage.

3.3.5 Summary of the MES construction

A series of experiments were conducted to study the individual effects of reactor design, configuration, membrane, external resistance and reactor size on both the stability without toxicants and sensitivity when exposed to toxicants of the MES. After phase 1 (Chapter 4) when the optimization of the sensor was finished, the optimal MES was used in the phase 2 (Chapter 5) and 3 (Chapter 6) for further studies. The information is summarized in Table 3.2.

Table 3.2 Summary of the MES used in different phases.

Optimization parameters	Reactor type	Configuration type	Membrane	R_{ext} (Ω)	Reactor Size (cm^3)	Figure
Phase 1-1: Optimization of the sensor device (Chapter 4)						
Membrane	WO Channel	MEA	Nafion, Selemion, PTFE, Isopore, Biomax	5000	28	Fig. 3.4a
External resistance	WO Channel	MEA	Selemion	5, 430, 5000	28	Fig. 3.4a
Configuration	WO Channel	MEA	Selemion	5	28	Fig. 3.4a
		SAC-P				Fig. 3.4b
		SAC-m				Fig. 3.4c
Reactor size	WO Channel	SAC-m	Selemion	5	14/28	Fig. 3.4c
Reactor type	WO Channel, With Channel	SAC-m	Selemion	5	28	Fig. 3.4c Fig. 3.5
MFC/MEC	With Channel	SAC-m	Selemion	5	40	Fig. 3.5
Phase 1-2: Sensing material optimization (Chapter 4)						
Biofilm	WO Channel	SAC-m	Selemion	5	28	Fig. 3.4c
Phase 2 and Phase 3 (Chapter 5 and 6)						
	With Channels	SAC-m	Selemion	5	40	Fig. 3.5

3.4 Operating conditions

MESs were firstly inoculated and enriched for 2 months and then applied into toxicity testing. Therefore, the operation condition of the MESs was divided into two periods: the enrichment periods and the toxicity testing periods as discussed in the following sub-sections.

3.4.1 Enrichment period

3.4.1.1 Electrolyte and inoculum

Domestic wastewater (COD of 300-400 ppm) was used as the inoculum and fuel for the MESs. The anodic compartments were fed continuously with effluent collected from the primary clarifier of the Ulu Pandan Water Reclamation Plant, Singapore. Prior to feeding, the effluent was filtered with a screen of 200-μm pore size. Other chemical parameters characterizing the wastewater are listed in Table 3.3.

Table 3.3 Characteristics of the influent wastewater.

Component	Concentration	Component	Concentration
COD (ppm)	346.0 ±77.0	F^- (ppm)	0.18 ±0.08
SCOD (ppm)	114.2 ±60.4	Cl^- (ppm)	98.1 ±64
TSS (ppm)	227.3 ±108.0	Br^- (ppm)	0.06 ±0.06
TDS (ppm)	114.2 ±60.4	NO_3^- (ppm)	2.15 ±2.15
VSS (ppm)	185.3 ±80.0	PO_4^{3-} (ppm)	6.58 ±3.38
pH	7.37 ±0.24	SO_4^{2-} (ppm)	62.72 ±12.38
Conductivity (mS/cm)	0.852 ±0.093	Na^+ (ppm)	45.75 ±28.75
		NH_4^+ (ppm)	22.96 ±11.14
Temperature (℃)	24.55 ±1.45	K^+ (ppm)	8.94 ±3.54
		Mg^{2+} (ppm)	2.14 ±1.14
		Ca^{2+} (ppm)	15.04 ±3.54

In one set of the experiments, Ni(II) (Sigma-Aldrich Pte. Ltd., Singapore) was continuously added into the inoculum, resulting in 1 and 2 ppm of Ni(II) in the influent feed during the 2 months enrichment period in order to investigate the response of the MES inoculated under toxic conditions with a final purpose to increase the sensor selectivity.

3.4.1.2 Shear stress

Different shear stress was applied on the MESs during the enrichment period controlled by the flow rate and intermittent nitrogen sparging. Except where noted otherwise, the MESs were usually run in an upflow mode at a constant flow rate of 1.3 mL min^{-1} during the enrichment period of 2 months, maintained through a peristaltic pump (Masterflex 07523-70, Cole-Parmer, USA) (Table 3.4).

For the optimization of sensing material, different enrichment shear stress were applied during the 2-month enrichment period (Table 3.4). Eight MESs (two for each shear condition) were inoculated in an upflow mode at four different flow rates, i.e., 1.3 mL min^{-1} (hydraulic retention time (HRT) of 20 min), 12 mL min^{-1} (HRT of 2 min), 12 mL min^{-1} (HRT of 2 min) and 24 mL min^{-1} (HRT of 1 min). For one of the two MES sets that were operated at a flow rate of 12 mL min^{-1}, nitrogen sparging was applied twice a week. Nitrogen sparging was carried out by stopping the feed to the MESs and aerating the MESs with nitrogen at a flow rate of 300 mL min^{-1} for 10 min.

Table 3.4 Summary of the shear stress applied during the enrichment period in different phases.

	Shear stress during enrichment period	
	Flow rate (mL min^{-1})	**Nitrogen Sparging**
Phase 1-1: Optimization of the sensor device (Chapter 4)		
MES without Channel	1.3	No
Phase 1-2: Sensing material optimization (Chapter 4)		
MES without Channel	1.3 (HRT = 22 min)	No
	12 (HRT = 2 min)	No
	12 (HRT = 2 min)	300 mL min^{-1} for 10 min twice a week
	24 (HRT = 1 min)	No
Phase 2 and Phase 3 (Chapter 5 and 6)		
MES with Channel	1.3	No

3.4.2 Toxicity testing period

3.4.2.1 HRT

Five different flow rates were compared using MES without channels to investigate the HRT effect on the sensor response in the range of 1–22 min (Table 3.5). The optimal HRT of 2 min was chosen for the phase 2 and 3 studies for the MES with channels as summarized in Table 3.5.

Table 3.5 Summary of the flow rate tested for toxicity testing in different phases.

	Flow rate (mL min^{-1})	**Toxicant tested**
Phase 1-1: Optimization of the sensor device (Chapter 4)		
MES without Channel	1.3 (HRT = 22 min) 4 (HRT = 7 min) 8 (HRT = 3.5 min) 12(HRT = 2 min) 24(HRT = 1 min)	Acidic toxicity
Phase 1-2: Sensing material optimization (Chapter 4)		
MES without Channel	12 (HRT = 2 min)	5 ppm Cu(II) 7 ppm Cu(II)
Phase 2 and Phase 3 (Chapter 5 and 6)		
MES with Channel	16 (HRT = 2 min)	Extreme pH conditions, nitrate, NaCl cyanide, heavy metals, organics

3.4.2.2 Toxicant tested

Table 3.6 summarizes all the toxicant tested in different phases.

Table 3.6 Summary of the toxicants tested in different phases.

Toxicant kind	Toxicant species	Concentration
Acidic and alkaline toxicity	HCl	2 to 6
	NaOH	8 to 11
Inorganic anions	Cyanide	1 to 10 ppm
	Nitrate	0 to 0.8 mM
Single heavy metal	Pb, Cd, Ni, Zn, Cu	1 to 10 ppm
Binary heavy metal	Ni-Cd, Ni-Cu, Ni-Zn,	5 ppm each metal
	Cd-Cu, Cd-Zn, Cd-Pb	5 ppm each metal
	Cd-Cu	5ppm-5ppm, 2ppm - 8ppm, 8 ppm-2 ppm
Organics	Dichloromethane (DCM)	700 to 7000 ppm
	m-cresol	400 to 1200 ppm
	Toluene	400 ppm
	Chloroform (CFM)	3000 to 10000 ppm

Acidic toxic incident was created by adding HCl to the wastewater to alter its pH to 6, 5, 4, 3 or 2. Alkaline toxic incident was created by adding NaOH to alter its pH to 8, 9, 10, or 11. All experiments were run in duplicate. For the assay of heavy metals, the toxic metal substance used in this study was Cu(II), Cd(II), Pb(II), Zn(II) and Ni(II) solutions, as 10,000 mg L^{-1} M^{2+} in 1-2% nitric acid (Sigma-Aldrich Pte. Ltd., Singapore). During the toxicity assessment, different amount of the solution was injected into the MES and the changes in the generated current with time were

recorded. The Organics used in this study was m-cresol, toluene, chloroform, dichloremethane. All of them were purchased from Sigma-Aldrich Pte. Ltd., Singapore.

3.5 Metal Precipitation and Biosorption tests

Batch experiments with initial metal concentrations of 0 to 15 ppm were conducted in 250-ml flasks with only filtrate of the wastewater and wastewater to study the metal precipitation and biosorption in the wastewater, respectively. The filtrate of the wastewater was obtained by filtering the wastewater with a 0.45-μm pore sized membrane filter (GN-6 grid 47-mm, Gelman Science, Pall Corporation, Ann Arbor, Mich.). For the adsorption test, the pH, total suspended solids (TSS) and volatile suspended solids (VSS) of the wastewater were determined. Total contact time of heavy metals with the wastewater was 4 h.

3.6 Analytical Methods

3.6.1 Solution composition determination

3.6.1.1 Chemical oxygen demand (COD)

Total and soluble chemical oxygen demand (TCOD and SCOD, respectively) of wastewater samples were measured using the closed reflux method (HACH COD heater, Model 16500-10) in accordance to the Standard Methods (APHA, 2005).

3.6.1.2 Total suspended solids (TSS) and volatile suspended solids (VSS)

The TSS and VSS were determined according to the Standard Methods (APHA, 2005). The glass microfiber filters (GF/F, Whatman) were rinsed with 25 mL of distilled water and baked in a furnace (Thermolyne 48000, Omega Medical Scientific) at 550^{o}C for 20 min prior to analysis. The samples were then filtered through the filter to collect the TSS and then dried at 105^{o}C for 1 h. After that, the sample was cooled to room temperature in desiccators before being weighed. To determine the VSS, the filter with the collected TSS was further heated at 550^{o}C for 20 min and weighed after being cooled in the desiccator.

3.6.1.3 Conductivity measurement

The conductivity of the solution was measured by a conductivity probe (Thermo scientific Orion 4 star- pH – conductivity probe, USA). The conductivity probe was calibrated with NaCl as standard rinse solutions.

3.6.1.4 Ion chromatogram

Samples were passed through a 0.45-μm pore sized membrane filter (GN-6 grid 47-mm, Gelman Science, Pall Corporation, Ann Arbor, Mich.) prior to analysis. Cations of Na^{+}, NH_4^{+}, K^{+}, Mg^{2+}, Ca^{2+} and anions of F^{-}, Cl^{-}, NO^{2-}, NO^{3-}, Br^{-}, PO_4^{3-}, and SO_4^{2-} was measured using an Ion Chromatogram (Dionex-dx 500IC).

3.6.1.5 Metal concentration

Soluble metal concentration

Samples were passed through a 0.45-µm pore sized membrane filter (GN-6 grid 47-mm, Gelman Science, Pall Corporation, Ann Arbor, Mich.) prior to analysis. Soluble Cu(II), Zn(II), Ni(II), Cd(II) and Pb(II) were determined by an inductively coupled plasma-optical emission spectrometry (ICP-OES) (Perkin-Elmer DV 4300). The standard curves were calibrated with standard ICP solutions as 10,000 mg L^{-1} M^{2+} in 1-2% nitric acid (Sigma-Aldrich Pte. Ltd., Singapore).

Total metal concentration

The total metal concentration was measured in accordance to the Standard Methods (APHA, 2005). Five mL of concentrated Nitric Acid (Sigma-Aldrich Pte. Ltd., Singapore) and a few glass beads were added to the sample in a flask (250 mL). It was brought to a slow boil on a hot plate and evaporated until about 50 mL was lft when digestion was completed as shown by a light-colored, clear solution. Then the exact volume of the evaporated sample was measured and the metal concentration present was analyzed by the ICP-OES.

3.6.2 Biofilm characteristics determination

3.6.2.1 Sampling

In the phase 1-2 biofilm optimization study (Chapter 4.2.2), to investigate the biofilm characteristics affected by shear stress during the inoculation period, the MES was

dismantled at the end of the experiment and the anode carbon cloth was removed from the MESs, cut into 16 pieces of 1 cm^2 squares and collected in Phosphate Buffer Saline (PBS) (1X, pH 7.0). Different pieces were used for the respective VSS, EPS and SEM analysis as described in Fig. 3.6.

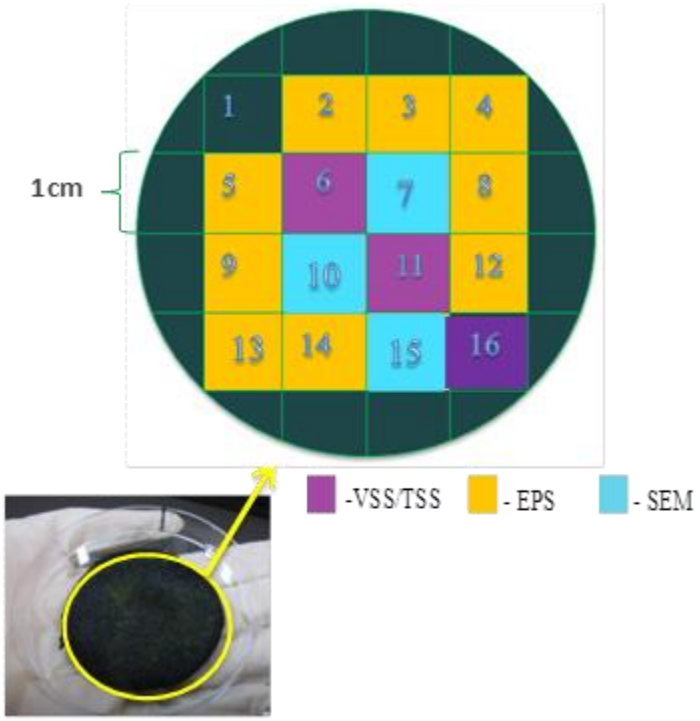

Figure 3.6. Arrangement of the anode carbon cloth from MES without channels for VSS/TSS, EPS and SEM tests.

In the phase 3 mechanism study (Chapter 6), to investigate the toxicant effect on the biofilm characteristics, the biofilm samples were taken at different toxicant exposure time as shown in Fig. 3.7: before the 10 ppm Cd(II) exposure (S-0), at the 1^{st} h (S-1), 4^{th} h (S-4), 6^{th} h (S-6) exposure and after 1^{st} h (S-7), 2^{nd} h (S-8) recovery.

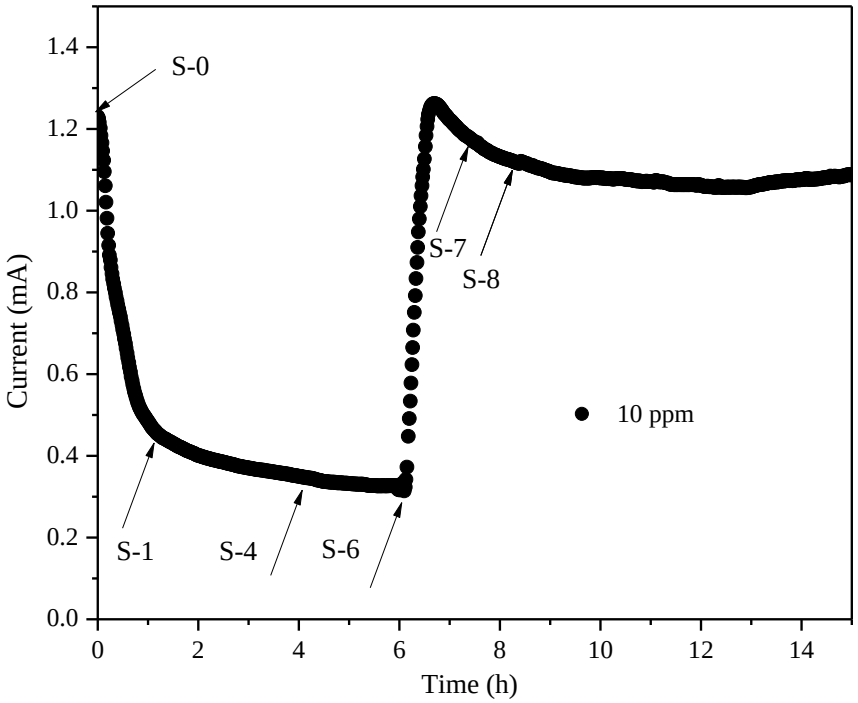

Figure 3.7. The biofilm samples were taken before the 10 ppm Cd(II) exposure (S-0), at the 1st h (S-1), 4th h (S-4), 6th h (S-6) exposure and after 1st h (S-7), 2nd h (S-8) recovery.

Pieces (1 × 0.6 cm) of each carbon cloth were cut with a sterile surgical blade. The pieces of carbon cloth were then processed for different analysis as summarized in the Fig. 3.8.

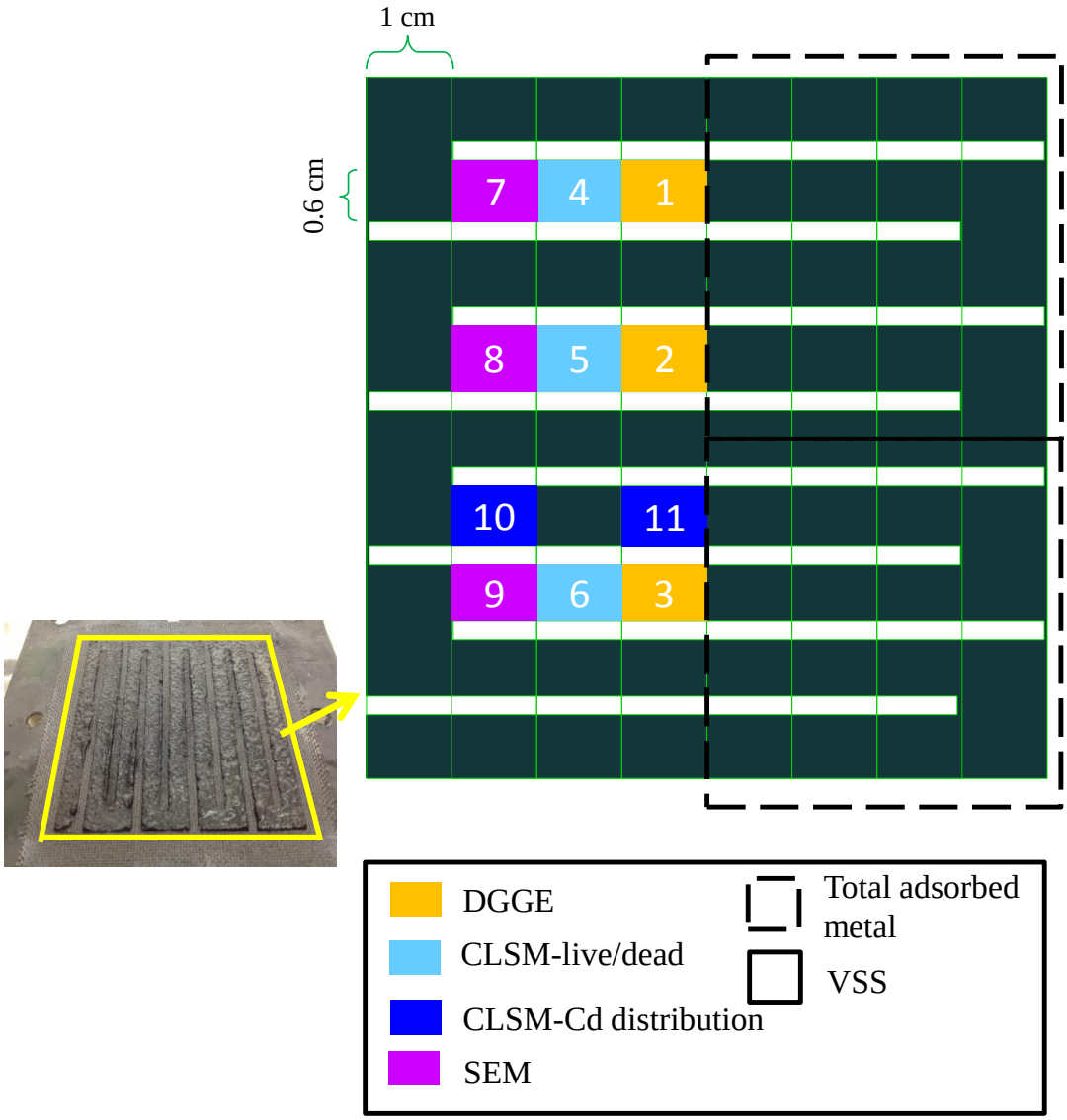

Figure 3.8. Arrangement of the anode carbon cloth from the MES with channels for DGGE, CLSM, SEM, total absorbed metals and VSS analysis.

3.6.2.2 VSS and biofilm density

VSS were recovered by centrifugation (5,000 rpm; 1 min) according to Xing et al. (2010). VSS were analyzed according to the Standard Methods (APHA, 2005). Biofilm density (D, g VSS L^{-1}) was determined as $D = m/L \times 10^4$, where m (mg cm^{-2}) is the VSS content of the biofilm collected from the $1cm^2$ carbon cloth and L is the thickness of the biofilm (μm).

3.6.2.3 Extracellular Polymeric Substances (EPS)

EPS were recovered by centrifugation (5,000 rpm; 1 min) according to Xing et al. (2010). The protein and carbohydrate concentrations of EPS were determined by the modified Lowry method (Frolund et al., 1995) using glucose as the standard and the Dubois phenol-sulphuric acid method using bomin serum albumin (BSA) (Dubois et al., 1956), respectively.

3.6.2.4 Scanning Electron Microscopy (SEM)

Scanning electron microscopy (SEM) was carried out to investigate both the surface and the thickness of the biofilm. The samples were first soaked in a 2.5% Glutaraldehyde solution for 30 min at room temperature (25^{o}C) for fixation. They were then dehydrated through an ascending ethanol series (25, 50, 75, 90, and 100% for 15 min each) at room temperature. Prior to observation, the samples were critical-point dried and coated with gold in a sputtering device. Three different points for each sample were observed under a SEM (Philips XL30 FEG).

3.6.2.5 Fluorescent Staining

To detect the bacteria viability and the distribution of Cd(II) within the biofilm, two sets of fluorescent probe kits, the LIVE/DEAD BacLight Viability kit (L-7012) and the Measure-iT Assay kit (M36353) (Life Technologies Holdings Pte. Ltd., Singapore), were used. The LIVE/DEAD BacLight Bacterial Viability Kits utilize mixtures of SYTO®9 green-fluorescent nucleic acid stain and the red-fluorescent nucleic acid stain, propidium iodide. Live cells with intact membranes fluoresce green,

while dead cells with damaged membranes fluoresce red (Invitrogen, 2004) due to the difference of the stains both in their spectral characteristics and in their ability to penetrate healthy bacterial cells. The SYTO 9 stain generally labels all bacteria in a population including those with intact membranes and damaged membranes. In contrast, propidium iodide penetrates only bacteria with damaged membranes, causing a reduction in the SYTO 9 stain fluorescence when both dyes are present.

Biofilm specimens were collected on the slide and dipped in Phosphate Buffer Saline (PBS) (1X, pH 7.0), which was tenfold dilution of the original 10X PBS (1st BASE PTE. Ltd., Singapore). The process was handled in petri dishes and gentle shaking was applied to remove any unbound or loosely bound organics that was not part of the attached biofilm. Then the biofilm specimens were stained by incubating for 15 min in 1 mL of PBS (1X, pH 7.0) containing 1.5 uL of propidium iodide and 1.5 uL of Syto 9 from the LIVE/DEAD BacLight stain kit under dark conditions. Excess dye was removed by gently washing the sample with PBS (1X, pH 7.0) and excess PBS was further drained away surrounding the section with a piece of KimWipe. A few drops of VectaShield were added as mounting medium and a cover slip was added by placing one of the ends on the slide and slowly lowering it like a sandwich.

3.6.2.6 Confocal Laser Scanning Microscopy (CLSM) and Image Analysis

After staining, the biofilm specimen was immediately examined using a Leica TCS SP5X Confocal Microscope System (German) under a 100× magnification objective. The 488-nm line of an argon laser was used as the excitation light for all the fluorescent probes used in this research. Two channel imaging was selected, and a

585-nm long pass filter and a 505-550-nm band pass filter were used for red and green fluorescent light, respectively.

The image analysis program COMSTAT (Heydorn et al., 2000) was used to analyzed the images stained with the LIVE/DEAD Bac Light viability stain, which recognizes the relative biomass that fluoresces green (live) and red (dead) at levels above a user-defined threshold value and reports the percentage of biomass that is alive and the percentage of biomass that is dead in each slice in a stack of images.

3.6.2.7 Molecular Biology Based Techniques for the analysis of the biofilm community

DNA extraction from bacterial cells present in the MES

Genomic DNA was extracted using a Qiagen DNeasy Blood and Tissue Kit (QIAGEN GmbH, Hilden, Germany). The procedure followed the manufacturer's instructions except that 45 µl of proteinase K (25 mg ml^{-1}), 20 µl of lysozyme (100 mg ml^{-1}) and 10 µl of achromopeptidase (25 mg ml^{-1}) were used (Cheng et al., 2009; Chow et al., 2010).

PCR amplification and cloning of bacterial 16S rRNA genes

PCR-denaturing gradient gel electrophoresis (PCR-DGGE) analyses were carried out by using two different sets of primers: (a) 341FGC (5'-CGCCCGCCGCGCGCGGCGGGCGGGGCGGGGGCACGGGGGGCCTACGGGAGGCAGCAG-3') and (b) 518R (5'-ATTACCGCGGCTGCTGG-3') (annealing

temperature: 60 ℃). PCR-amplified fragments were electrophoresed on an 8% polyacrylamide gel with a 30–60% urea-formamide gradient for 16 h at 120 V and 60 ℃ (Cheng et al., 2009).

DGGE screening of cloned 16S rRNA gene fragments

Cloned 16S rRNA gene fragments were analyzed by denaturing gradient gel electrophoresis (DGGE) to screen clones prior to sequencing. DGGE analysis was conducted using the D-Gene DGGE system (Bio-Rad, Hercules, CA, USA). Polyacrylamide gels (10% polyacrylamide, acrylamide:*N*,*N*′-methylenebisacrylamide, 37.5:1; 0.75 mm thick; 16×16 cm) were run in a 1 X TAE buffer (40 mM Tris-acetate, 1 mM EDTA pH 8.3). A gradient ranging from 30 to 60% denaturant (100% denaturant is 7 M urea plus 40% vol/vol formamide in 1 X TAE) was used. Gels were run at 60 ℃ for 4 h at a constant 200 V and stained for 30 min in SYBR green I (Sigma, Poole, UK; diluted 1/10,000 in 1 X TAE). Stained gels were viewed and documented using a Fluor-S Multilmager (Bio-Rad, Hercules, CA, USA). Clones with different migration characteristics in DGGE analysis were selected for sequence determination.

Sequencing and phylogenetic analysis of cloned rRNA gene fragments

Interesting bands were excised from the gel and amplified by PCR again, following being sequenced with primer 518R. Bands identification was determined by comparing the sequences against NCBI nucleotide database for highest similarity.

3.6.3 Electrochemical measurements

3.6.3.1 Sampling

During the inoculation period of a MES, the first polarization test was conducted 3 d after the startup of the reactor and then was conducted twice a week. During the toxicity testing period, the polarization tests were conducted before and after the toxic event. For the phase 3 (Chapter 6), PC, CV and EIS were taken during the toxicity dosing period as shown in Fig. 3.7: before the 10 ppm Cd(II) exposure (S-0), at the 1^{st} h (S-1), 4^{th} h (S-4), 6^{th} h (S-6) exposure and after 1^{st} h (S-7), 2^{nd} h (S-8) recovery.

All of the tests were conducted in the two-electrode mode, in which the anode served as the working electrode and the cathode acted as both reference and counter electrode. It was assumed here that the variation of the electrochemical characteristics of the whole cell was due to the anode conditions since the cathodic potentials were almost identical in all cases due to the use of the same electron acceptor (Yuan et al., 2011).

3.6.3.2 Polarization Curve

Polarization curves represented the voltage as a function of the current, and were obtained by varying the applied external resistance connected across the MESs, and recording the pseudo steady-state voltage every minute while the current was calculated using the Ohms law (Logan et al., 2006). Before that, the MESs were kept in the open circuit mode until the open circuit voltage became stablilized (around 2 h).

The value of the internal resistance, R_{int}, of the MESs was determined using a linear regression on the linear part of the polarization curve that corresponded to the Ohmic zone. The E_{emf} (V) was estimated as the intercept of the regression with the Y-axis (Watanabe, 2008).

3.6.3.3 Cyclic Voltammetry

The electrochemical activities of the biofilm were examined by the Cyclic Voltammetry (CV) with a potentiostat (VersaSTAT 3, Princeton Applied Research, US). CV was conducted at a scan rate of 1 mV/s, in the potential range from -0.5 to 0.5V, starting at the open circuit potential (2 scans).

3.6.3.4 EIS

EIS was conducted with a potentiostat at an applied potential of 0.6 V (VersaSTAT 3, Princeton Applied Research, US), over a frequency range of 100 kHz to 100 mHz with a sinusoidal perturbation of 5-mV amplitude. The R_p+R_s and R_s were analyzed using the Bode plot (He and Mansfeld, 2009).

CHAPTER 4 Optimization of MES

4.1 Introduction

MES has shown potential to be used as online biosensor for the detection of toxic compounds in water (Kim et al., 2007). Kim et al. (2007) successfully used an MES to detect Pb(II) and Hg(II) at a concentration of 1 ppm; however, Patil et al. (2010) showed that in the presence of Pb(II) and Hg(II) at concentrations in the range of 0.41-12.48 ppm and 0.83-8.33 ppm, respectively, planktonic cells were inhibited, while the electrochemically active biofilm was not affected. The contradiction between these two studies suggests that the behavior of an MFC-based toxicity sensor can be influenced by several factors which need further optimization and investigation.

A MES is composed of two elements (Thévenot et al., 2001): a bioreceptor that is an immobilized sensitive biological element sensing the analyte (i.e., the electroactive biofilm of the MESs) and a transducer that is used to convert the activity of the biofilm into the current signal. It is influenced by many factors, such as reactor configuration (Liu et al., 2005a; Fan et al., 2007), proton exchange membrane (Oh and Logan, 2006), distance between the electrodes (Ghangrekar and Shinde, 2007; Cheng et al., 2006), electrode material (Park and Zeikus, 2003) and external resistance (Aelterman et al., 2008).

The objective of this chapter was to optimize the MES in terms of the anodic biofilm and the transducer to develop an ideal sensor for online screening of toxicity present in influent wastewater as shown in Fig. 4.1. It implies that the MES should provide (i)

a stable baseline in the absence of toxicity (Stein et al. 2010); (ii) high sensitivity when exposed to toxicity; and (iii) good recovery capability following the toxic event.

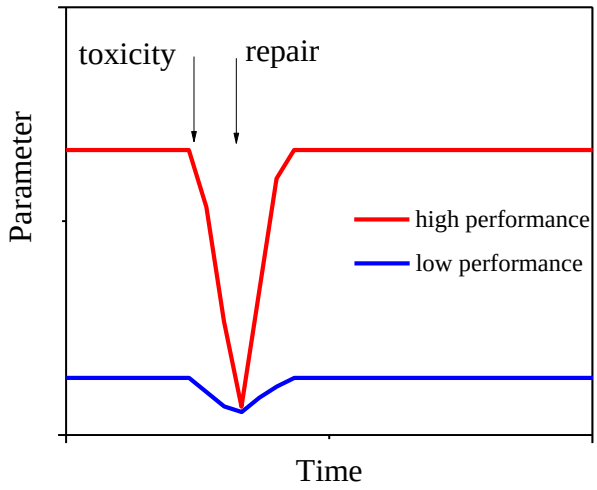

Figure 4.1. The basic criteria of an optimized biosensor for toxicity screening of wastewater: high and stable baseline, fast response, good recovery ability.

In the first part, different configurations, membranes, size and external resistances were compared to get the optimal MES toxicity sensor design by being evaluated with the occurrence of an acidic toxic event (HCl at various pH).

In the second part, the sensitivity of the MES was improved through modification of the biofilm structure. Hydrodynamic shear rates are known to affect mass transfer conditions, biofilm structure and the production of extracellular polymeric substances (EPS) (Celmer et al., 2008), all of which are factors that can affect the diffusitivity of toxicants and their interaction with the biofilm (Henriques and Love, 2007; Liu and Tay, 2002). As such, shear rates play an important role in biofilm reactors and shear rates have already been shown to impact on the density of MFC biofilms (Pham et al., 2008). Both intensive mixing and nitrogen sparging have been validated as effective methods to regulate the shear rate (Celmer et al., 2008). Thus we assessed the characteristics of the electrochemically active biofilm of an MES under different

shear rates – controlled by the flow rate and intermittent nitrogen sparging – and these characteristics were further correlated to the MFC sensitivity to Cu(II).

4.2 Results and Discussions

4.2.1 Optimization of the transducer

4.2.1.1 The startup of the MESs

Fig. 4.2 showed an example of the start-up of the MESs. Once the wastewater started to be continuously fed into the MESs, the initial voltages were generated immediately and increased quickly during the first 3 d. The reason is likely due to both chemical and biological factors based on the difference of the potential between the electrodes (Min et al., 2005). A lag phase of 17 d were seen, followed by a fast increase during the next 10 d and eventually stabilized at maximum values of 4.5 mV after 45 d of acclimation. The stable maximum voltages indicated that the effective exoelectrogenic biofilm had been enriched successfully on the surface of anodic materials (Min et al., 2005). Polarization curves were done regularly and the E_{emf}, R_{int} and P_{max} values are shown in Fig. 4.2. It could be seen that the trend of the P_{max} were the same as the voltage evolution and thus the average maximum power of 1-month operation following an acclimation period of approximately 1-month was used as the indicator to compare the baseline performance of different subsequently operational conditions.

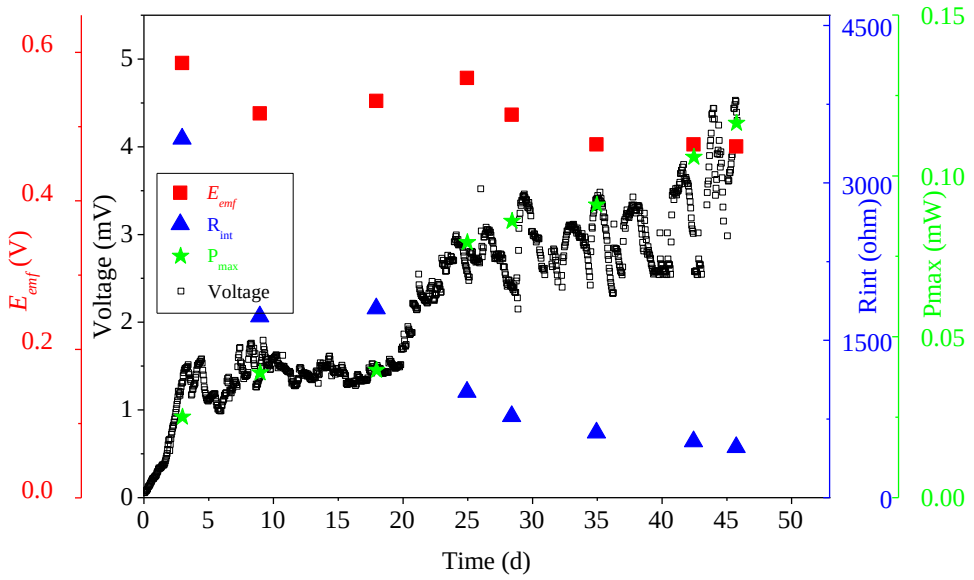

Figure 4.2. Voltage outputs (□), E_{emf} (■) R_{int} (▲) and P_{max} (★) variation over time during 45 d acclimation of MFCs operation. (MEA-MES with selemion membrane under the external resistance of 5 Ω)

4.2.1.2 Comparison of different types of membranes

Five different membrane types were tested in the MEA-MES design (Type A). No current was generated by the MESs with Biomax and PTFE membrane (data not shown). The average maximum power attained with the Nafion, Selemion and Isopore membranes are shown in Fig. 4.3. Isopore could provide high power during the first week but dropped dramatically during the subsequent three weeks, which was reflected by its high standard deviation. Both Nafion membrane and Selemion membrane could work continuously over a long period of time; however, the maximum power with Selemion (0.085 ± 0.015 mW) was higher and more stable than that achieved with the Nafion membrane (0.068 ± 0.027 mW).

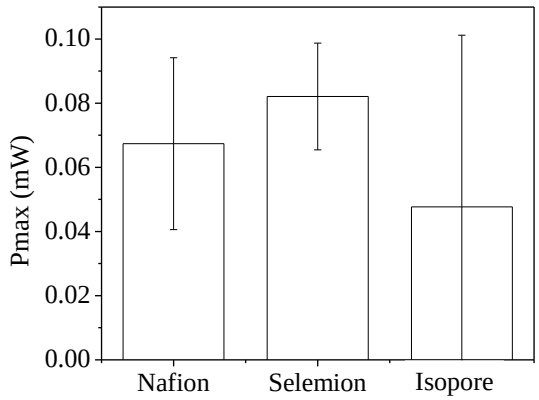

Figure 4.3. Average maximum power of MEA-MESs with Nafion, Selemion and Isopore membranes.

Both the Nafion and Selemion membranes were proton exchange membranes (highly selective for protons), but were not the case for the other three membranes. This result was consistent with the finding that the higher the selectivity for protons, the lower the resistance of the membrane and the higher the performance would be (Rabaey et al., 2005). And one possible reason for the comparatively lower and less stable performance of the Nafion membrane than the Selemion membrane was its high permeation to oxygen shown as shown in Table 4.1 (Chae et al., 2007; Lefebvre et al., 2011b). The highest D_O value (0.90×10^{-6} cm^2 s^{-1}) was observed with the Nafion membrane, and the lowest was seen with the Selemion membrane (0.08×10^{-6} cm^2 s^{-1}), suggesting that the Nafion membrane allowed the most O_2 to be diffused into the MES which was harmful to the system. Another likely reason was that the sulfonic acid groups in the Nafion membrane would bind with ammonia in the solution, leading to pollution of the membrane (Rabaey and Verstraete, 2005; Chae et al., 2007). Therefore, the Selemion membrane was found to be the most suitable membrane among those tested and it was used for subsequent experiments.

Table 4.1 Mass transfer coefficients (K_O) and diffusivities of oxygen (D_O) for various membranes tested in single-chamber MFC set-ups. (Lefebvre et al., 2011b)

	Nafion	**Selemion**	**Isopore**	**PTFE**	**Biomax**
Material	Nafion	Hydrocarbon	Polycarbonate	PTFE	Polyethersulfone
Thickness (μm)	180	150	15	80	120
K_O ($\times 10^{-4}$ cm s^{-1})	0.5	0.05	3	0.3	0.4
D_O ($\times 10^{-6}$ cm^2 s^{-1})	0.90	0.08	0.45	0.24	0.48

4.2.1.3 Effect of the external resistances

External resistance can affect the potential of the anode and thus the microbial activity and the performance of MESs (Clauwaert et al., 2008). MEA-MESs were operated under three different values of external resistance, ranging from 5 to 5,000 Ω. As shown in Fig. 4.4a, the MESs with the lowest resistance of 5 Ω achieved the highest maximum power of 0.126 mW with low standard deviation ± 0.016 mW, demonstrating high baseline performance with good stability. With higher external resistance, as expected, the MESs produced lower maximum power − 0.08 ± 0.012 and 0.05 ± 0.02 mW for the MESs with external resistance of 5,000 and 430 Ω, respectively. These results agreed with the finding by other studies that MFC performance increases with decreasing applied external resistance (Aelterman et al. 2008, Liu et al. 2005b).

In terms of sensitivity to an acidic toxic event, the MESs with the lowest external resistance of 5 Ω had the highest sensitivity to a pH 4 toxic event, as shown by the sharper voltage drop in Fig. 4.4b that reached 80% inhibition after 4 h of exposure. For the MESs under external resistance of 430 and 5,000 Ω, the inhibition after 4 h of exposure were just 50%, showing that operation of the MESs under low external resistance would improve its sensitivity as a sensor significantly. Because starting up

at different external resistance would affect the biofilm formation in the MFCs, Zhang et al. (2011) found that a loose biofilm structure with more void spaces was developed under a low external resistance of 10 Ω, which was beneficial for toxicants transport within the biofilm. Hence operation of the MES under a low external resistance is recommended for biosensor application.

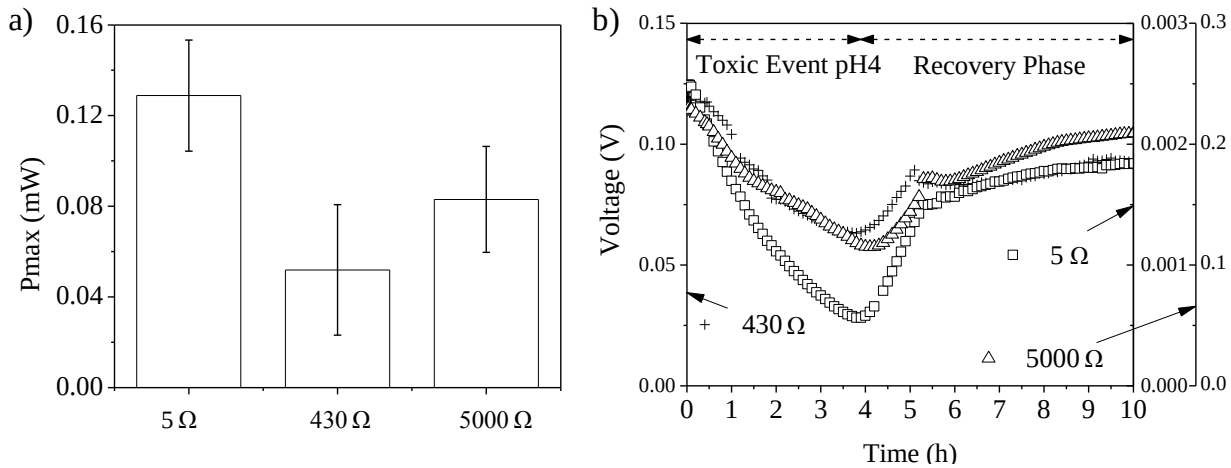

Figure 4.4. Baseline performance and toxicity test of MEA-MESs under different external resistances. a) Average maximum power during one month operation after inoculation; and b) Voltage evolution during (0-4 h) and after (4-10 h) exposure to pH 4 toxic event. The arrows indicate the respective axis.

4.2.1.4 Comparison of different configurations and wet-proofing method

Fig. 4.5a showed the baseline performance of the three different types of MESs. The MEA-MES (Type A) achieved a lower maximum power (0.126 ± 0.016 mW) than the MESs with separate anode and cathode configuration (Type B and C). With regards to the wet-proofing method applied for the separate anode and cathode configuration (Type B and C), the maximum power of Type B (PTFE) was 35% higher than that of Type C (membrane), but the larger standard deviation (± 0.13 mW) of Type B demonstrated poor stability, making it unacceptable as a sensor since it might result in false warning. When equipped with a Selemion membrane, the MESs were able to provide an average maximum power of 0.23 ± 0.023 mW, which met the basic

requirements of having both high and stable baseline performance for a sensor. The lack of the membrane in Type B MESs would make oxygen diffusion into the anode very easily and thus the aerobic bacteria would consume most of the substrate and decrease the voltage generation of MFCs (Liu and Logan, 2004), leading to the high fluctuation of the baseline performance of Type B MFCs. Besides, the biofilm could grow easily on the cathode without the protection of the membrane, affecting the activity of the catalyst (Liu and Logan, 2004). Thus the absence of the membrane (i.e., Type B) is not suitable for a stable baseline performance.

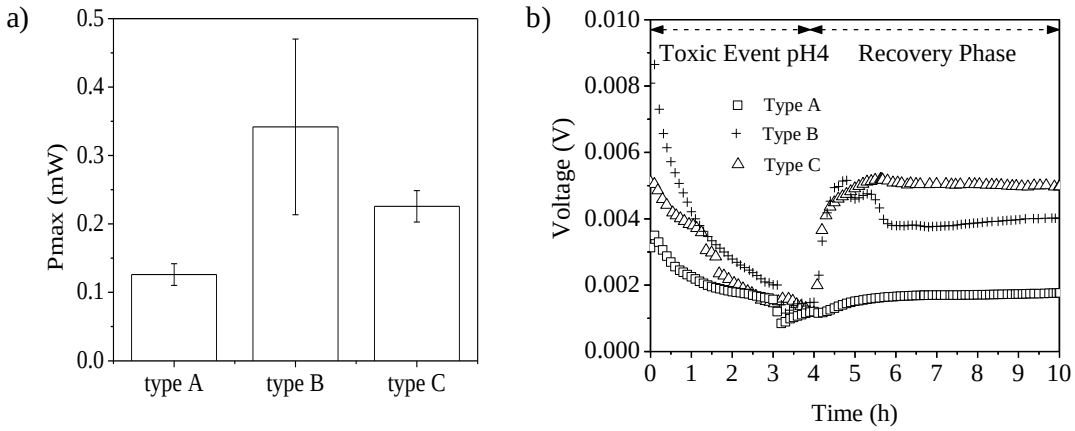

Figure 4.5. Baseline performance and toxicity sensitivity comparison of MESs with different configurations and different wet-proofing methods. a) Average maximum power attained during one month operation following inoculation; and b) Voltage evolution during (0-4 h) and following (4-10 h) exposure to a pH 4 toxic event.

In terms of sensitivity to an acidic toxic event, the Type B and C MFCs experienced a sharper voltage drop than Type A MFCs as shown in Fig. 4.5b, showing higher sensitivity. However, only for Type C the voltage could recover to its original level within hours following the toxicity event. There are many possible reasons for the difference in the recovery of these MFCs that can only be answered with a better understanding of the characteristics of the electrochemically active bacteria and how they transfer electrons to the anode surface. For Type A MFC with MEA, the anode and cathode were pressed together on either side of the membrane that was permeable

to oxygen, and therefore, oxygen diffusion would be more severe than that of Type C where the anode was located further from the cathode. In addition, for Type A MFC, the oxygen concentration in the inner layer of the biofilm (growing on the anode surface) that was closed to the anode would be higher than the outer layer of the biofilm, which was in contrast to the case of Type C MFC. Consequently, direct electron transfer via membrane bound cytochromes and electronically conducting nanowires would be lesser for Type A MFC with MEA because of the existence of oxygen as an alternative electron acceptor (Bond and Lovley, 2003; Kim et al., 2006a; Schröder, 2007). MEA-MFCs would involve more of the mediated electron transfers via the primary and secondary metabolites. The recovery and reproduction of these metabolites after being damaged by toxicants would take time and energy (Rabaey et al., 2004b), which led to the incomplete recovery of MEA-MFCs**.**

4.2.1.5 Effect of HRT

The HRT was changed between 0.9 and 22 min (Fig. 4.6). With a 22-min HRT, the voltage drop was slow and it took 13 h for the voltage to drop to 20% of its original voltage when the MESs were subjected to an acidic toxic event of pH 4. When HRT was decreased, the voltage drop was sharper and the recovery was faster (recovery data for HRT of 22 min was not shown here). This was due to the increase in the rate of mass transport, which enhanced the sensitivity of the system. However, the effect of further decreasing the HRT below 3.5 min was negligible because the mass transport rate was no longer the limiting factor. As such, 3.5 min can be considered as the optimum HRT for the biosensor MFC.

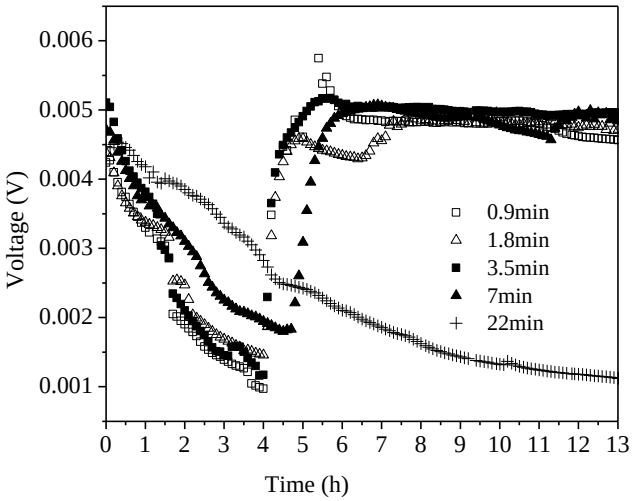

Figure 4.6. Voltage evolution during and following an acidic toxic event of pH 4 under different HRTs. Toxic event ceased when the voltage dropped to 20% of its original voltage.

4.2.1.6 Effect of the distance between anode and cathode

The distance between the anode and cathode were reduced from 1 to 0.5 cm to investigate the effect of electrode spacing. At the same time, the reactor volume was decreased by half to 14 mL. The maximum power density was found to decrease from 0.23 ± 0.023 to 0.12 ± 0.037 mW with decreasing the electrode space and the stability was much lower as shown by its larger standard deviation.

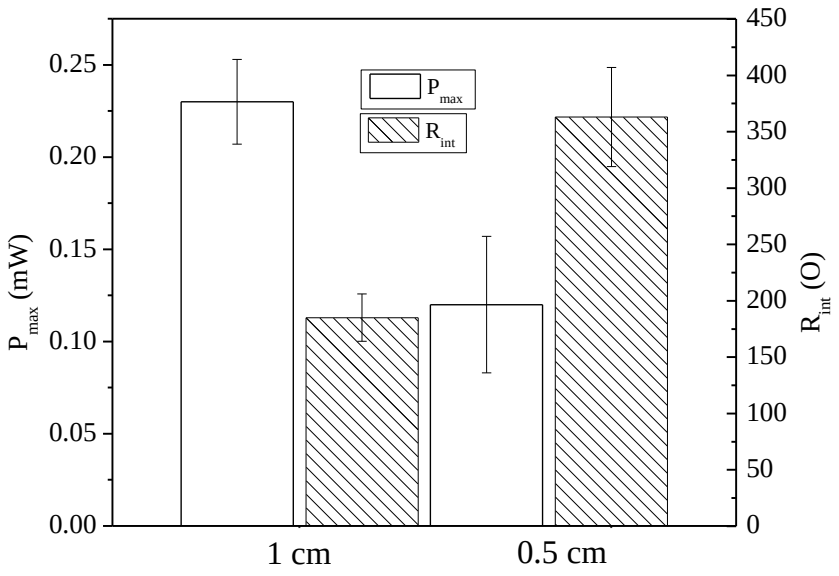

Figure 4.7. Average maximum power (P_{max}) ( ) and internal resistance (R_{int}) ( ) of MESs with different electrode space of 1 and 0.5 cm.

This result may appear contradictory to the findings of Liu et al. (2005a), which the maximum power density increased with decreasing the electrode space from 4 to 2 cm. The increase of the maximum power in Liu et al. (2005a) is due to the decrease of the internal resistance with narrower electrode space. However, in our study, the internal resistance was instead increased from 185±21 to 363±44 Ω when the electrode spacing was decreased from 1 to 0.5 cm (Fig. 4.7). The reason was that the internal resistance of the optimal MFC was low enough and there was not much improvement when the the electrode spacing was further reduced (Liu et al., 2005a). Instead, decreasing the electrode space to 0.5 cm was unfavorable to the water flow and increased the settlement of the suspended solids and biomass inside the MFCs and the probability of clogging. This accumulation of the suspended solids and biomass increased the internal resistance and had a negative influence on bacterial activity (Rabaey et al., 2003).

4.2.1.7 Effect of the different flow condition

Long-term stability is one important factor that needs to be considered for a biosensor. Fig. 4.8 shows values of the maximum power achieved through polarization curves over 8-month period of operation following an acclimation period of approximately 1 month. Different flow conditions were compared: non-serpentine flow in the MESs without channels and serpentine flow in the MESs with channels. Both of them exhibited very good stability over an operational period of 2 months. Subsequently, the performance of the MFCs without channels started to decrease gradually, whereas constant power generation from wastewater was obtained with the MESs with channels over a period of 8 months. The P_{max} in the MESs with channels kept stable at 0.33 mW and the total variation during the full period of operation was only 10%. The average power density (79.71 ± 7.4 mW/m^2) was comparable to other studies such as that by Min and Logan (2004) at 72 ± 1 mW/m^2 using the same MFC design fed by domestic wastewater.

Suspended solids and biomass were found to be seriously accumulated inside the MFCs without channels after 2 months of operation, which stopped the effective contact between the biofilm and the substrate, affecting the activity. The disadvantage of the circular MESs without channels has been shown in the literature, whereby a dead zone usually happened (Mench et al., 2001) and the maximum suspedned soilds and biomass accumulation often occurred near the single inlet and corners of the MFCs (dead zones) (Pea et al., 2000). The advantage of the serpentine flow path is that any obstruction in the path, such as a water droplet, will not block all activity downstream of the obstruction and ensure minimal loss of active area (Mench et al., 2001).

Although white deposit was observed on the cathode side of both the two different type of MES after 2 months of operation, the system performance was only affected marginally, which is also reported by Di Lorenzo et al. (2009b).

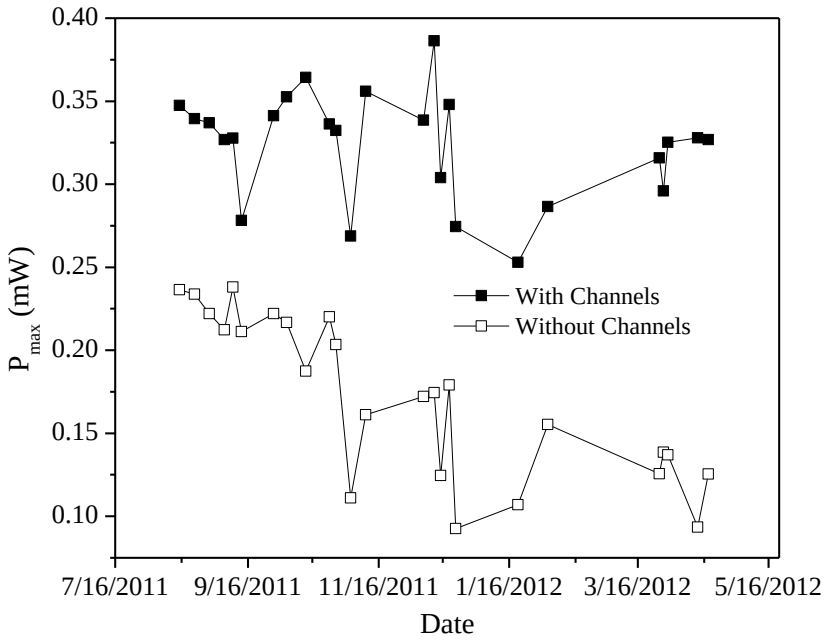

Figure 4.8**.** Comparison of the long-term stability of two different flow conditions: non- serpentine flow in the MFCs without channels and serpentine flow in the MESs with channels. $\boldsymbol{P_{max}}$ obtained by polarization curves during the 8 months of operation following an acclimation period of approximately 1 month. Data are the average from the twoMESs.

4.2.1.8 Comparison of the MES and MEC-MES

One group of optimal MES was switched from MFC mode to MEC mode (denoted hereafter as MEC-MES) by connecting the anode and cathode to the potentiostat at an applied voltage of 0.6 V. It took 2 h for the current of the MEC-MES to stabilize at 1.1 mA after operation and it was kept stable for the next 16 h as the control MES group did (Fig. 4.9).

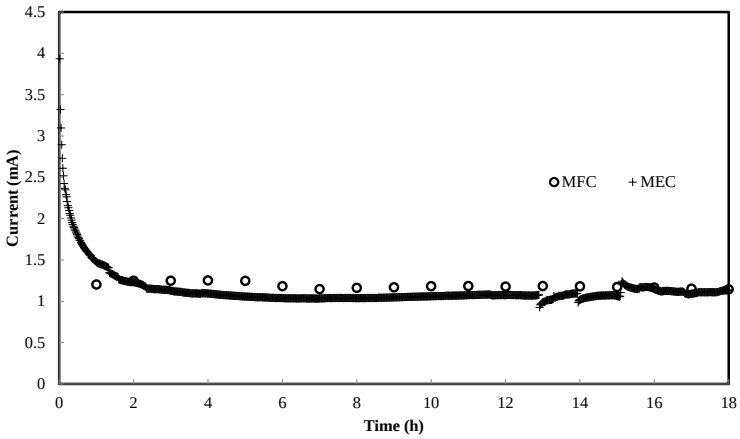

Figure 4.9. The baseline current evolution of the MES (○) and MEC-MES (＋), at time 0 the MES was switched from MFC to MEC mode, and current was recorded per min.

When injected with 10 ppm of Ni(II), the current of the MEC-MES started to decrease and the response behavior was quite similar with that of the MFC-based MES (Fig. 4.10). It showed that the key component of the MFC-based MES that was impacted by the toxicity present in the feed wastewater was the biofilm.

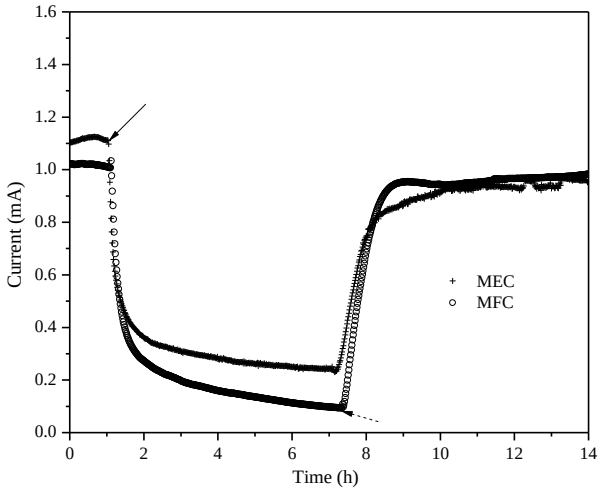

Figure 4.10. Current evolution of the MFC-based MES (○) and MEC-MES (＋) during and following an toxic event of 10 ppm of Ni(II). Arrows indicated the start (↙) and stop (↖) of the toxicity injection.

4.2.2 Optimization of the anodic biofilm characteristics

4.2.2.1 Response of MESs enriched under different shear rates to Cu(II) toxicity

After steady state was achieved, toxic incidents were created by spiking Cu(II) either at 5 or 7 ppm to the wastewater. An immediate decrease in voltage was observed after exposure to Cu(II) (Fig. 4.11). The inhibition ratios of the MESs by Cu(II) at 5 and 7 ppm under enrichment flow rate of 12 and 24 mL min^{-1} were similarly low, with inhibition extended beyond 2 h of Cu(II) exposure. Inhibition ratios at 5 ppm of Cu(II) after 4 h were around 30% for both 12 and 24 mL min^{-1}, and around 50 and 60% at 7 ppm of Cu(II) for 12 and 24 mL min^{-1}, respectively. However, the degree of inhibition was inversely proportional to the shear rate, and the highest inhibition to the toxic event was observed at a flow rate of 1.3 mL min^{-1}, which after 2 h of Cu(II) exposure led to a 60% inhibition ratio at 5 ppm of Cu(II) and 85% inhibition ratio at 7 ppm of Cu(II) after 4 h. Intermittent nitrogen sparging increased the extent of inhibition after 2 h of Cu(II) exposure from 30 to 40% at 5 ppm of Cu(II) and from 40 to 85% at 7 ppm of Cu(II), showing a stronger effect at higher Cu(II) concentration.

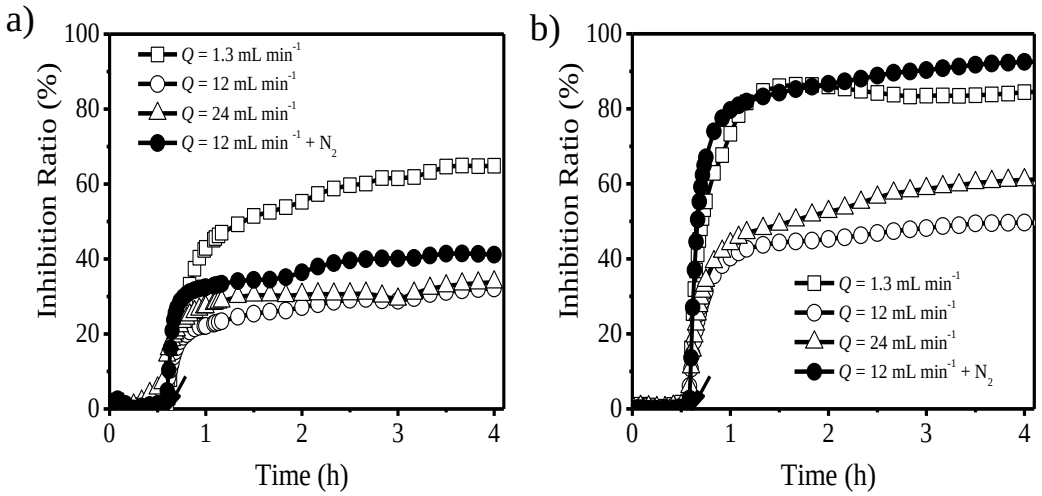

Figure 4.11. Inhibition ratio of MESs enriched under different flow rates (Q) exposed to Cu(II) at a concentration of (a) 5 ppm; and (b) 7 ppm. The arrow indicates the beginning of the toxic event.

The result showed that an MES had been successfully developed as a toxicity biomonitoring system, giving a quick response to a Cu(II) toxic event. The fast drop of the performance of the MES may appear contradictory to the findings of Patil et al. (2010), in which no effect on the biofilm of the MFC was observed even at 6 ppm of Cu (II). This apparent contradiction, however, proved from the findings in this study that the biofilm was a key factor determining the sensitivity of the MFC to toxicity, and the shear rate could be an effective enhancement parameter.

4.2.2.2 Effect of the shear rate on the biofilm structure

The operating conditions applied to each set of the MESs and their effect on the biofilm characteristics are summarized in Table 4.2.

Table 4.2 Volatile suspended solids (VSS), thickness, density and EPS content (protein and carbohydrate) of the anodic biofilm of a MES enriched under different shear rates.

Flow Rate (mL/ min)	**Nitrogen sparging**	**VSS (mg/cm^2 of electrode)**	**Thickness (μm)**	**Density (g VSS/L of biofilm)**	**Protein content (mg/g of VSS)**	**Carbohydrate content (mg/g of VSS)**
1.3	No	3.67 ±0.31	295.5 ±0.7	124	2.37 ±0.48	1.70 ±0.16
12	No	3.43 ±0.54	202.5 ±2.1	170	6.19 ±3.12	2.87 ±0.63
24	No	3.83 ±0.59	101 ±5.6	380	6.48 ±1.87	2.66 ±0.55
12	Yes	3.79 ±0.11	200 ±15.5	190	2.35 ±0.31	1.37 ±0.03

The VSS averaged 3.68 mg VSS cm^{-2} of electrode at all flow rates, showing insignificant effect of the shear rate; nevertheless, the biofilm thickness was impacted. At a flow rate of 1.3 mL min^{-1} (low shear stress), the thickness of the biofilm was about 300 μm. When the flow was increased to 12 mL min^{-1}, the thickness further decreased to about 200 μm (33% reduction) and finally dropped to about 100 μm (67%

reduction) under the highest flow rate of 24 mL min^{-1}. As a result, the biofilm density increased with flow rate up to 380 g VSS L^{-1} of biofilm at the highest flow rate of 24 mL min^{-1}, indicating that high shear rates resulted in stronger aggregation and a denser biofilm. Denser colonization of the anode under higher shear rate was further confirmed by the SEM analysis (Fig. 4.12). The electrode surface enriched under high shear rate was covered much more densely with bacterial cells and appeared less porous in contrast with that enriched under low shear rate. Intermittent nitrogen sparging on the other hand did not significantly affect the biofim thickness or density (Table 4.2).

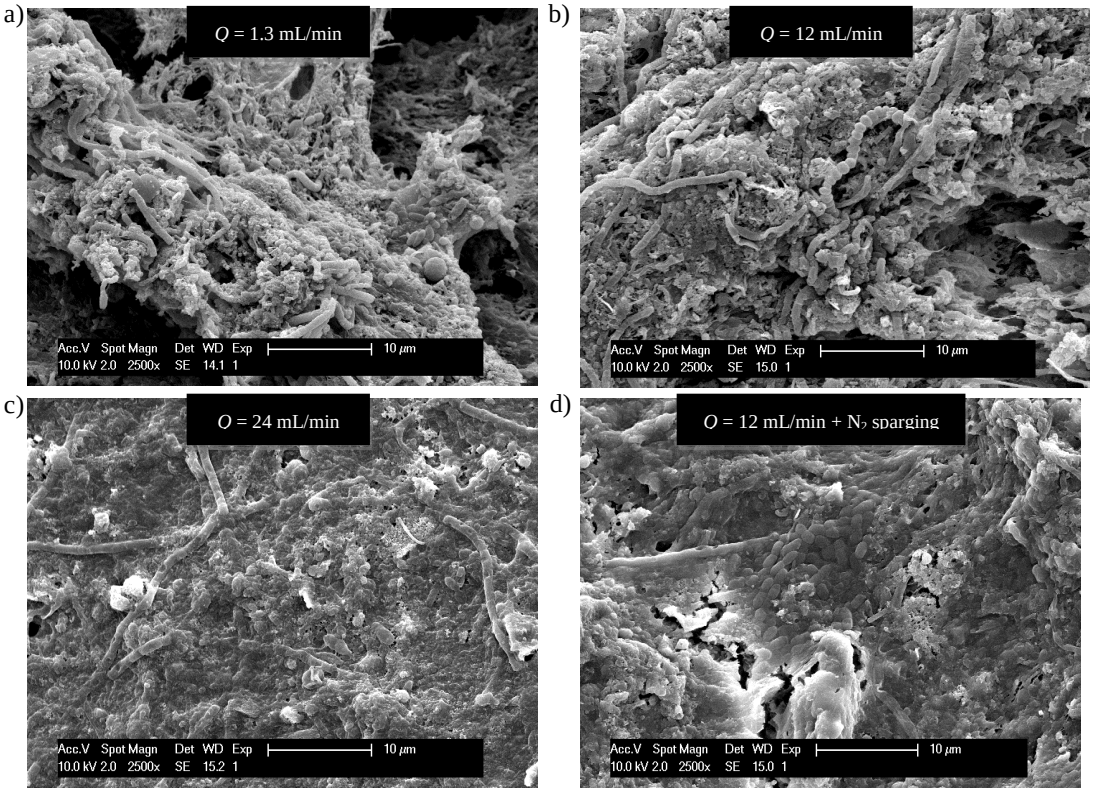

Figure 4.12. Scanning electron micrographs (×2500) of the anodic biofilm of MESs enriched under different flow rates (Q).

Our results supported the hypothesis that increasing flow rate resulted in increasing shear rate that modified the biofilm characteristics, making the developed biofilm denser and more compact with reduced porosity (i.e., less porous). The thickness of

the biofilm also decreased up to 65% with increasing flow rate. This observation is in good agreement with the works of Kwok et al. (1998) and Celmer et al. (2008), but contradicted with the conclusions of Pham et al. (2008) and Rochex et al. (2008). The latter two studies showed that the biofilm thickness increases with shear stress due to increased mass transfer and biomass production. However, the increased shear rates in our study caused the detachment of the top layer of the biofilm, which has also been shown by Coufort et al. (2007) whereby about 60% of the biofilm mass was fragile and easily detached. In our study, nitrogen sparging did not further impact on the biofilm structure, probably because its intermittent nature (twice a week) made it insignificant as compared to the effect of the flow rate.

The relationship between the modified biofilm structure and the improved sensitivity of the electrochemically active biofilm enriched under low shear rates can be explained by the one-dimensional mass transport model used by Hu et al. (2007), which describes the spatial distribution of Cu(II) in biofilms. According to this model, the retardation factor (R_f) for diffusive transport of Cu(II) can be described as $R_f = 1 + (D/\Phi) \times K_d$, where D is the density (g L^{-1}), Φ is the porosity and K_d is the metal-biomass partition coefficient. Therefore, low cell density along with the increased porosity observed under low shear rates are expected to increase the diffusivity of Cu(II) in the biofilm and hence, enhance the toxic effect, which explains the results observed in this study.

Another interesting finding from the present study is that the thick biofilm obtained under low shear rates did not hinder the mass transfer of Cu(II). In some cases such as the study conducted by Hu et al. (2007), Cu(II) could only penetrate the first 150 μm

of the biofilm instead of the whole thickness of the biofilm after exposure for 2 h at a concentration of 0.2 mM. However, in our study, with the fact that EAB only persist up to tens of micrometers away from the anode and inhabit the inner layer of the biofilm (Marcus et al. 2007), the highest inhibition observed with the MFCs operated under the lowest flow rate (Fig. 4.11) that had the highest biofilm thickness of nearly 300 μm, suggesting that Cu(II) penetrated much deeper into the biofilm in our study. And it can be concluded that biofilm density and porosity have a stronger impact on the MES sensitivity than its actual thickness.

4.2.2.3 Effect of the shear rate on the EPS content of the biofilm

High shear rates led to over production of EPS (Table 4.2). When the flow rate was increased from 1.3 to 12 mL min^{-1}, the protein and the carbohydrate content of the biofilm increased from 2.37 to 6.19 mg g^{-1} of VSS (161% increase) and from 1.70 to 2.87 mg g^{-1} of VSS (69% increase), respectively. However, increasing the flow rate to 24 mL min^{-1} did not further affect the EPS content. Scattered nitrogen sparging, on the other hand, significantly decreased the protein and the carbohydrate content from 6.19 to 2.35 mg g^{-1} of VSS (62% reduction) and from 2.87 to 1.37 mg g^{-1} of VSS (52% reduction), respectively.

Our results suggested that high flow rates - hence high shear rates - led to EPS overproduction (Table 4.2) which resulted in a loss of sensitivity of the MFC sensor. Stoodley et al. (2002) explained that the overproduction of EPS under high shear rates aimed at protecting the biofilm from the physical environment. However, intermittent nitrogen sparging produced the opposite effect as it significantly decreased the EPS production by 50 to 60%. In addition, intermittent decrease or increase of the shear

rate might be beneficial to reduce the EPS content and a probable mechanism is the breakdown of the EPS matrix and simultaneous release of EPS into the bulk liquid as explained by Henriques and Love (2007). Reduced levels of EPS were associated with improved sensitivity of the MFC sensor and this can be related to the nature of the polysaccharides and proteins that constituted the EPS, and which functional groups (e.g., carboxylic acids and amino acids) can bind positively-charged metal ions (Fang et al., 2002). Hence, reduced EPS content improved the sensitivity of the MES under low shear rates and scattered nitrogen sparging.

4.2.3 Summary

An optimal MES was developed in this study that allows the fast monitoring of the acidic toxicity and heavy metals present in wastewater by recording the current generated by the MFCs. The MES was targeted at high and stable baseline, fast response to the toxic event and good recovery ability by optimization of both the cell design and biofilm characteristics.

The results showed that the MESs with separate anode and cathode configuration and made water-proof by way of a Selemion proton exchange membrane (Type C) served as an ideal toxicity sensor. Serpentine flow was found to reduce suspended solids or biomass accumulation inside the MESs. In addition, low external resistance was recommended to be applied to the MESs to generate a looser electroactive biofilm with more void spaces on the anode surface, which would facilitate mass transport and increase the MES sensitivity to toxicants. When the HRT was decreased from 22

to 3.5 min, the sensitivity further increased substantially due to the increase of the rate of mass transport.

It has been shown in this study that the biofilm is the key to the biosensor and biofilm density, porosity and EPS content of the biofilm affect the sensitivity of MES to heavy metals. Flow rate and nitrogen sparging swere found to be two operational parameters that can be easily used to control the characteristics of the biofilm developed on the anode of MESs. It can be concluded that to enhance the sensitivity of MES as a toxicity sensor for heavy metals, MES should be operated under low flow rate and intermittent nitrogen sparging.

CHAPTER 5 Application of the MES

5.1 Introduction

In general, biological treatment activity can only be maintained stable within certain range of variation of the typical composition of the wastewater such as COD, pH, temperature and inorganic ions. Extreme changes of those characteristics sometimes would cause severe treatment upset and shall be considered as a toxic event. For example, chemical wastes like acid mine drainage can alter the pH of the wastewater as low as 2.4 (Carnicero et al., 2009), severely affecting the biomass activity.

Besides of the extreme condition of typical wastewater compositions, a wide variety of toxicants which could lead to the upset of the ASP. Heavy metals such as Zn(II), Ni(II), Cu(II), Cd(II) and Pb(II) are often found to reach quite high levels in the industrial effluents such battery manufacturing, coil coating, copper forming, electrical and electronic components manufacturing, electroplating, iron and steel factory (Çeçen et al., 2010). In some cases, industrial effluents are discharged into centralized wastewater treatment plant without pretreatment, which could affect the activity and viability of activated sludge, impeding the performance of the biological treatment process (Halling-Sørensen, 2001; Lin et al., 2003). Cyanide, widely used in industrial applications such as electroplating and mining process, is a deadly poison which also needs serious monitoring (Registry July 2006; Nakanishi et al., 1996). Organic chemicals are also another important cause for the disturbance of wastewater treatment process, broadly used in industries, e.g., paper manufacturing, chemical

processing, and domestic products such as detergents and insecticides (Ren and Frymier 2002).

These effects can be avoided if protective actions are taken in advance by developing an upstream toxicity sensor which should be stable, quick response, simple to operate and on-line. More importantly, the information should be relevant to the ASP performance (Ren, 2001). The application of the MES in monitoring the above toxicants is discussed in this Chapter.

For the application of MES, it is important to differentiate the sensor response due to the normal fluctuation of the typical components of the wastewater or the toxic event to avoid false alarm. The performance of MES is usually affected by many operating conditions imposed on the MES, such as wastewater strength (Min and Logan, 2004; Liu et al., 2004), substrate loading rate (Reddy et al., 2010; Mohan et al., 2007), ionic strength (Liu et al., 2005a) and pH (Gil et al., 2003). Therefore, in the first part, the MES stability and its response to normal and extreme change of common wastewater characteristics were studied.

After the study on the stability, we qualitatively and quantitatively analyzed the MES characteristics during their application in the toxicity screening influent wastewater. Toxic compounds that were tested included individual heavy metals, binary mixtures of heavy metals, cyanide and organic chemicals that represented two different chemical structures - halogen substituted alkanes and aromatics. Regression was used to fit the current versus time data and dose-response curve to achieve a better understanding of the response behavior. The MES's characteristics of stability, IC_{50}, sensitivity and detection limit were discussed, and their relativity with the toxicants

effect to the ASP was investigated. To investigate the MES's selectivity, one MES was continuously inoculated with wastewater containing Ni(II).

5.2 Results and discussion

5.2.1 MES baseline stability

The wastewater characteristics and typical ionic composition of the influent wastewater were measured weekly basis and the results are summarized in Table 5.1.

Table 5.1 Characteristics and Ionic Composition of the wastewater utilized.

Component	Concentration	Component	Concentration
COD (ppm)	346.0 ±77.0	F^- (ppm)	0.18 ±0.08
SCOD (ppm)	114.2 ±60.4	Cl^- (ppm)	98.1 ±64
TSS (ppm)	227.3 ±108.0	Br^- (ppm)	0.06 ±0.06
TDS (ppm)	114.2 ±60.4	NO_3^- (ppm)	2.15 ±2.15
VSS (ppm)	185.3 ±80.0	PO_4^{3-} (ppm)	6.58 ±3.38
pH	7.37 ±0.24	SO_4^{2-} (ppm)	62.72 ±12.38
Conductivity (mS/cm)	0.852 ±0.093	Na^+ (ppm)	45.75 ±28.75
		NH_4^+ (ppm)	22.96 ±11.14
Temperature (^oC)	24.55 ±1.45	K^+ (ppm)	8.94 ±3.54
		Mg^{2+} (ppm)	2.14 ±1.14
		Ca^{2+} (ppm)	15.04 ±3.54

The stability of the baseline current of the MESs fed with real domestic wastewater was examined by operating MESs under two different feeding procedures (Fig. 5.1): batch feeding (48 h) and continuous feeding (continuous supply of domestic

wastewater). In the continuous feeding where the wastewater characteristics was relatively constant, the current generation was found to be stable with only 8.3% fluctuation of the current (Fig. 5.1). Although only 26 h of data were shown in Fig. 5.1, it reflected the long-term operational performance of the MESs. During the long-term operation of the MESs, the normal fluctuation of the water parameters, as shown in Table 5.1, usually affected marginally on the current generation of the MESs and the fluctuation was smaller than 10%, showing good stability of the MESs continuously fed with domestic wastewater which characteristics was relatively constant.

In the batch feeding tests where the COD was decreased from 320 to 250 ppm after 12 h, and was further dropped to 130 ppm after 24 h (Fig. 5.1), the current of the MESs was maintained stable at 1.2 mA during the first 10 h and started to decrease gradually with the decrease of COD till 0.45 mA. The replacement of the fresh wastewater with high COD at 300 mg/L led to the recovery of the current generation immediately.

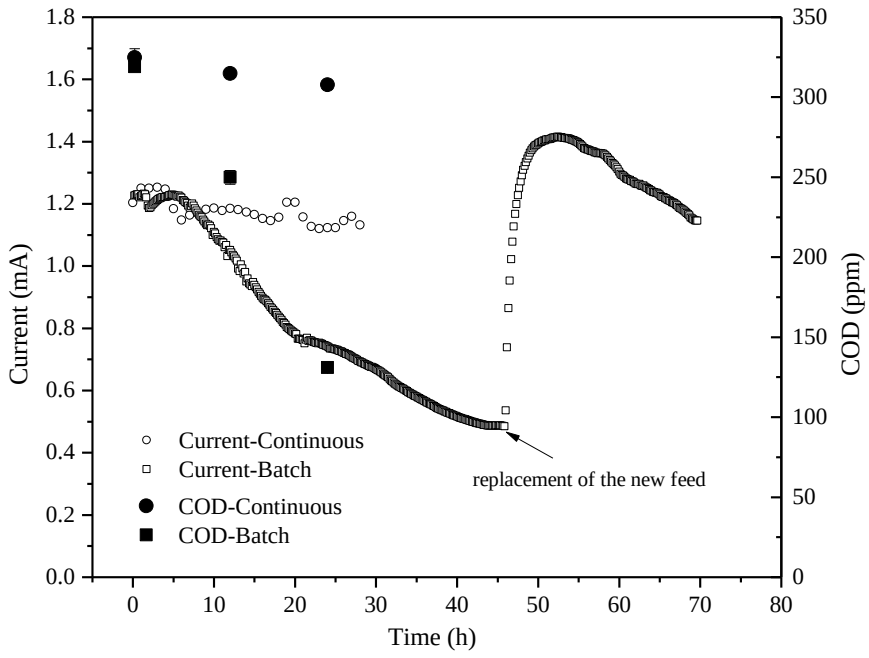

Figure 5.1. Evolution of the cell current (open symbol) and COD (closed symbol) during operation of the MFCs in batch mode (□) and in continuous mode (○).

The detailed impact of the normal fluctuation and extreme variation of common wastewater characteristics (i.e., COD, pH, ionic strength and nitrate) on the current generation of the MESs will be discussed in the following sub-sections.

5.2.1.1 Current generation as a function of wastewater strength

To further determine the relation of the current generation of the MESs with the concentration of organic matter in the wastewater, the cells were continuously fed at a targeted COD for 6 h each, decrease stepwise from 360 to 180 ppm and increase to 360 ppm again as shown in Fig. 5.2. The targeted COD was obtained by diluting the original wastewater (COD of 360 ppm) with deionized water. Fig. 5.2a shows the dynamic response of the generated current under different COD concentration. The response profile of the current generation to the change of the COD was different from that to the toxicant as shown in Chapter 1, which had a sharp drop within 1 h. When a new COD was fed into the MESs, the current generation will be changed much more gently than due to the toxicant effect, and after that, the MES gave reasonably constant values of current response when the input COD was similar. For example, when the MESs were fed with a feed wastewater having 360 ppm COD, the current output was 1.18 mA with a standard deviation of 0.09 mA. With 180 ppm of COD, the current output was 0.79 mA with a standard deviation of 0.02 mA. This made it possible to differentiate whether the current drop was due to COD change or toxicant effect. Fig. 5.2 shows the variation in current with COD concentration. A saturation-type trend was shown as a function of the wastewater strength. The current generation was limited by other factors instead of substrate concentration at COD concentrations higher than 280 ppm. As discussed elsewhere (Gil et al., 2003), those

factors include electron transfer from the bacteria to the anode, proton permeability across the membrane, and chemical reaction in the cathode compartment. A linear response was obtained with the COD ranging from 180 to 280 ppm (r^2 = 0.999). For COD ranging from 280 to 360 ppm, the generated current of the MESs was kept stable.

The targeted COD of the wastewater could reach higher than the highest COD presence in original watsewtaer as shown in Table 5.1. To achieve these high COD concentration (ranging from 400 to 1200 ppm) in the feed wastwater, sodium acetate was added into the original wastewater (Fig. 5.2c). The current generated by the MECs started to increase once the COD was increased and it stabilized after about 2 h. It seemed contradictory with the conclusion above which the current stabilized once the COD reached 280 ppm and above. The most probable reason was that acetate is a preferred aqueous substrate for electricity generation in MFCs or MESs and the power generation was usually larger with acetate than domestic wastewater (Min and Logan 2004, Liu et al. 2005b). The saturation-type trend was shown again as a function of the wastewater strength showing that the current would keep stable once the COD reached some value (Fig. 5.2d).

It was concluded that during the normal variation of the COD values of 346.0±77.0 ppm, the current of the MFCs kept stable since the substrate concentration was no longer a limiting factor. Even though the COD range varied too far, it's possible to differentiate the response with the toxicant effect to prevent the false alarm.

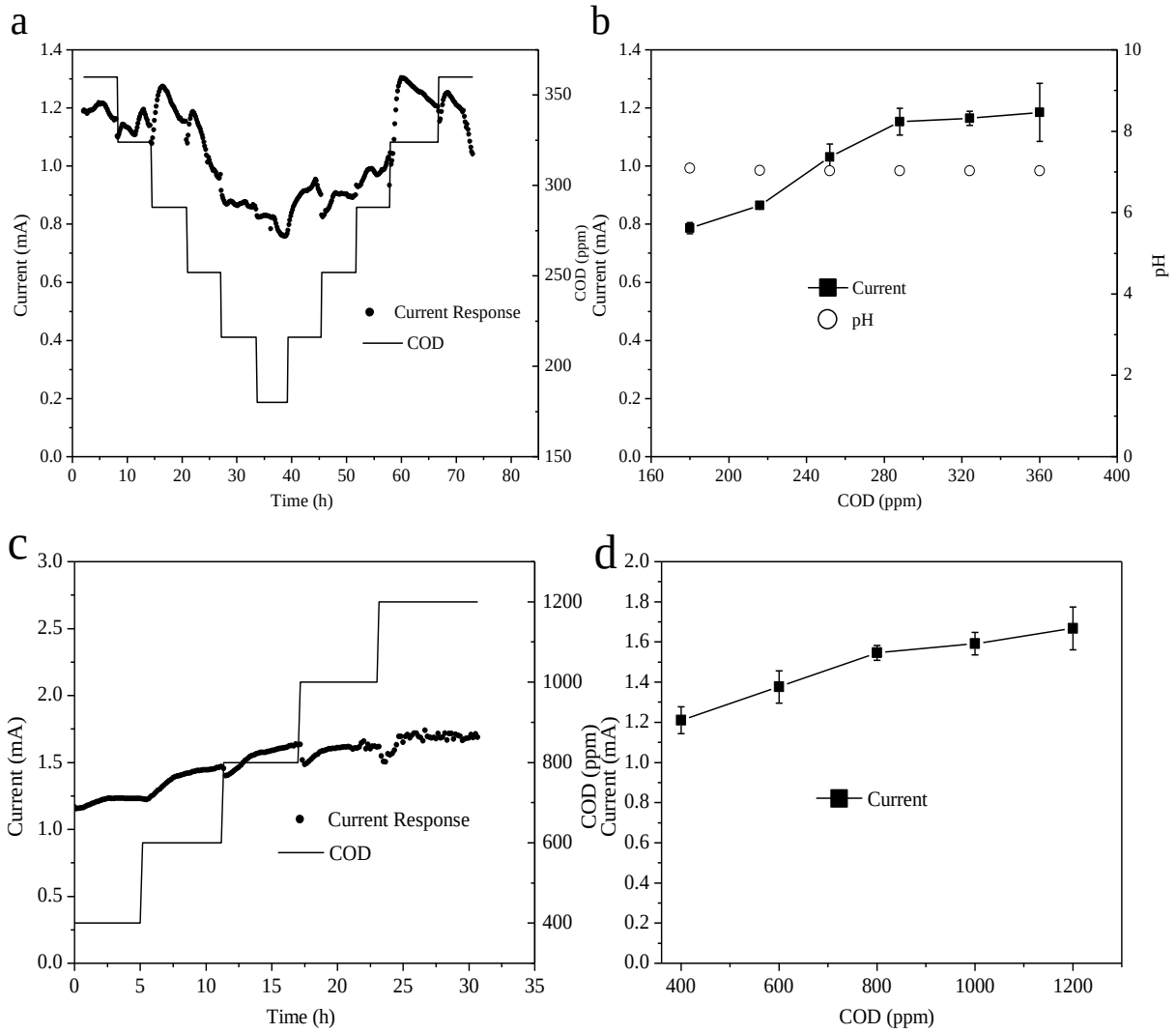

Figure 5.2 Current response to COD concentration. Current profile with different COD concentrations. (a) MESs were fed with different concentrations of COD (by diluting the original wastewater) for 6 h each. The line (—) represented the COD in the feed. (b) Average current (■) in relation to the feed COD. (c) MESs were fed with different concentrations of COD (by adding sodium acetate into the original wastewater) for 6 h each. The line (—) represented the COD in the feed. (d) Average current (■) in relation to the feed COD. Data are the average from two MESs.

It is possible that diluting the wastewater with deionized water, which has a lower conductivity, or adding the sodium acetate would change the conductivity of the feed and thus altered the power generation (Min and Logan, 2004). However, as shown in the next paragraph, the changes in conductivity did not affect power generation in our system. pH was also stable during the operation as shown in Fig. 5.2b. Therefore the change of the current is only due to the variation of the COD of the wastewater.

To confirm that the drop of the current with the existence of toxicant was not due to the decrease of COD, four batch experiments (lasting for 6 h) were conducted and the COD in the culture vessel were measured with time (Fig. 5.3). In the control MESs, wastewater in the culture vessel was not fed into the MESs, while in the other three, the wastewater was fed into the MESs and the effluent were recirculated back to the vessel. Among those three experiments with wastewater feed, one experiment was conducted with no toxicants dosing which served as a control, while for the other two experiments, one was fed with 10 ppm of Cd(II) and the other fed with 10 ppm of Ni(II).

It could be seen that both the total COD and sCOD were unchanged during the 6 h of toxicant exposure in all the cases. It thus suggested that the drop of the current was only attributed to the toxicants and not the COD. Besides, the exposure to the Ni(II) did not affect the COD as well.

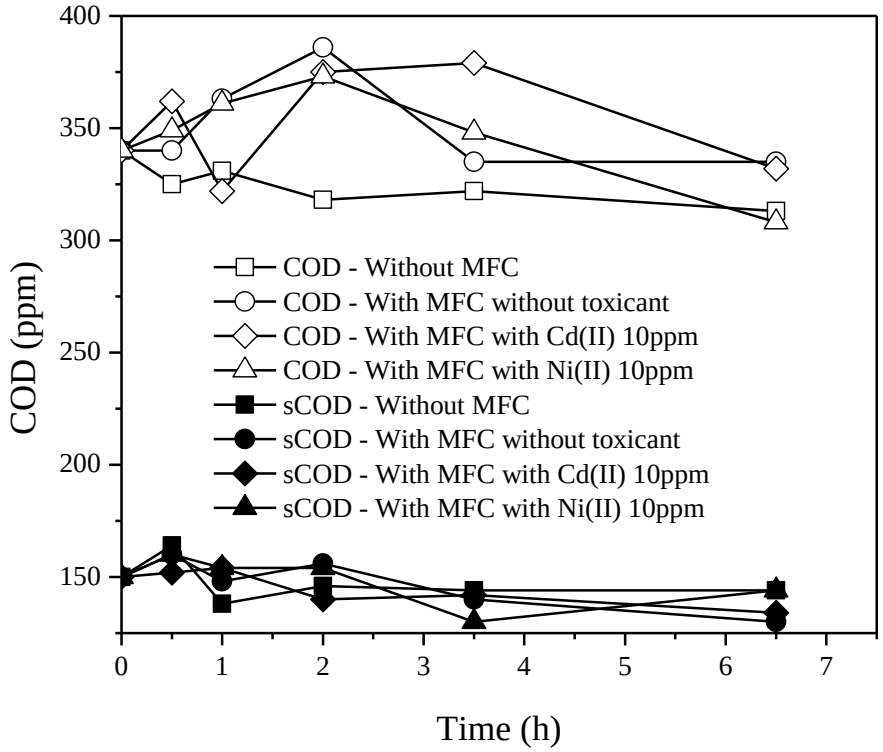

Figure 5.3. Change of total COD (open symbol) and sCOD (closed symbol) in four culture vessels with time. One set of MESs was without feeding (Control, □), one set of MESs was with their effluents recirculated back to the vessel without toxicant dosing（○）, one set of MESs was with their effluents recirculated back to the vessel with 10 ppm Ni(II) dosed at 0^{th} h（◇ and one set of MESs was with their effluents recirculated back to the vessel with 10 ppm Cd(II) dosed at 0^{th} h（△）. The batch tests lasted for 6 h.

5.2.1.2 The effect of ionic strength of the wastewater

NaCl was added into the MESs to yield different conductivity of the wastewater ranging from control to 30 mS/cm (35 times higher than that of the normal wastewater range) to investigate the sensor response to extreme ionic strength. Conductivity instead of ionic strength was used here since the measurement of conductivity is generally a rapid way of determining the ionic strength. Fig. 5.4 shows the current response profile of the MESs within 10 h of exposure to wastewater of different conductivities. No obvious difference was observed between wastewater with different conductivity and control, showing that the MES has strong tolerance to the

change of high ionic strength. This is consistent with the research done by Liu et al. (2005a), in which the power generation ability was not decreased by the high dosing of NaCl at 300 mM. Instead, in their cases, the power output was increased when the dosed NaCl was raised from 100 to 300 mM due to the decrease of the ohmic resistance by increasing the solution conductivity. And when the ohmic resistance is small enough and the further decrease of the ohmic resistance is neglectable, the increase of the current stopped. However, in Fitzgerald et al. (2012) the increase of the current with increasing concentration of $CaCl_2$ (up to 1.4 mM) is due to biological aggregation instead of the ionic effects.

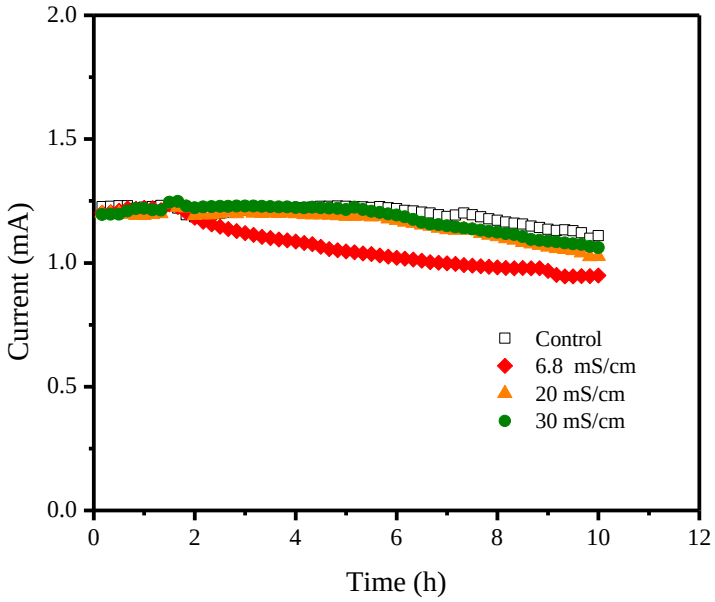

Figure 5.4. Chart of current output of MESs vs. time fed by wastewater of different ionic strength at 6.8 (◆), 20 (▲) and 30 mS/cm (●) controlled by adding 60, 190, and 320 mM NaCl, respectively. The feed started at time 0 and lasted for 10 h. Normal wastewater without NaCl addition was used as a control (□).

A comparison of polarization curves from MESs fed with wastewater of different conductivities (Fig. 5.5) were made and it was found that the polarization behavior was consistent and no significant differences were observed in both the internal resistance as represented by the slope and the maximum power. This trend indicates that the general performance of the MES in our study was not affected by the addition

of NaCl due to the fact that the ohmic resistance was low enough and there was no further decrease potential.

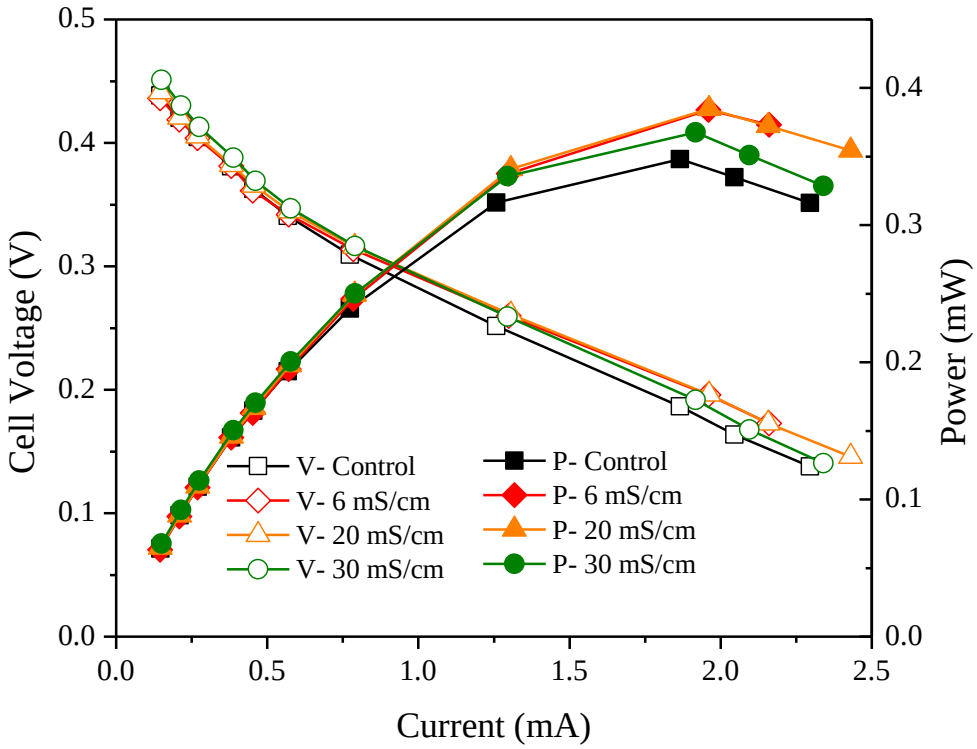

Figure 5.5. Power (closed symbol) and cell voltage (open symbol) vs. current for MESs with wastewater of different ionic strength 6.8 mS/cm (◆), 20 mS/cm (▲) and 30 mS/cm (●) controlled by adding 60, 190, and 320 mM NaCl, respectively. Normal wastewater without NaCl addition was used as a control (■).

5.2.1.3 Nitrate effect

The effect of extreme nitrate concentration on the current generation of the MES was investigated (Fig. 5.6). Fig. 5.6 a shows the current response profile to different nitrate concentrations (ranging from 0 to 0.8 mM nitrate). The current was not affected once the dosed nitrate concentration was lesser than 0.32 mM, which was 10 fold higher than the normal nitrate range encountered in typical domestic wastewater (0.035±0.035 mM) as shown in Table 5.1. With 0.4 mM nitrate in the feed wastewater, the current dropped gradually during the first 3 h of exposure and then started to increase slowly in the next 3 h of exposure. While for both cases with

nitrate concentration of 0.48 and 0.8 mM, continuous decrease of the generated current were observed during the first 3 h of exposure time and the current were maintained stable at the minimum value during the next 3 h of exposure instead of increasing. In general, current produced by MESs was lower when exposed to higher nitrate concentration. Once the nitrate ceased to be fed into the MESs, gradual increase in current generation was observed for all cases; however, the higher the nitrate concentration, the longer the time it took for the full recovery. For example, it only took 1 h for the current production being inhibited by 0.4 mM of nitrate to recover to its baseline value, while it took 3 h for the one with 0.4 mM and 12 h for the one with 0.8 mM.

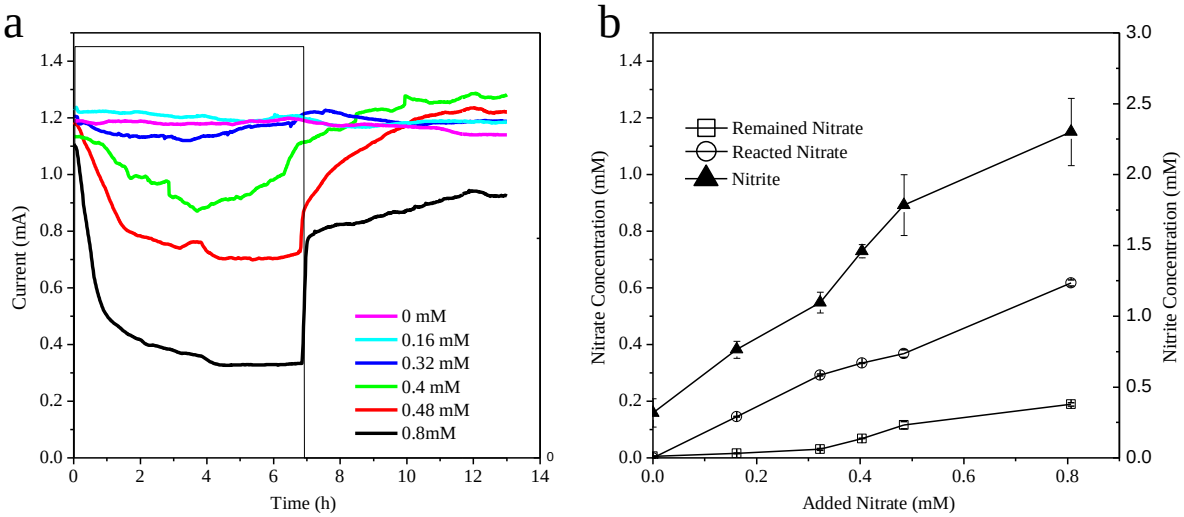

Figure 5.6 (a) The current generation by MESs fed with wastewater containing different nitrate concentration (0, 0.16, 0.32, 0.4, 0.48 and 0.8 mM) (b). Remained Nitrate (□), reacted Nitrate (○) and Nitrite (▲) in the effluent.

The nitrate and nitrite concentration in the effluent were measured and the results are shown in Fig. 5.6b. It could be seen that the nitrate in the effluent was much lower than the dosed concentration while the nitrite concentration was increased, showing that the conversion of nitrate to nitrite happened in the MESs, which consumed the electrical current. It has been shown in the literature that the electroactive bacteria on the anode could switch from using the anode as the electron acceptor to using the

nitrate as the chemical terminal electron acceptor due to its higher redox potential (Morris and Jin, 2009; Gregory et al., 2004). Chang et al. (2005) had also proven that the current generation from MFCs decreased in the presence of electron acceptors of higher redox potential such as nitrate and oxygen.

It was interesting to find that the remained nitrate (i.e., present in the effluent) was close to 0 for dosed nitrate concentration lesser than 0.32 mM where no inhibition of the current was seen. While for dosed nitrate concentration of 0.4 mM, the remained nitrate was also very low (0.05 mM) and almost the entire nitrate was consumed. This information may give us an idea why the current response was different as described above for different concentrations. There might be two groups of bacteria existed on the anode and both of them could utilize the anode as electron acceptor yet showed different electron pathways in response to the presence of nitrate (Sukkasem et al., 2008). One group still used the anode as the electron acceptor while the other group would switch to use nitrate as electron acceptor. Thus the current generation was still possible with high concentration of nitrate present in the solution since the first group of bacteria transferred electrons to the circuit but current generation would be lower. When the nitrate was consumed, the second group of bacteria would switch back to transfer electrons to the circuit, recovering the current generation. This explained why the current decreased at first and started to increase during the 0.4 mM nitrate exposure.

Morris and Jin (2009) had also proposed another possibility that it was due to the aggravated depletion of dissolved organic content (DOC) in the MFCs by the growth of denitrifying bacteria that utilized nitrate as an electron acceptor. But it could not be

the case in our study since the current drop was immediate and the short term exposure did not allow the enrichment of the denitrifying bacteria.

5.2.1.4 pH effect

pH is crucial to both the activated sludge activity and the anodic microbial activities in the MESs. The pH of the toxic event was allowed to vary between 3 and 11. No effect was seen on the current generation of the MESs during the change of pH from 7 to 10, showing that the normal fluctuation of the pH (7.37 ± 0.24) (Table 5.1) in the wastewater would not lead to the fluctuation of the current generation by the MESs. This result is consistent with Gil et al. (2003), who showed that the same highest current was observed between pH 7 and 8, and with He et al. (2008), who concluded that the peak current was relatively stable between pH 8 and 10. The possible reason for the current of MESs to keep constant during high alkaline pH, which is harmful to the ASP, is that the anodic bacterial activities might be inhibited by pH (8–10) to some extent, but cathodic reaction was also improved at the same time, and thus the overall performance was maintaned unchanged (He et al., 2008) .

Acidic pH was found to have a severe effect on the current production of the MESs as shown by the current response profile in Fig. 5.7a. The injection of the acidic toxicity would lead to a fast drop of the current generation immediately. The current dropped drastically during the first 4 h and then slowed down subsequently. The decrease continued as long as the MESs were exposed to the acidic pH except for pH of 6. During the 10-h exposure to pH of 3 to 5, no stabilized minimum current were observed, which showed different response of the MESs to the extreme nitrate case, which the current stabilized at minimum values after 4 h of exposure (Fig. 5.6). The

extent of inhibition observed was found to be correlated to different acidic pH, and the inhibition after 10 h of exposure were 88, 75, 55 and 35% for pH 3, 4, 5 and 6, respectively, showing the existence of dose-response relation. It took 4 h for the MES to recover to the baseline current, longer than the nitrate cases. However, for the pH 3 case, the current could not recover to the baseline even after 14 h. It is likely that the activity of the bacteria was only temporarily inhibited when they were exposed to pH of 4 to 6, while some bacteria might be killed by the very low pH of 3, instead of temporary inhibition.

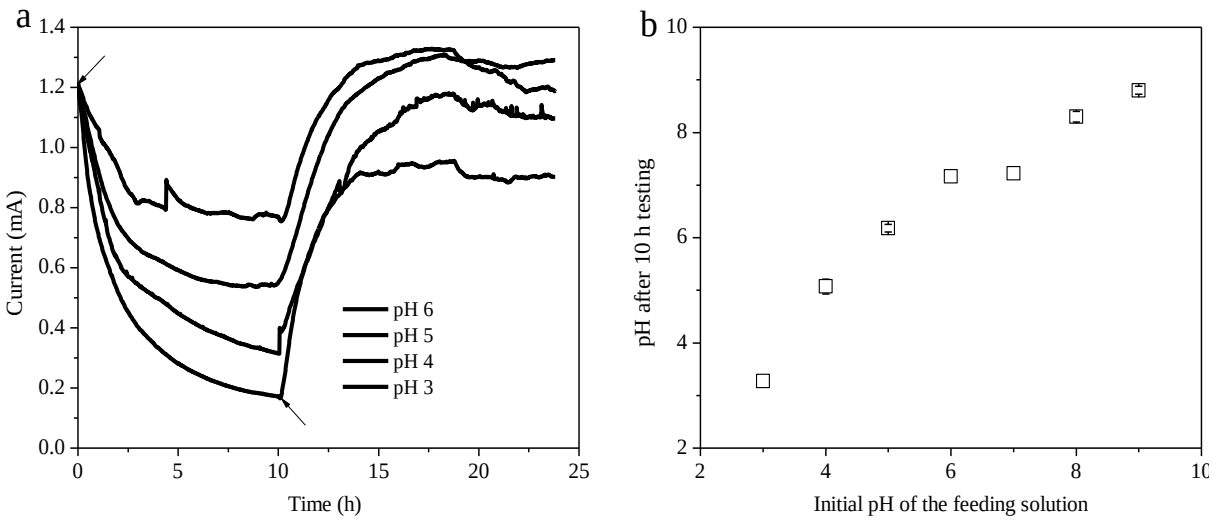

Figure 5.7. a) Current evolution during (0–10 h) and following (10-24 h) an acidic toxic event of pH varying between 3 and 6. Arrows indicate the start (↙) and the end (↖) of the toxic event. b) The pH of the feed wastewater after 10 h of testing is presented as a function of the intial feed solution pH. Error bars represent standard deviation from duplicate experiments.

Fig. 5.7b showed that the pH was increased after 10 h of reaction when the intial pH of the feed wastewater was lower than 6, while no change of the pH was observed when the pH values were 7 and above. The initial pH of 6 was increased to 7 after 10 h of testing, which explained the stop of further decrease of the current after 4 h when the MESs were exposed to pH of 6 (Fig. 5.7a). The result is similar but also different from He et al. (2008) who observed pH increase for initial feed pH values lower than 8 and pH decrease for initial feed pH values equal or higher than 8 as well. The

increase of the pH is due to proton consumption by the oxygen reduction on the cathode electrode (Zhao et al., 2006; Rozendal et al., 2006) .

He et al. (2008) analyzed that the reason why pH decreased at high initial feed pH values was due to the weak acid compounds produced by the bacterial metabolism. It should be noted that the MFC in their case is a batch-operated system where the buffering effect via bacterial metabolism was more important than in a continuously operated MESs in this study. This showed that the constant flux of fresh feed might overwhelm the change of the electrolyte inside the MESs induced by the biological reactions, which is an advantage for a sensor since the accumulation effect is neglectable and the sensor displays the real time response.

The results here showed that MES was sensitive to monitor the acidic toxicity of the wastewater and the baseline current during the normal fluctuation of the pH (7.37 ± 0.24) was stable enough to prevent a false alarm.

5.2.2 Assays of single heavy metal

5.2.2.1 MES characteristics, IC_{50}, sensitivity, detection of limit

To investigate the MES performance toward heavy metals and the characteristics of the MES, typical heavy metals of Pb(II), Cd(II), Ni(II), Zn(II) and Cu(II) were injected individually into the MESs as target toxicants. Their real-time current responses upon exposure to 6 h pulses of various metal concentrations ranging from 1 to 10 ppm are shown in Figs. 5.8a-e. It could be seen that the MES allowed the monitoring of the activity of the anodic biofilm in the absence and presence of the

different metals with various concentrations by recording the current it generated. In the absence of the toxic agents, the current of the MESs were maintained stable at 1.2±0.02 mA. The patterns of the current drop due to the presence of toxic metals followed a similar trend. Upon the injection of the toxic agents, a continuous and reproducible decrease in the current generation was observed immediately and the decreasing rate was dependent on both the type of heavy metal and its concentration. After a rapid decrease, the rate of the current generation inhibition slowed down. When the toxicant injection was stopped, the current recovered to nearly the initial basal value within 1 h.

The extent of the current generation inhibition by different metals was however, different, giving the possibility of differentiating them. For example, the inhibition of the MES by Ni(II) (Fig. 5.8b) was higher than those to other metals shown by its larger current difference at the same concentration. The current generation inhibition to 5 ppm Ni(II), Cd(II), Zn(II) and Cu(II) after 6-h exposure was 55±1.22, 40±1.69, 40±1.72 and 50±3.64%, respectively. The response of the sensor to Pb(II) was much smaller compared to other heavy metals. The MES only encountered 30% current generation inhibition even at 10 ppm of Pb(II), while at this concentration, the MES showed huge current drop to Ni(II) (95% inhibition).

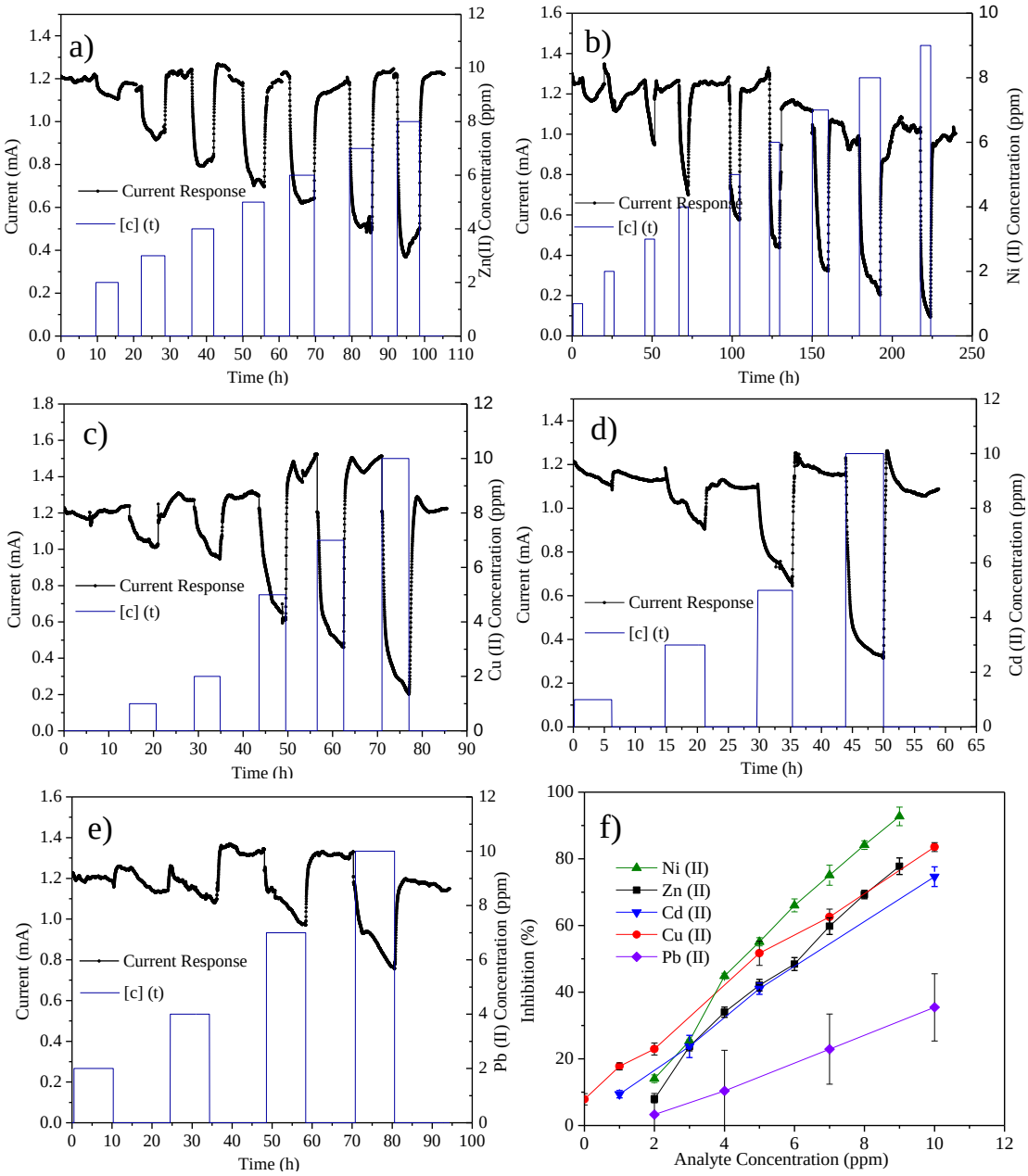

Figure 5.8. The real-time i-t response curve (a-e) obtained by MES with different concentrations and the plot of inhibition verses different concentration of MES (f) upon exposure to different concentrations of target metals (a) Zn(II), (b) Ni(II), (c) Pb(II), (d) Cd(II) and (e) Cu(II).

The response enhancement with the increase of target heavy metal concentration was observed in a range of 1-10 ppm for all the studied heavy metals, indicating the existence of a dose-response relationship. A linear dose-response relationship was confirmed by plotting the current generation Inhibition (I) (%) after 6-h exposure to the toxicants versus heavy metal concentrations (c) (ppm). The calibration curves

between the current generation Inhibition and respective heavy metal concentrations were obtained from least-square linear regressions of the data points (Fig. 5.8f), $Inhibition\ (I)\ (\%) = a \cdot c + b$ (Equation 1), where a and b are the regression coefficients. The dose-response regression results are shown in Table 5.2. Linear response often offers advantage in MES application as a sensor since sensitivity is constant over a certain range of concentrations (1 to 10 ppm), defined as the slope (a) of the calibration curve (dI/dc). The important MEC characteristics such as detection of limit, sensitivity and IC_{50} could be achieved through the dose-response calibration curve.

Table 5.2 Summary of the MES characteristics (dose-response calibration, detection of limit, sensitivity and IC_{50}) in response to different heavy metals of Zn(II), Cd(II), Cu(II), Ni(II) and Pb(II).

	Regression (r^2)	**DL** (ppm)	**Sensitivity** (%/ppm)	**IC_{50}** (ppm)	**Conc. affecting the ASP** (ppm)
Zn(II)	I =9.5329 c-7.0562 (0.9906)	2	9.5 ±0.42	6	2.1 (Madoni et al. 1996)
Cd(II)	I =7.2696 c+2.6693 (0.9977)	1	7.2 ±0.26	6.5	3 (Zarnovsky et al. 1994)
Cu(II)	I =7.6006 c+9.3913 (0.9937)	< 1	7.6 ±0.16	5.3	5 (Cabrero et al. 1998)
Ni(II)	I =11.264 c-4.7796 (0.9837)	1	11.3 ±0.8	4.9	5 (Ong et al. 2004)
Pb(II)	I =4.048 c-5.2614 (0.999)	4	4.0 ±0.07	13.6	17 (Madoni et al. 1999)

Table footnote: DL represents detection limit. The column of the *Conc. Affect the AS system* showed the lowest concentration of respective heavy metal that affect the ASP summarized from Table 2.1

Detection limit

On the basis of the signal-to-noise characteristics of the data (S/N=3), the variation of 10% is considered as the detection limit. The detection limit (DL) of the five metals are summarized in Table 5.2, which were low enough to detect the heavy metal concentration which would have negative impacts on the ASP (Table 2.1).

Sensitivity

The sensitivity of the MES toward each heavy metal was obtained and the results are shown in Table 5.2. The MES showed highest sensitivity toward Ni(II) (11.3 %/ppm) and the lowest sensitivity to Pb(II) (4.0%/ppm). The sensitivity to Cu(II) (7.6%/ppm) and Cd(II) (7.2%/ppm) were quite similar and both were lower than the sensitivity to Zn(II) (9.5%/ppm).

The sensitivity is an important characteristic of MES, representing the sensor ability to detect the toxicants. It can be used to give information of the toxicants according to the signal, such as infer toxicity at other concentrations or determine the toxicant concentrations according to the current generation inhibition. Moreover, the higher the sensitivity to one heavy metal, the clearer signals the MES could respond to its various concentrations. Thus in our case, the MES is suitable for detecting Ni(II), Cu(II), Cd(II), Zn(II) and Pb(II).

IC_{50}

As mentioned in the introduction, another parameter frequently used as an indicator of the MES characteristics toward the toxicant is the IC_{50} (the toxicant concentration eliciting a 50% inhibitory effect). The IC_{50} of different heavy metals were determined by substituting value of Inhibition (I) = 50% in the respective calibration curves and the results are shown in Table 5.2. Also listed are concentration ranges of heavy metals from the literature that negatively affect the ASP, which are comparable to the IC_{50} obtained in our study. For example, the IC_{50} calculated by the equation for Ni(II) was 4.9 ppm, which was comparable to the literature that 5 ppm of Ni(II) would lead to a 22% reduction of TOC removal (Ong et al., 2004). The relativity of the

information to the ASP is an advantage over other sensors, which IC_{50} values are either too high or too low.

The comparison between the MES characteristics with other toxicity biosensor methods is difficult and not useful in this study since the biosensor methods are dependent on the bacteria, testing method, testing time and wastewater conditions. The toxicity order of the heavy metals, the EC_{50} values in the literature, the detection limit, characteristics to sense water all varied largely among different researches. For example, Dalzell et al. (2002) compared the toxicity data for metals using five different rapid toxicity assays and found that the EC_{50} value was different among different assays. Taking Cu(II) as an example, the EC_{50} value was 28 ppm for a 2-h nitrification inhibition test, 24 ppm for a 3-h respirometry test, 3 ppm for a 30-min ATP luminescence test, 0.3 ppm for a 30-min *V. fischeri* test and 12 ppm for a 15-min enzyme inhibition test (the data was read from the graph in Dalzell et al. (2002)). The toxicity information among different literatures was even more different.

Thus it is more important to compare with the concentration that would affect the ASP treatment efficiency to see whether the information is related. These data suggest that the MES is appropriate for screening the influent toxicity for the ASP. However, the accuracy of the method could not be determined, as there were no available theoretical values of inhibition of these reference substances for ASP and also no available data on other MFC-based biosensors.

The limitation observed in the MES response is its low specificity to different heavy metals, mainly due to the complexity of the interaction between the heavy metal and

the biofilm. It suggests that the influent monitoring using MES alone might not give full information of the toxicant immediately, but it did give early warning signals and primary information, alerting operator for the further detailed investigation. Several approaches including the mathematical modeling of the sensor response curve and inoculating the MES under one constant toxic condition to make it acclimatized to a specific toxicant were being investigated in this study to minimize this disadvantage.

5.2.2.2 Kinetics study-Response time and exposure time

Fig. 5.9 showed the enlarged part of the current response curves of the MFC-based biosensor to the exposure to Zn (II) (4 ppm), Ni (II) (5 ppm) and Cu (II) (10 ppm) originally in Fig. 5.8 to display the typical sensor response profile so as to further reveal the kinetic response characteristics and toxicants exposure time effect.

Exposure time effect

Exposure to 4 ppm of Zn(II) yielded a dramatic decline in current generation within the first hour and stabilized at a minimum current at 0.8 mA. Longer exposure (9 h) led to no change in the current inhibition response (Fig. 5.9a). Different exposure time didn't affect the current response profile in the Ni (II) (Fig. 5.9b) and Cu (II) (Fig. 5.9c) case either. The recovery was independent of the exposure time in all the cases, which was not affected even at longer exposure (24 h) to Cu (II).

Although the current response pattern was the same to the different tested metals (i.e., dropped fast during the first hour and tend to be slower), it appears clearly that only

exposure to Zn(II) approached an equilibrium state after 1 h of injection. For the other metals, the minimum steady-state current can't be reached up to 6 h exposure.

6 h was selected as the exposure time for the device because sizeable distinctions were yielded between varying levels of metal exposures and the change of current was not so sharp after 6 h exposure.

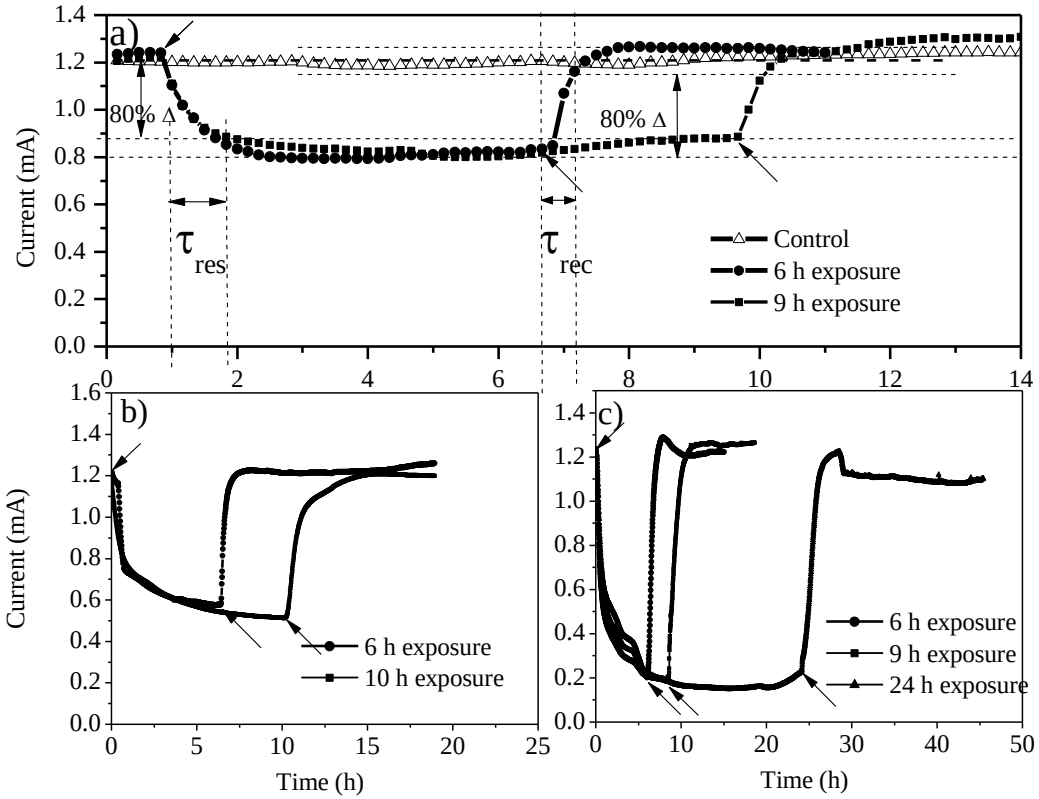

Figure 5.9. The enlarged part of the current response curve of the sensor response to (a) 4 ppm of Zn(II) (b) 5 ppm of Ni(II) and (c) 10 ppm of Cu(II). The calculation of the response time **(τ_{res})** and recovery time **(τ_{rec})** was shown and different exposure time effect was also compared.

Response time

The response time is defined as the time taken for a measurement (current in the case of MES) to reach a given percentage (80% in this case) of the difference between the two steady-states after switching from one concentration to another (Ménil et al., 2005). The 80% response time (τ_{res}) of the MES fed with wastewater containing 4 ppm of Zn(II) was 50 min and the 80% recovery time (τ_{rec}) was 23 min as shown in

Fig. 5.9. The summary of the MES τ_{res} and τ_{rec} in the case of heavy metals at different concentrations are shown in Table 5.3.

It was found that the response time varied from one heavy metal to the other; however, a similar trend of decreasing τ_{res} with increasing heavy metal concentration was found for every heavy metal. For example, τ_{rec} were 80, 75, 50, 65, 55, 42 and 40 min to detect the Zn at concentration of 2, 3, 4, 5, 6, 7, and 8 ppm (Table 5.3), respectively. It is likely due to the diffusion of the metal - when the concentration of heavy metal was higher, higher number of metal ions could reach and diffuse through the biofilm, which promoted rapid achievement of steady-state conditions. However, this trend was not observed for the τ_{res}, which is dependent on neither the toxicant concentration nor metal species. The τ_{res} was below 60 min and shorter than the respective response time in all cases. It is likely because that during the recovery, the diffusion of fresh water within the biofilm at similar rate and the slight difference in the heavy metal concentration in the ppm range did not have much impact on the back diffusion of heavy metal to the bulk solution.. Therefore, it could be concluded that the concentration of heavy metal in the bulk solution will impact the diffusion of the heavy metal in the biofilm and hence the MES response.

Table 5.3. Summary of the response time **(τ_{res})** and recovery time **(τ_{rec})** of the MES with different concentration of heavy metals.

Conc. (ppm)	2	3	4	5	6	7	8	9	10
Zn(II)									
τ_{res} (min)	80	75	50	65	55	42	40	/	/
τ_{rec} (min)	60	15	23	32	21	19	21	/	/
Ni(II)									
τ_{res} (min)	/	/	160	75	55	160	90	45	/
τ_{rec} (min)	/	/	58	40	42	25	31	46	/
Cu(II)									
τ_{res} (min)	105	/	/	110	/	56	/	/	52
τ_{rec} (min)	48	/	/	17	/	16	/	/	45
Cd(II)									
τ_{res} (min)	/	72	/	56	/	/	/	/	45
τ_{rec} (min)	/	15	/	20	/	/	/	/	20
CN^-									
τ_{res} (min)	31	38	28.5	40	/	32.5	/	/	41
τ_{rec} (min)	84	65	30	56	/	76	/	/	62

The τ_{res} values obtained in this study was not comparative with other sensing assays such as the bioluminescent bacteria (Shk1)-based monitoring system, which τ_{res} was only 5 min (Ren and Frymier, 2003). However, the τ_{res} values obtained in this study were still significantly shorter than those of the respirometry-based test methods, which typically take hours. This showed one of the major limitations of the usage of MES as a sensor because heavy metal has to diffuse through the biofilm to the electrochemically-active bacteria (EAB) that are growing on the surface of the anode, resulting in a slow response as compared to cell or enzyme-based biosensors.

The τ_{res} was usually affected by the exposure time and was different from the time to trigger the alarm that indictae the presence of toxic heavy metals in the wastewater. The 1-h data showed that the easrliest response started after about 5 min of toxicants injection (Fig. 5.10), which was close to the HRT of the MES feed tubing and the MESs, indicating that there was an intrinsic time delay of at least 5 min. The significant decrease of the current during the preliminary period of the exposure time

(less than 30 min) can allow practical application of the MES as a sensing device by triggering the alarm when a preset percentage drop in the current is detected or a based on a preset duration (sufficient enough for preventive action to be carried out to to protect the downstream ASAP) such as 1 h after the current continues to drop.

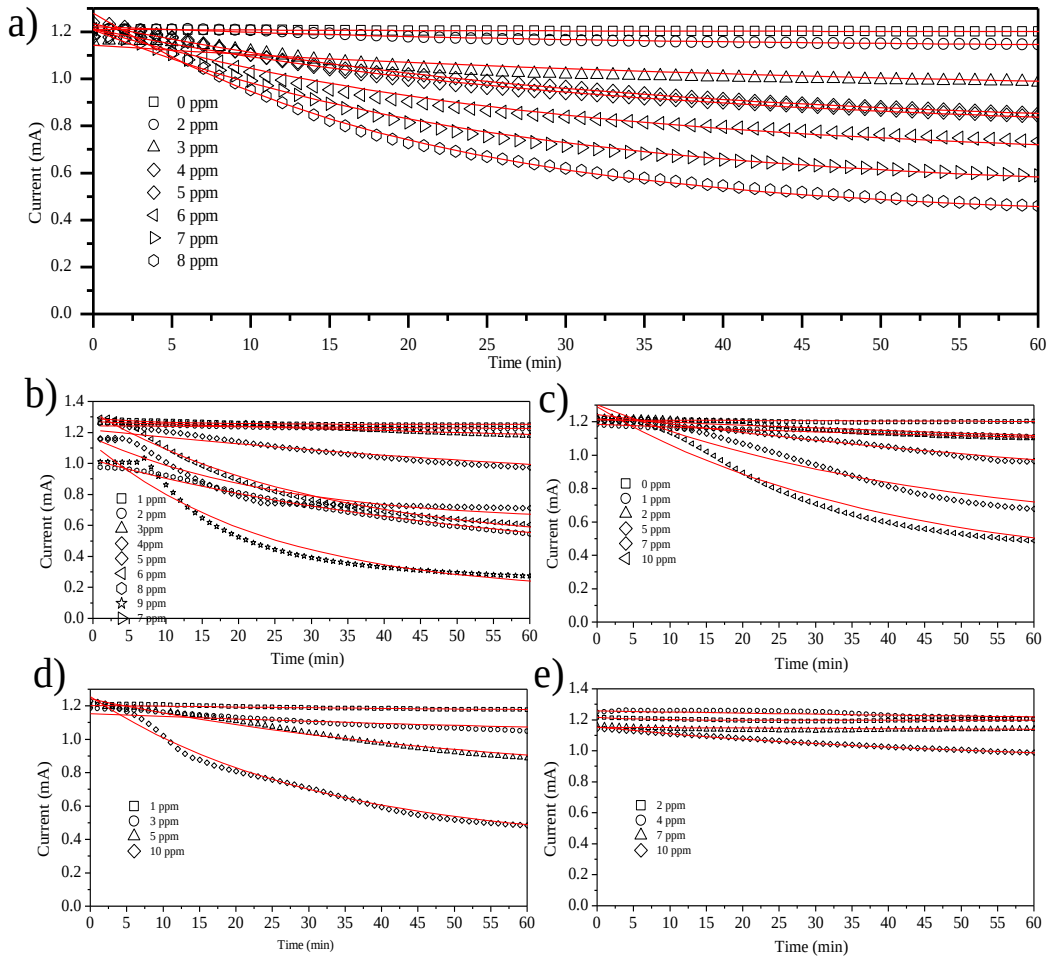

Figure 5.10. The first 1 h of the MES *i*-t response profile after exposure to (a) Zn(II), (b) Ni(II), (c) Cu(II), (d) Cd(II) and (e) Pb(II). The red lines showed a single exponential fit to Exponential decay by using the fitting method of ExpDec-1 (Origin 8).

Modeling

The computational model of the response curve of the MES to toxicants was constructed with the aim to reproduce the short-term (i.e., min) current production after the addition of toxicant and also to have a primary judgment of the toxicant

information according to the MES response, making it possible to differentiate the toxicants.

According to Motulsky (2004), the following shape of the graph which is close to the current response profile of our study is can be described by the modified decay equation:

$$\mathbf{Y = (Top - Bottom) \cdot e^{-kt} + Bottom} \quad (5.2)$$

where Top is the initial signal value and Bottom is the final signal value as shown in Fig. 5.11.

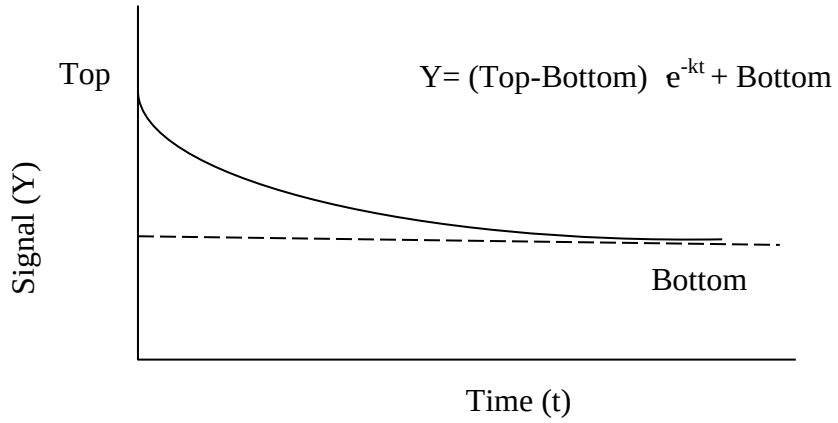

Figure 5.11. An example of the exponential decay graph.

Thus regression was used to fit the current versus time data to the modified exponential decay curves:

$$i(t) = (i_0 - i_{\min})e^{(-kt)} + i_{\min} \quad (5.3)$$

where $i(t)$ is the current (mA) at time t (min) after injection of toxicant, i_0 is initial current (mA) before toxicant injection and i_{min} is the final current (mA) during exposure to toxicant and k is an coefficient and a large k value is indicative of a steep

decay curve. The fitting of curves were done using ExpDec1 model (Origin 8). Regression coefficients, standard errors, and coefficient of determination (r^2) were thus determined for each heavy metal at different concentrations and the results are summarized in Table 5.4 .

It could be seen that the coefficient of determination values were high. Model calculations showed that the response curves follow a single exponential decay as demonstrated by the exponential decay fit (continuous red line) in Fig. 5.10. For most of the cases, the first order exponential decay curves adequately described the current decrease due to the metal toxicants effect. A deviation from this behavior can be seen at the very first few minutes, which was the intrinsic time delay for the toxicants to have an effect on the EAB of the MESs as discussed earlier.

Table 5.4 Regression coefficients for current of individual compounds at different concentrations with time, *i(t)*, using the exponential decay curve of Eq. 5.3.

	Conc.(ppm)	2	3	4	5	6	7	8	9	10
Ni	i_0- $i_{\min\,(mA)}$	-	0.47	0.49	0.54	0.86	0.79	0.70	0.97	-
	1/k (min)	-	311.47	97.44	25.80	30.86	143.86	54.13	24.55	-
	$i_{\min\,(mA)}$	-	0.80	0.73	0.62	0.47	0.25	0.33	0.16	-
	r^2	-	0.994	0.986	0.901	0.989	1.000	0.995	0.964	-
Zn	i_0- $i_{\min\,(mA)}$	0.01	0.10	0.22	0.46	0.48	0.57	0.71	-	-
	1/k (min)	29.69	51.27	46.98	28.09	43.05	33.28	25.95	-	-
	$i_{\min\,(mA)}$	1.20	1.12	0.93	0.80	0.72	0.63	0.52	-	-
	r^2	0.974	0.940	0.987	0.990	0.987	0.994	0.970	-	-
Cu	i_0- $i_{\min\,(mA)}$	0.30	-	-	0.64	-	0.79	-	-	1.00
	1/k (min)	149.28	-	-	108.77	-	44.44	-	-	38.12
	$i_{\min\,(mA)}$	0.92	-	-	0.61	-	0.51	-	-	0.30
	r^2	0.976	-	-	0.997	-	0.983	-	-	0.983
Cd	i_0- $i_{\min\,(mA)}$	-	0.19	-	0.51	-	-	-	-	0.90
	1/k (min)	-	109.30	-	55.62	-	-	-	-	30.95
	$i_{\min\,(mA)}$	-	0.96	-	0.73	-	-	-	-	0.36
	r^2	-	0.971	-	0.988		-	-	-	0.991

Since τ_{res} was defined as the response time consists in measuring the time to reach a 80% of the final change, substituting $i_0 - i(\mathrm{t}) = 0.8\,(i_0 - i_{\min})$ into the Eq. 5.3, we obtained $= -\frac{\ln 0.2}{\tau_{res}}$. As seen above, Inhibition $(I)(\%) = \frac{i_0 - i_{min}}{i_{min}} \cdot 100 = a \cdot c + b$, where a was the sensitivity and b was related with the IC_{50} in the way of $b = 50 - a \cdot IC_{50}$. Thus rewriting Eq. 5.3, we can get

$$\boldsymbol{i(t) = \frac{(ac+b)i_0}{100} e^{\frac{ln0.2}{\tau_{res}}t} + i_0 - \frac{(ac+b)i_0}{100}} \qquad (5.4)$$

It showed that the MES characteristics (i.e., sensitivity, IC_{50} and τ_{res}) could be used to describe the shape of the MES output current signal decay in response to the respective heavy metals. The actual mechanisms of toxic action by which heavy metals inhibit the current generation of the MESs were not discussed in this chapter and not being included when considering the mathematical modeling. We used a simple mathematical model similar to the first order exponential decay to describe the

current decrease in response to the heavy metals. The format of this equation is suggested by the shape of the current decay and does not suggest a fundamental mechanism. Use of such a model provides more intuitive metrics for comparison and permits more reliable use of shorter measurement times to characterize the MES response.

5.2.3 Assays of binary metal mixtures

Different binary metal mixtures with various combinations of component species and concentrations were investigated. Cd(II) and Ni(II) were chosen as the two base heavy metals to combine with the other metals, and the combination of the metals tested were Cd(II) with Cu(II), Cd(II) with Ni(II), Cd(II) with Zn(II), Cd(II) with Pb(II), Ni(II) with Zn(II) and Cu(II) with Ni(II). The concentration of each metal in each mixture was 5 ppm except as otherwise noted. For the mixture of Cd(II) and Cu(II), three different combination of concentrations were tested, i.e., 2ppm Cu(II) with 8 ppm Cd(II), 8ppm Cu(II) with 2 ppm Cd(II) and 5ppm Cu(II) with 5 ppm Cd(II). The observed response to binary mixtures of heavy metals after 6 h of exposure were calculated and the results are shown in Fig. 5.12. Additive function ($f(x+y) = f(x) + f(y)$) was proposed to calculate the response to the toxicity of mixtures based on the additivity hypothesis (Gälli et al., 1994; Ribo and Rogers, 1990). The results of experiments using individual Ni(II) or Cd(II) with concentration of 10 ppm were also included for comparison. The results of the duplicate MESs of 6-h exposure to eight binary mixtures of heavy metals were highly reproducible between replicates.

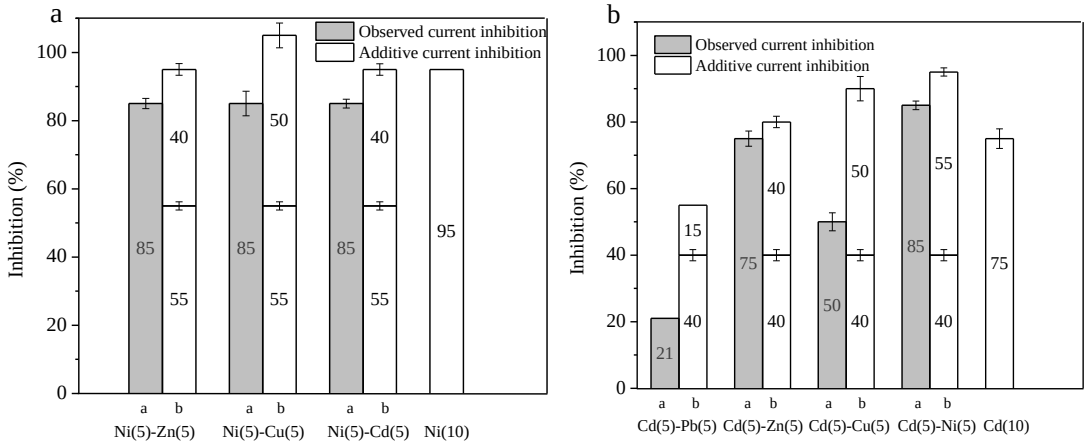

Figure 5.12. The observed (■) and predicted (□) current inhibition of the MES to (a) Ni-metal and (b) Cd-metal binary mixtures after 6 h of exposure. The predicted current inhibition was calculated based on the additive function using the single metal response data. The results using individual Ni(II) or Cd(II) with concentration of 10 ppm was also included for comparison.

It could be seen from Fig. 5.12a that for all the Ni(II) combination cases (5 ppm Ni(II) with 5 ppm Zn(II), 5 ppm Ni(II) with 5 ppm Cu(II), 5 ppm Ni(II) with 5 ppm Cd(II)), 85% inhibition of the current generation were observed, which were smaller than the predicted additive effect and lower than the single Ni(II) effect of 10 ppm (95% inhibition), showing antagonistic effects.

But in the Cd(II) cases, the result was different as shown in Fig. 5.12b. The responses to Cd(II)-metal mixtures were different among different metal combinations. For example, the inhibition were 50% for mixture of 5 ppm Cd(II) with 5 ppm Ni(II), 21% for mixture of 5 ppm Pb(II) and 5 ppm Cd(II), which were smaller than the single 10 ppm Cd(II) effect (75%). In contrast, the inhibition were 85% for mixture of 5 ppm Cd(II) with 5 ppm Ni(II), which were larger than the single 10 ppm Cd(II) effect. For the mixture of 5 ppm Cd(II) with 5 ppm Zn (II), the inhibition were 75%. All the observed inhibitive response of the different mixtures were smaller than the predicted addictive response, also showing antagonistic effects as Ni-metal mixtures did. Besides, the effect of the mixtures were different from that of the single metal. For

example, the single 5 ppm of Cu(II) gave higher inhibition than 5 ppm of Zn(II), but the effect of the mixture of x ppm of Cd(II) with x ppm of Zn (II) was, however, larger than that of x ppm of Cd(II) with x ppm of Cu (II). The response to different concentration of heavy metal in mixtures was also investigated. The combination of Cd(II) with Cu(II) gave 50% inhibition regardless of the concentration ratio (2 ppm Cd with 8 ppm Cu, 5ppm Cd with 5 ppm Cu or 8 ppm Cu with 2 ppm Cd).

A general rule for the effect of interaction of heavy metals in binary mixtures was not suggested by our data, which was expected since it is known that different metal pairs exhibit different interaction patterns. The literature reported results that are often contradictive, even for similar type of microbial systems (Ribo and Rogers, 1990). The interaction is sometimes observed to change from synergism to antagonism and vice versa as the concentrations or metal species change. What can be derived from the literature is that the toxic effects to microorganisms usually do not follow the rule of additivity, all three possible interactions (synergy, additivity and antagonism) have been reported (Gikas, 2008). In our study, antagonism effects were observed in all the tested mixtures. The mechanism of such interactions might be particularly complex, affected by many factors such as the combinations of heavy metals and biofilm characteristics (Cabrero et al., 1998), which requires further investigation.

Although the results somehow only demonstrated the interactive effects at the combinations of metal concentrations that were investigated and conclusions cannot readily be extended to mixtures with different concentration combinations, it were still informative and offered a qualitative estimation of the toxicity of metal mixtures, given knowledge of the toxicity of mixture metals, i.e., whether the toxicity of the

mixture is higher than, lower than, or equal to the sum of the toxicity of the mixture components. Further investigation is recommended to study about the mechanism and ternary or more complex mixtures.

5.2.4 Specificity study

To improve the sensor specificity, MESs were inoculated under two constant toxic conditions (1 ppm and 2 ppm of Ni(II)) for 1 month and after that, their response to metal toxicity (Ni(II) and Zn(II)) was investigated and the results were discussed below. A control group of MESs with normal inoculation (i.e., without the presence of toxicants) were also included as comparison.

The startup and acclimatization for the MESs inoculated under toxicant condition was the same as the control MESs. It took 1 month for the MESs to produce stabilized current for all the three conditions, but the steady-state current generated was different. For MESs inoculated under 1 ppm of Ni(II), the baseline current was 1 ± 0.02 mA, lower than the control MESs inoculated without Ni(II) (1.2 ± 0.02 mA), and the MESs inoculated under 2 ppm of Ni(II) produced even lower steady-state current of 0.45 ± 0.01 mA, showing that inoculating under Ni(II) conditions affected the growth condition of the anodic biofilm of the MESs, giving lower basal current.

It could be seen from Fig. 5.13 that with the injection of 5 ppm Ni(II) into the above three MESs, the response of the MESs with 1 ppm Ni(II) inoculation was almost the same as the control one, only 10% less inhibited than the control condition (50% inhibition), suggesting that inoculating the MESs with 1 ppm of Ni(II) did not affect

the biosensor performance. For the MESs under 2 ppm of Ni(II) inoculation, the difference was significant, where the inhibition only reached 25%. In other words, MESs inoculated with 2 ppm of Ni(II) condition made the sensor less responsive to Ni(II) toxicity.

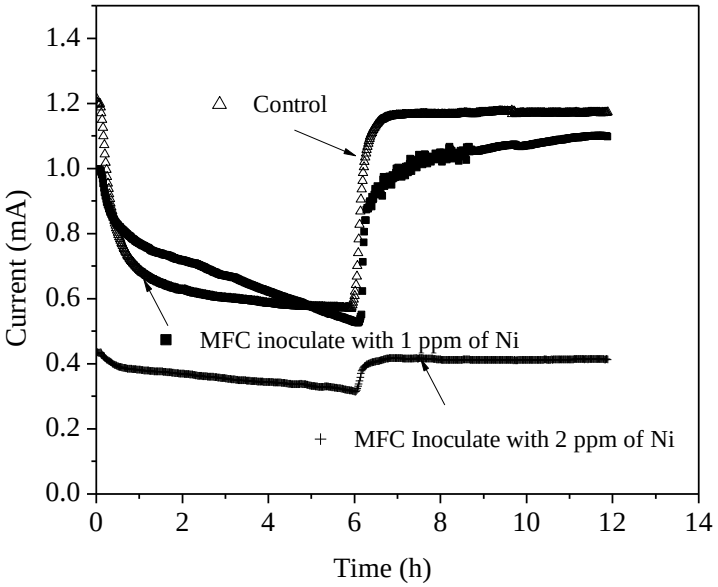

Figure 5.13. The real time *i*-t response profile to 6-h exposure of 5 ppm Ni(II) of the MESs inoculated under 1 ppm of Ni(II)(■), 2 ppm of Ni(II) (+) and 0 ppm of Ni(II) (△) as the control. At time 0, the toxicity injection started and the MESs were exposed to 5 ppm of Ni(II) for 6 h.

However, as shown in Fig. 5.14, when the MESs inoculated with 2 ppm of Ni(II) were further exposed to 10 ppm of Ni(II), larger inhibition (65%) was observed, and it also displayed similar inhibition to 10 ppm of Zn(II) (65%), which showed no significant difference from the response of the MESs without Ni(II) inoculation. It suggested that inoculating the MESs with Ni(II) did not make it specially acclimatized to it and the MES selectivity could not be improved.

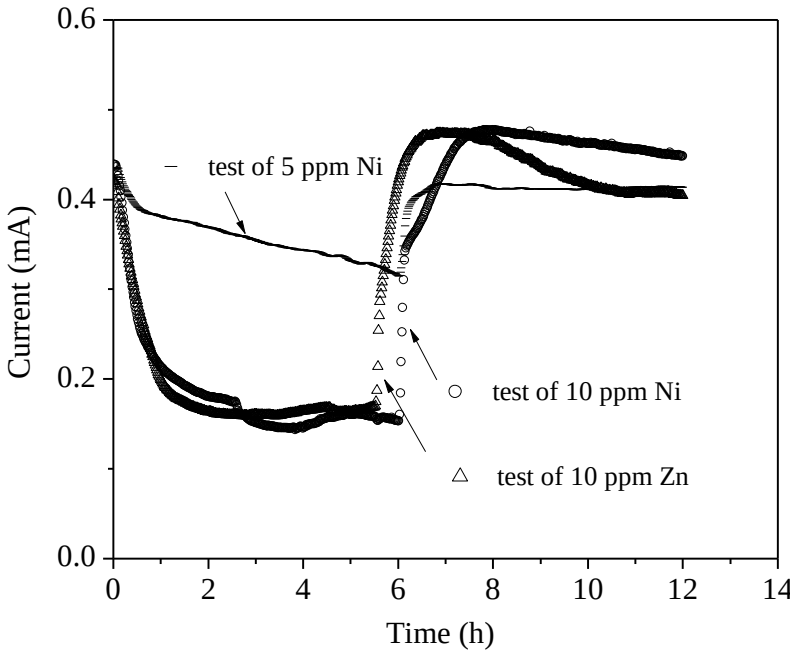

Figure 5.14 The real time *i*-t response profile to 6-h exposure of 5 ppm Ni(II) (—), 10 ppm of Ni(II) (○) and 10 ppm of Zn(II) (△) of the MESs inoculated under 2 ppm of Ni(II). At time 0, the toxicity injection started and continued for 6 h.

Through the contrasting response of the MESs inoculated with 1 ppm of Ni(II) and 2 ppm of Ni(II), it could be found that the main reason for the smaller inhibition for the MESs inoculated with 2 ppm of Ni(II) is mainly due to its lower baseline current, which led to the smaller measurement range of current produced under the toxicant. Inoculating the MFCs with Ni(II) did not make it specially acclimatized to it and the sensor selectivity could not be improved. However, on the other hand, the observation is beneficial to the MES as a heavy metal sensor since exposure to the toxicants would not affect subsequent sensitivity of the sensor during the long-term operation, giving stable performance. The enzyme sensors usually are highly specific for substrates due to their specific working enzymes, yet the enzymes employed are generally expensive and unstable.

5.2.5 Toxicity screening of Cyanide (CN^-)

Cyanide was dosed in the particulate form of potassium cyanide (KCN) to yield initial concentration of 1–10 ppm. Fig. 5.15 shows the cyanide sensing response profile of the MESs. The line represented the step change in the feed CN^- concentration. Sharp decreases and rises in *i* values could be seen when the CN^- were injected and discharged, respectively, indicating that the MESs were of fast response and recovery (in the presence of up to 10 pp,m cyanide) to cyanide toxicity. The different generated current variations can be distinctly observed. The detection limit was estimated to be 2 ppm (S/N=3).

Fig. 5.15a shows the dynamic response of the MES towards CN^- at different concentration while Fig. 5.15b shows the first 600 min of the dynamic response of the MES towards 5 ppm CN^-, which is a typical response profile of the MES detecting CN^-. The current generated by the MES decreased immediately and at samilarly high rate for the first 30 min when CN^- was introduced into the MES. Subsequently, it approached slowly to 0.7 mA and it maintained stable during the whole exposure period. Compared with the MES response to pH and heavy metal, it could be seen from Fig. 5.15 that it take shorter time (less than 60 mins) for the generated current to become stabilized, further proven by the shorter response time summarized in Fig. 5.16.

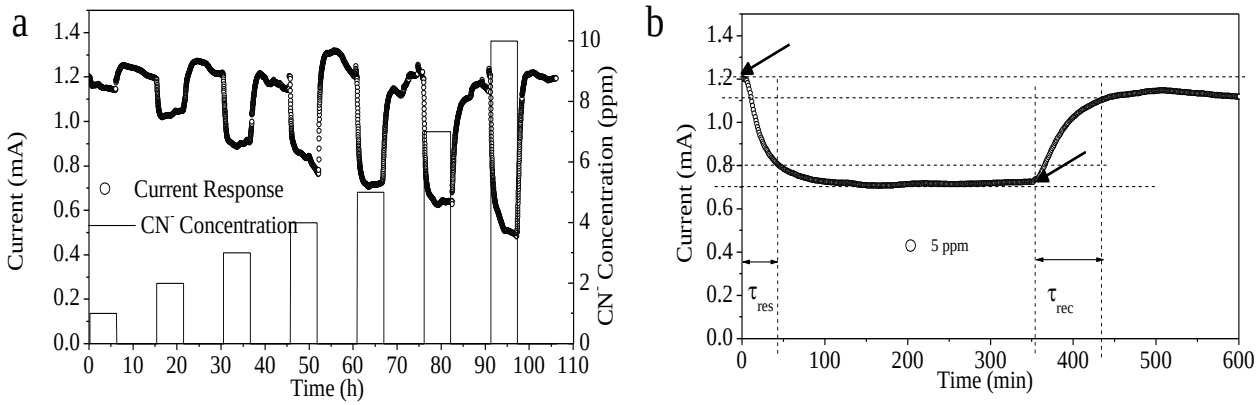

Figure 5.15 (a) The real-time *i*-t response curve obtained with different CN^- concentrations. The line represented the CN^- concentration. (b) The first 600 min of the current response curve of the MES exposed to 5 ppm of CN^-.

The τ_{res} was less equal or less than 40 min for all CN^- concentrations except with 10 ppm CN-, τ_{res} was at 41 min. In comparison, the average τ_{res} of all heavy metals tested earilier was around 80 mins (Fig. 5.19). Another difference between the response of CN^- and heavy metals was the recovery from toxicant event. It took longer time (around 2 h) for the MES to recover to its basal current for CN^-. However, for heavy metals, the the average recovery time was 28 min, much shorter than the CN^- cases.

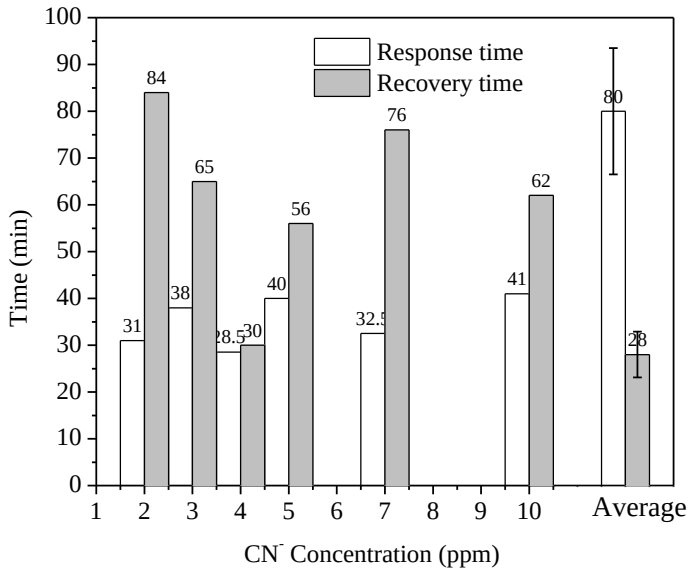

Figure 5.16. The response time (τ_{res}) (□) and recovery time (τ_{rec}) (■) at various dosed CN^- concentrations. The average response time and recovery time at various concentrations for all the heavy metal cases were calculated based on the data from Table 5.3 and also included as a comparison.

The generated currents for the first hour exposure to CN- of different concnetration were shown in Fig. 5.17. Similar to heavy metals, it also took 5 min for the MESs to show reaction to the CN^-, confirming that 5 min is the intrinsic time delay for the MES that was close to the HRT of the feed tubing and the MESs. Despite this short response time, the significant decrease of the current during the preliminary period of the exposure time (less than 30 min) can ensure the practical application of the MES as a sensing device, triggering the alarm fast enough to protect the ASP.

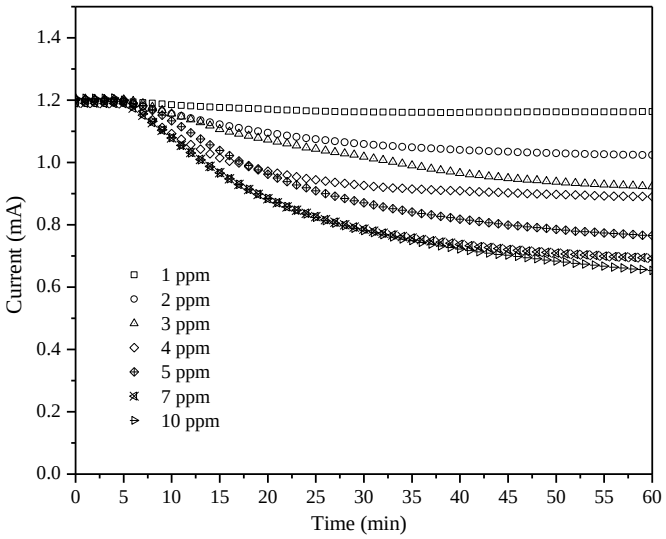

Figure 5.17. The current response curve of the MESs during the first hour of exposure to different concentrations of CN^-.

Fogure 5.18 a showed that the inhibition did not increase linearly with CN^- concentration, showing that the sensitivity was not constant within the tested range. A plot of i_0/i_{min} vs. *c* demonstrated that the inhibition was similar to the non-competitive inhibition.

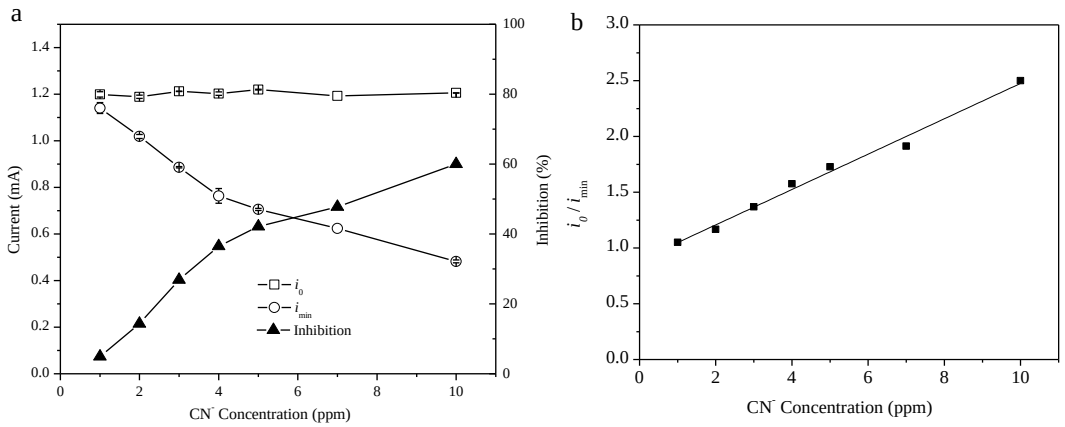

Figure 5.18. (a) The plot of inhibition verses different concentration. (b). A plot of (i_0/i_{min}) vs. concentration.

In general, cyanide did not seem to be as toxic to EAB as compared to heavy metals. The highest dosage in this set of testing was 10 ppm. Even at this high dosage, the inhibition was only 60%, much lower than the response to Ni(II), Cu(II) and Cd(II). This could likely be attributed to the fact that cyanide is negatively charged and bacterial cell surfaces possess a net negative electrostatic charge (Dickson and Koohmaraie, 1989), thus cyanide does not penetrate into the EAB as easily as the positively charged heavy metals. Its expression of toxicity is limited by its low level of absorption into the cells. Different regression was achieved and made it possible to differentiate the MES response to the metal cases.

5.2.6 Toxicity screening of organic chemicals

Four different kinds of organic compounds were tested using the MES toxicity sensor, representing various groups of organics, i.e., Dichloromethane (DCM) and Chloroform (CFM) (halogen substituted alkanes), Toluene and m-Cresol (aromatic hydrocarbon).

The response profiles for DCM and CFM are shown in Fig. 5.19. For both DCM and CFM, inhibition effect was only noticeable with concentrations that were beyond thousands of ppm, which was not realistic in real life. For example, the MES showed no response to DCM as high as 700 ppm and CFM at 3,000 ppm. The IC_{50} obtained from the MES was far higher than the that affecting the ASP, for example, the EC_{50} to the ASP given by Ren and Frymier (2002) for DCM was 2,935 ppm and 700 ppm for CFM. However, in our study, IC_{50} for DCM was 7,000 ppm and 5,000 ppm for CFM. The reason could be that the biofilm had a high degree of resistance against DCM and CFM by impedicting diffusion of DCM and CFM deep into the biofim where EAB were growing on the anode surface. However, the real mechanism is yet to be further investigated.

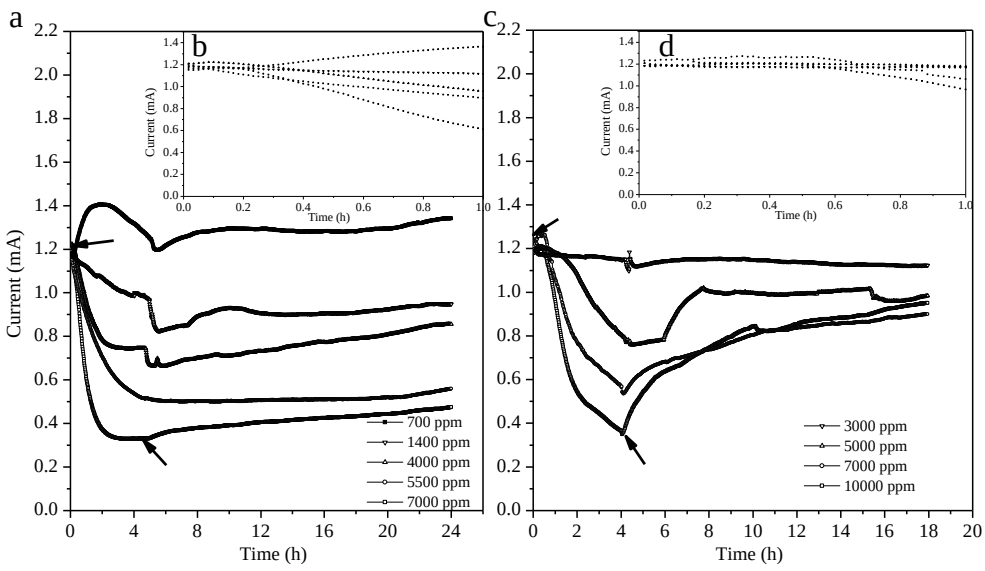

Figure 5.19. The real time i-t response profile of MES when exposed to (a) Dichlomethane (DCM) and (c) Chloroform (CFM). Arrows indicate the start (↙) and stop (↖) of the toxicant. Inserted graph showed the current response curve of the MES for the 1st hour exposed to (b) Dichlomethane (DCM) and (d) Chloroform (CFM).

The first hour of the current response curve of the MES (Fig. 5.19b and Fig. 5.19d) showed that it took much longer (around 35 min) for the generated current to decrease when exposed to DCM and CFM compared to the responses to metal toxicity. In

addition, recovery was also more difficult as the generated current did not revert to the basal current even after 10 h when the inflow of VOCs has been stopped. Approximately 2 d were needed for complete recovery to the baseline current (data not shown). The longer response and recovery time taken for the MESs exposed to VOCs as compared to the heavy metals showed that diffusion of VOCs through the biofilm into the depth whether EAB was growing on the anode surface was impeded and also for VOCs to diffuse from the biofim out to the bulk solution. The major reasons are due to high adsorption capacity of VOCs by the biofilm, high volatility (low boiling point) and low solubility of the toxic organics. Späẗh et al. (1998) has reported that 80% of the toluene is sorbed onto the EPS of the biofilm and only 20% is taken up by the bacterial cell in the biofilm. Thus, regardless of the amount of toxicants that was dosed into the MESs, only a small proportion was taken up by bacteria which can exert a toxic effect. This could explain the low sensitivity of the MES to organics.

In the case of detecting the aromatic hydrocompound of Toluene (Fig. 5.20a) and m-Cresol (Fig. 5.20b), the decrease of the current was also only observed at very high concentratons (i.e., 1,200 ppm for m-cresol), which was not realistic in real life.

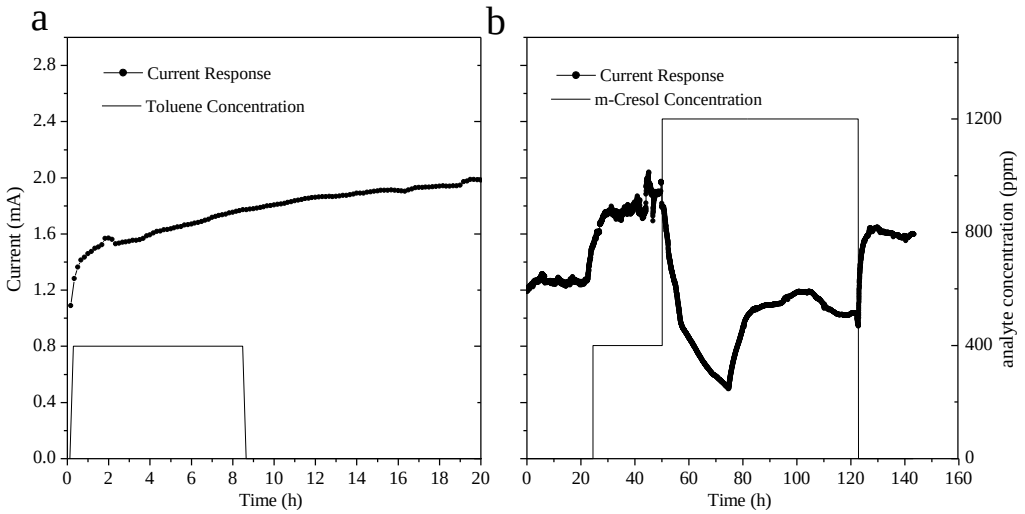

Figure 5.20. The real time *i*-t response profile of MES when exposed to (a) Toluene and (b) m-Cresol at different concentration as represented by the line.

However, it was interesting to find that the generated current increased instead when the MESs were exposed to 400 ppm of toluene (Fig. 5.20a) and 400 ppm of m-Cresol (Fig. 5.20b), showing the possibility of MESs utilizing those two aromatic hydrocompounds as the substrate. This has been proven in the literature that a diversity of aromatic hydrocarbons under anaerobic conditions can be utilized and degraded by the microorganisms in the MFCs (Luo et al., 2009; Zhang et al., 2010). *Geobacter metallireducens* has been reported as the first pure culture found to anaerobically oxidize aromatic hydrocarbons such as toluene, benzene, phenol and p-cresol (Lovley et al., 1989; Lovley and Lonergan, 1990), which was one of the common bacteria in the MFCs/MESs. The results in this study have proven that m-Cresol could also be utilized by the MESs, showing the great advantage of MFCs as the wastewater treatment method. The increase of the generated current due to the degradation of those aromatic hydrocarbons also shed light on the idea of monitoring those pollutants by analyzing the increased current since increased electron production were related with the substrate the MESs utilized. Much further research,

including the quantative analysis and a broader screening of aromatic hydrocarbons, is necessary.

5.2.7 Repeatability and long-term operational stability

5.2.7.1 MES repeatability

For real applications, the sensors should operate reliably during long-term operation. Fig. 5.21 shows two examples of the repeatability of the MESs. The response curves of the MES under repeated exposure to 5 ppm Ni(II) (Fig. 5.21a) and 10 ppm of CN^- (Fig. 5.21b) were shown. In both the cases, the MES repeatedly recovered its original basal current. Furthermore, the magnitude of the current response and valley shapes were identical and variations in the response were less than 5%, suggesting that the MES could be subjected to long-term operation without performance degradation.

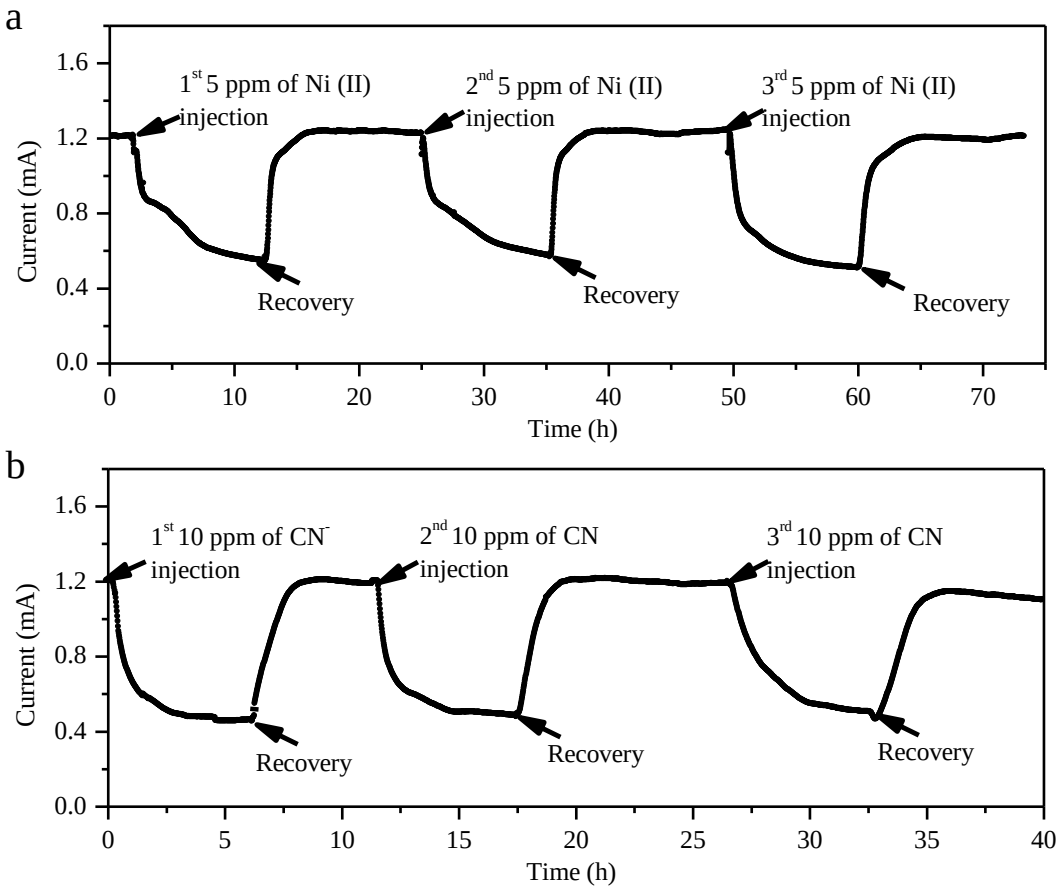

Figure 5.21. The real time *i*-t response profile of MESs for three consecutive injections at (a) 5 ppm of Ni(II) and (b) 10 ppm of CN^-. Arrows indicate the start (↙)and stop (↖) of the toxicant injection.

5.2.7.2 Long-term operational stability

The flat plate single-chamber air-cathode MESs with drilled channels used in our study had been operated for more than 2 years and neither the sensor basal current nor the response to the same toxicant was significantly changed (within 10%) after 2 years of operation.

This is an advantage over many other kinds of sensors in which either the sensing material or the transducer or both are unsuitable for the long-term operation. For

example, the immobilized activated sludge based biosensor (Liu et al., 2000) utilizes immobilized microorganisms in combination with a dissolved oxygen electrode probe, in which the electrode probe is easily oxidized and regularly change is necessary (Liu and Mattiasson, 2002). Besides, after some short-time operation, the immobilized microorganisms would start to lyse and the lysis rate might vary in different microbial strains during the sensor storage, leading to different response even for assimilation of the same organic substrate.

However, it was not the case for MESs. The two components of the MES: the sensing material and the transducer are both suitable for long-term operation. The anodic biofilm was stable once it was mature and neither the viability nor bacteria community was changed after 2 year operation, which will be discussed in next chapter. It has also been shown in the above Specificity study that the exposure to the toxicants did not affect the sensitivity of the MES during long-term operation, making the long-term operational stability possible. Kim et al. (2003) has shown a microbial fuel cell-type BOD sensor that had been operated over 5 years without any services, suggesting that the operational life time of the MES could be very long. However, in our study, regularly cleaning with ultrasound once a month was needed since suspended solids/niomass would otherwise start to accumulate inside the MESs, which would decrease current production and sensor sensitivity. Nevertheless, the procedure of the cleaning was very simple.

5.3 Summary

The MES was successfully developed in study as a real-time on online biosensor to detect the presence of various toxicants or extreme pH, nutrient concentration conditions in real wastewater, triggering the alarm within one hour to allow immediate action and further analysis. The MES allowed the monitoring of the activity of the anodic biofilm in the presence of heavy metals with different concentrations by giving specific current responses modeled by linear dose-response and exponential decay regression. Important MES characteristics such as the IC_{50}, sensitivity, response time and detection limit were given and found to be related with the toxicity information to the ASP. They are also the key to describe the shape of the sensor output current signal decay in response to different heavy metals. Continuous inoculating the MESs with small concentration of Ni(II) did not make the sensor acclimatized to the toxicant, showing the stable sensitivity to the toxicants and potential of long-term stability of the sensor. The resistance to common variation of the wastewater characteristics, fast and sensitive response to the toxicants, long-term operational stability (over 2 years), and relativity to the ASP made the MES suitable to serve as an early warning system to protect the downstream biological treatment process.

The major limitation to the use of biofilm as sensing material is the diffusion of compounds within the biofilm resulting in a slow response as compared to some other types of sensors such as the one utilizing suspended microorganisms. The diffusion of the compounds within the biofilm was the key to the different response to different toxicants such as positively charged metal ions, negatively charged cyanide ion and neutral organic compounds. In-depth investigation of the diffusion and interaction of

these compounds within the biofilm would give more information on the interpretation of the current output signal. Another limitation is the low specificity as compared to biosensors containing pure enzymes. However, modeling of the response curves, which are specific to different kinds of toxicants, showed potential to further optimize this method in order to achieve more information through the output signal.

The MES was found not suitable for detecting the presence of organics since the high IC_{50} found suggest the impracticality in real life. However, it was interesting to observe the increase of the generated current due to the degradation of aromatic hydrocarbons by the MESs, shedding light on the idea of monitoring those pollutants by analyzing the increased current. Further research, including a broader screening of organic compounds as well as the mixture effect of different toxicants, is necessary.

CHAPTER 6 Electrochemical and Biological Mechanism Study

6.1 Introduction

The MESs have been shown successful and advantageous to be used as an online biosensor for the influent wastewater toxicity screening by recording the change of the current generated by the MESs as discussed in the previous two chapters. To better relate the sensor signal with the toxicity information and further promote the application of the sensor, a better understanding of the effects of toxicants on electricity generation and the intrinsic reasons behind them are of utmost importance. However, little is known.

As discussed in Chapter 2, the current of the MESs is generated by the oxidation of organic compounds catalyzed by the bacteria in the anode biofilm, and both of the electrochemistry and biofilm kinetics have been shown to affect the electricity of the MESs (Logan et al., 2006; Bond and Lovley, 2003; Rittmann et al., 2008). The complexity of microbial and electrochemical processes make evaluation and interpretation of the toxicant effect on the current generation challenging. Investigation on both the microbial and electrochemical characteristics is needed in order to gain a better understanding of the mechanisms (Fricke et al., 2008).

In this chapter, we investigated the heavy metal effect on both the electrochemical and microbiological properties of the anodic biofilm with a view to understand the intrinsic mechanisms of current decrease due to the heavy metals. Molecular,

electrochemical, and microscopic tools were employed at different metal exposure time to fulfill this objective. PC, CV and EIS are standard tools in electrochemistry and has regularly been exploited to study and to gain valuable information on the electrochemical activity of the microbial biofilms (Logan et al., 2006; He and Mansfeld, 2009; Torres et al., 2009). DGGE and CLSM allow us to identify the members of the anodic electroactive biofilm community and viability changes in the presence of metal toxicant and their impact on biofilm activities (Torres et al., 2009; Kim et al., 2006). It is apparent that metal toxicity can also be heavily influenced by environmental conditions. Binding of metals to organic materials, precipitation, and ionic interactions are all important phenomena that must be considered carefully, which are also being investigated and discussed in this Chapter.

6.2 Results and Discussions

6.2.1 Electrochemical Analysis

6.2.1.1 Polarization Analysis

Polarization curves were measured at different exposure and recovery times to preliminary explain the current drop due to the Cd(II) toxicity (Fig. 6.1). Without exposure to 10 ppm of Cd(II), the maximum power density was 0.3 mW and the maximum power density was 75 mW/m^2, which was comparable with a flat-plate MFC using domestic wastewater as substrate as well (72 mW/m^2) (Min and Logan, 2004), but higher than a cylindrical chamber MFC (28 mW/ m^2) (Liu and Logan, 2004). This showed that the power densities produced by mixed cultures are often similar when the specific architecture, electrode spacing and solution conductivity of the fuel are similar (Logan, 2009), suggesting the advantage of repeatability of MES.

The slope of the polarization curve, referred as the internal resistance (R_{int}) of the cell includes the ohmic resistance, activation loss and concentration polarization (Fan et al., 2008). Fig. 6.1 showed that the slope of the polarization curves increased slightly when the MESs were started to be exposed to 10 ppm of Cd(II) and the further increase of the R_{int} with a longer metal exposure time could be observed. Those increases in the R_{int} were most likely due to the MES exposure to the toxicants which affected the electrochemical activity of the biofilm. The decrease of the maximum power due to the exposure to metal toxicant could also be observed (Fig. 6.1). The maximum power was restored when the recovery was started and the R_{int} was seen to decrease as well.

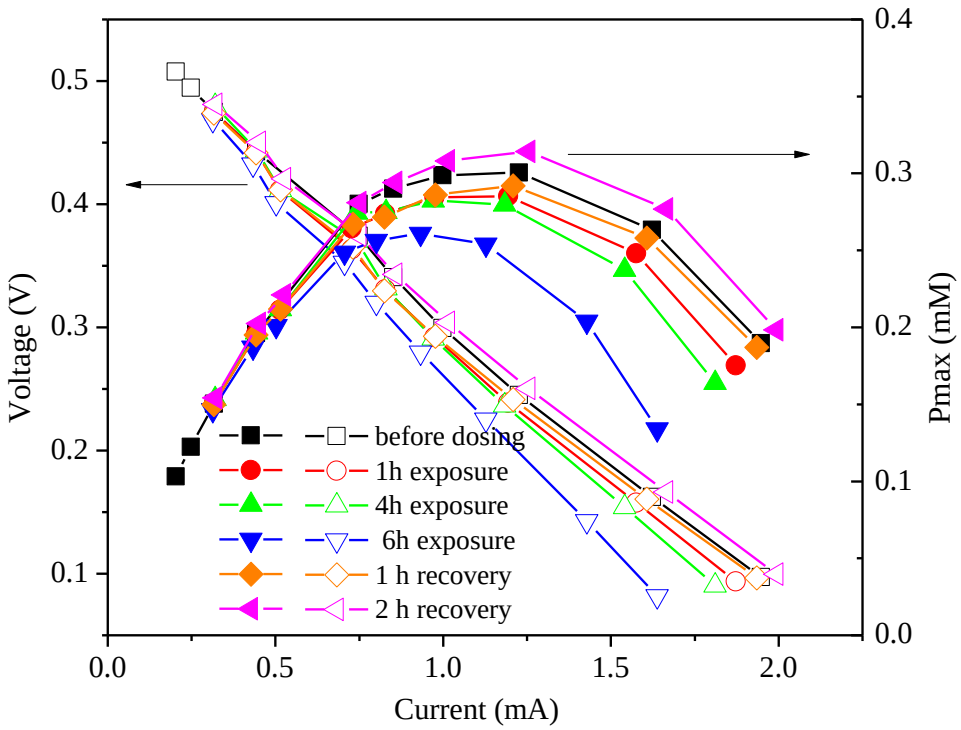

Figure 6.1. Polarization curve (open symbols) and power-current curve (closed symbols) before dosing (S-0) (□); at time 1st h (S-1) (○), 4th h (S-4) (△), 6th h (S-6) (▽) exposure of 10 ppm Cd(II); and at time 1st h (S-7) (◇), 2nd h (S-8) (◁) recovery.

Although polarization curves are useful for rapid investigation of MES behavior and are the direct way to determine the current generation of the MESs, the drawback of polarization curves is that they do not provide further detailed information about the composition of the internal resistance. CV and EIS were studied to better understanding the intrinsic reasons behind.

6.2.1.2 CV analysis

CV has been used for assessing the electrochemical activity of the microbial biofilm of MFCs in many studies (Logan et al., 2006; Kim et al., 2002; He et al., 2005; Liu et al., 2005b).The occurrence of the oxidation/reduction peak in the CV showed the electrochemical activity and the size of the peak indicated the quantity of the redox

active component involved in the current generation (Fricke et al., 2008,; Nicholson, 1965; Marsili et al., 2008; Allen and Larry, 2001).

In Fig. 6.2a, the oxidation peak was observed at 0.3 V before the MES was exposure to Cd(II), showing the electrochemical activity of the bacteria and gave a baseline of the CV in a control condition. The peak was not so distinctive compared to some of the studies where pure culture such as *Geobacter sulfurreducens* (Katuri et al., 2010) or *Shewanella putrefaciens* (Kim et al., 2002) was involved or excreted metabolites (Rabaey et al., 2004a) were extracted which redox components concentrations were all high. In this study, mixed culture was used and the lower peak intensity showed that the concentration of the involved redox species was low due to the complexity of the mixed culture anodic biofilm. For the MESs were exposed to the 10 ppm of Cd(II), no oxidation/reduction peak was observed regardless of the exposure time (1 to 6 h of exposure) (Figs. 6.2b to d), suggesting that the electrochemical activity of the bacteria was inhibited due to the exposure to Cd(II). After the injection of Cd(II) was stopped, the peak reappeared (Figs. 6.2e and f), indicating the recovery of the electrochemical activity of the bacteria.

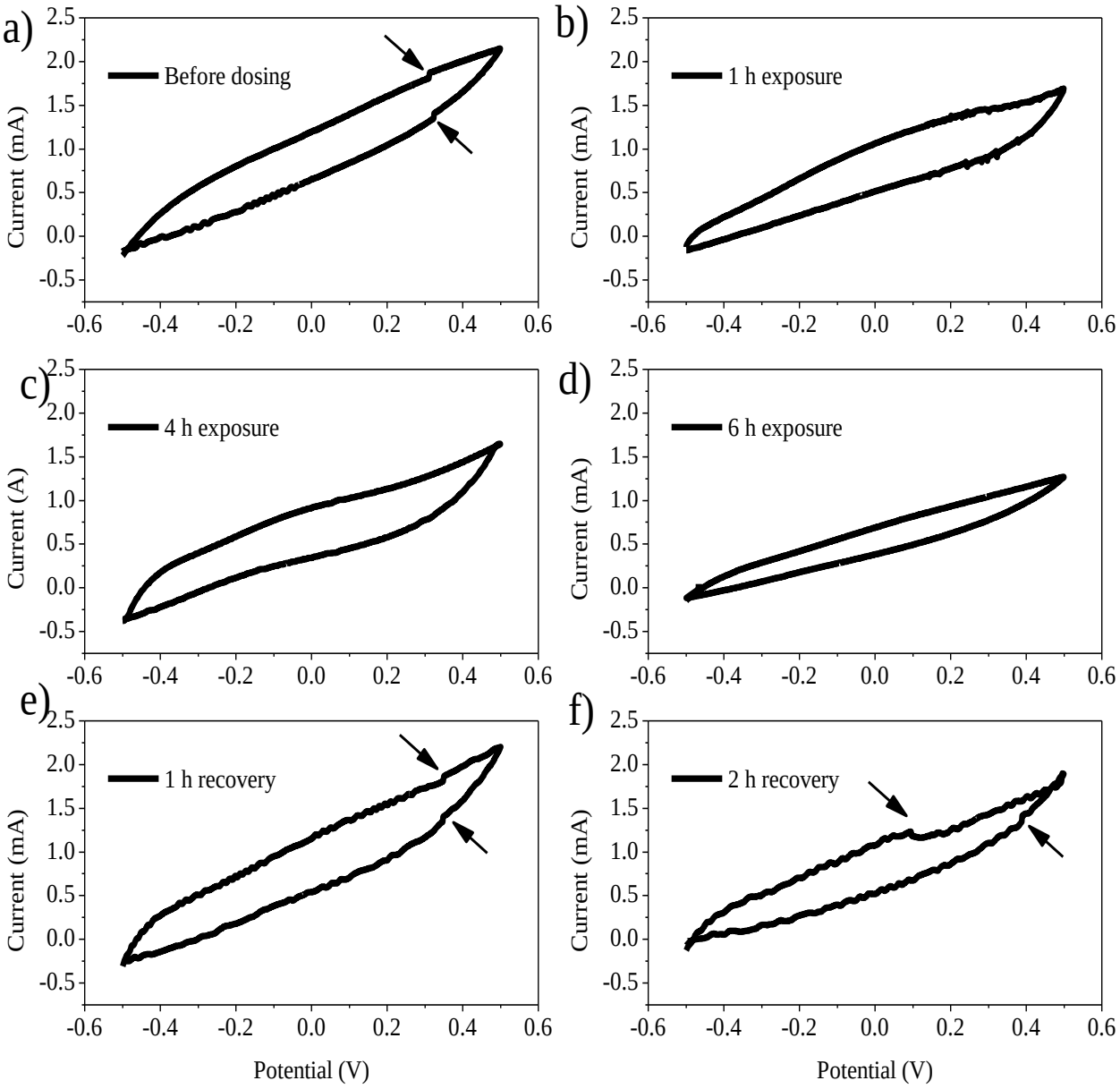

Figure 6.2. Cyclic voltammograms of the MESs taken before exposure to 10 ppm of Cd(II) (a), after 1 h (b), 4 h (c) and 6 h of exposure to 10 ppm of Cd(II), and after 1 h of recovery (e) and 2 h of recovery (f). Arrows indicated the oxidation/reduction peak.

6.2.1.3 EIS analysis

EIS measurement provide information on ohmic resistance (R_s) as well as polarization resistance (R_p) (or charge transfer resistance), which is affected by the kinetics of the electrode reaction. The Bode plot shows the impedance at different frequencies and

the low- and high-frequency data can be easily determined from the plot, representing R_p+R_s and R_s, respectively (He and Mansfeld, 2009). EIS was conducted here to identify the polarization resistance produced by different toxicant exposure time and toxicant kind. The tests were conducted in the two-electrode mode, in which the anode served as the working electrode and the cathode acted as both reference and counter electrode. It was assumed here that the variation of the electrochemical characteristics of the whole cell was due to the anode conditions since the cathodic potentials were almost identical in all cases due to the use of the same electron acceptor (Yuan et al., 2011).

Fig. 6.3 shows the Bode plots measured at different Cd(II) exposure time and recovery time. It could be seen that the impedance at high frequency of 10^6 Hz was all around 300 ohm among different toxicant exposure times, showing that the toxicant exposure did not affect the R_s. This is reasonable since ohmic losses in an MES are resulted from the resistance to the electrons flow through the electrodes and interconnections, and the ions flow through the membrane and the electrolytes (Logan et al., 2006), which are irrelevant with the toxicants effect.

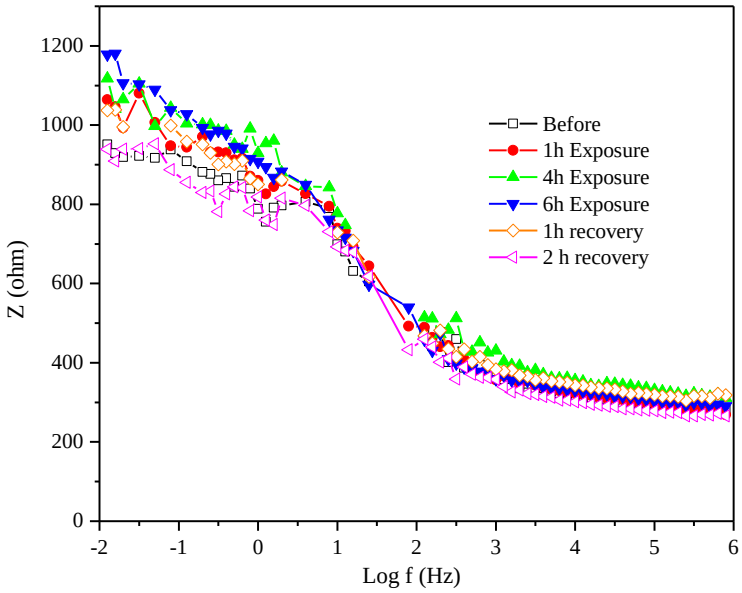

Figure 6.3. Bode Plot of the impedance of the MESs taken before exposure to 10 ppm of Cd(II) (□); at time 1st h (S-1) (○), 4th h (S-4) (△), 6th h (S-6) (▽) exposure of 10 ppm Cd(II); and at time 1st h (S-7) (◇), 2nd h (S-8) (◁) recovery.

It could be seen from Fig. 6.3 that the impedance at lower frequency of 10^{-2} Hz showed variation among different toxicant exposure times, meaning that R_p+R_s was affected by the toxicant. Since R_s was unchanged as shown above, it could be concluded that the change of the impedance at lower frequency was mainly due to the change of R_p and it was easy to calculate from the plot on how R_p was affected by exposure of the MESs to Cd(II). The R_p was calculated from the graph and shown in Fig. 6.4.

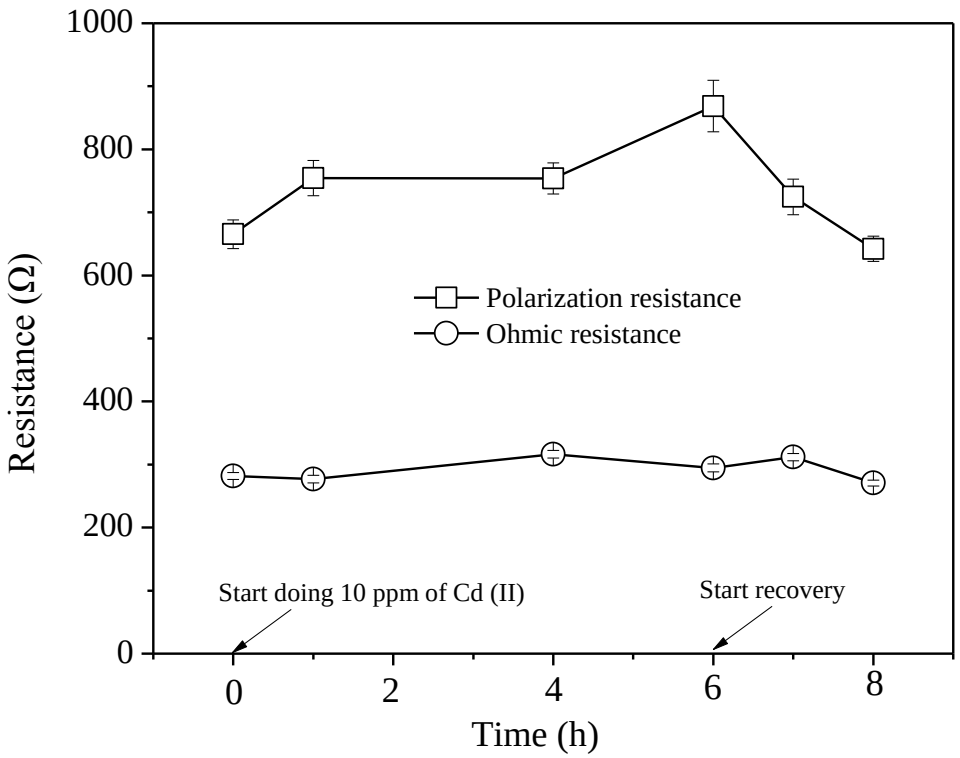

Figure 6.4. The change of polarization resistance (□) and ohmic resistance (○) with time of MESs exposed to 10 ppm of Cd(II) at time 0 and recovery started at the 6th h. The result was calculated from the Bode Plot from Fig. 6.3.

As shown in Fig. 6.4, before the toxicant exposure, the R_p of the MESs was 650 Ω and it increased to 750 Ω after 1 h exposure to Cd(II), was further increased to 800 Ω after 4 h of exposure and maximized at 900 Ω after 6 h of exposure to Cd(II). Once the recovery started, as shown in the last chapter, the current of the MESs showed immediate increase. The R_p started to decrease as well and it could be seen that it decreased to 750 Ω after 1 h of recovery and further decreased to 650 Ω, which was the same as it was before the toxicant exposure. The results were consistent with the above results measured by PC where small changes of the R_{int} were observed.

The polarization resistance (R_p) has been shown to be related with the bacterial electrochemical activity and the variation of the R_p reflected the change of the anodic microbial catalysis of the organic substrates (He et al., 2008). The higher the R_p, the

weaker the anodic bacterial activity is involved in the electricity generation. Thus it could be seen that exposing MESs to the toxicant inhibited bacterial electrochemical activity that might be through influencing the enzymatic activity of the bacteria. The toxicant might induce damage of the enzymes that are used for electron generation or transfer (ter Heijne et al., 2008) and thus led to a higher $R_{p,}$ resulting in the current drop.

R_p increased with increasing exposure time, indicating that the longer the exposure time, the more the electrochemical activity of the bacteria was inhibited. When the recovery started, the R_p started to decrease, showing that the electrochemical activity restored when toxicants were removed. After 2 h of recovery time, the R_p decreased back to the same as it was before toxicant exposure, which was consistent with the finding in last chapter that after 2 h, the complete recovery of the current could be seen. This showed that the inhibition effect of the metal toxicant on the electrochemical activity of the bacteria was temporarily and further proven the advantage of the MES on good recovery ability.

The measurement at low frequency region was not as stable as the impedance at high frequency, which is common in the EIS measurement of MES\s since impedance measurements at low frequencies usually require a long measurement time, and it is more difficult to keep the MES stable during the measurement (Fan et al., 2008; ter Heijne et al., 2008). However, it still reflected the trend of how toxicant exposure affected the bacterial activity.

EIS was also conducted to identify the polarization resistance produced by different toxic metals. Fig. 6.5 showed the EIS analysis of the MESs at the 6th h exposure to

different metal toxicant of Cd(II), Cu(II), Zn(II) and Ni(II) at the same concentration of 10 ppm. Both of the impedance at low- and high-frequency showed no significant difference among different toxicant types. The R_s (low-frequency impedance) of all of the toxicant cases were kept at 300 Ω since the toxicant did not affect any factors that determine the ohmic resistance. The R_p achieved from the high-frequency impedance was all around 900 Ω, indicating that the electrochemical activity was inhibited to the same extent by the different heavy metals. It was consistent with the results shown in the last chapter that the current inhibitions at 10 ppm of those metals toxicants were all around 75-95%.

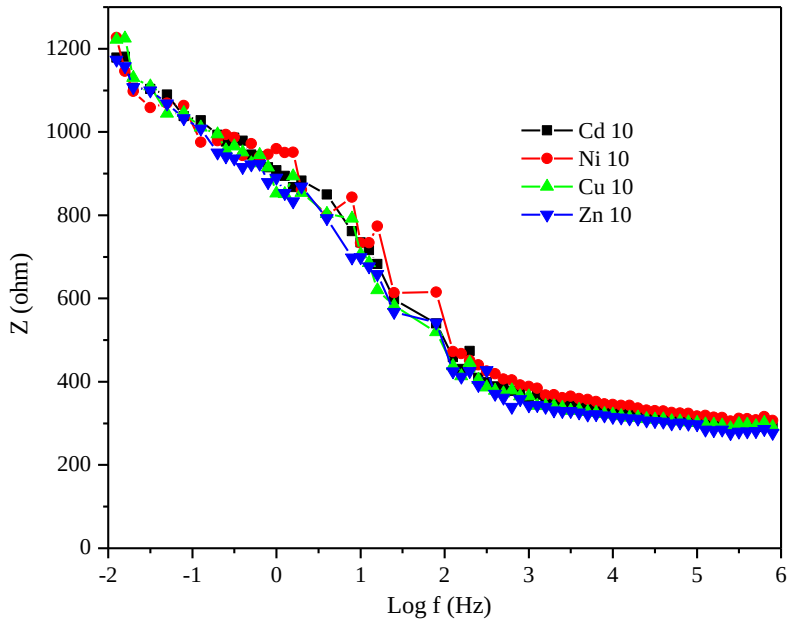

Figure 6.5. Bode Plot of the impedance of the MESs taken at the 6th h exposure to 10 ppm of Cd(II) (□); 10 ppm of Ni(II) (○), 10 ppm of Cu(II) (△), and 10 ppm of Zn(II) (▽).

6.2.2 Biological analysis

6.2.2.1 Preliminarily result of biofilm developed on the anode in the absence of toxicant

SEM, CLSM, DGGE were used to characterize the electroactive microbial biofilm developed in our MES in terms of structure, viability and communities. Biofilms were analyzed by SEM to characterize their biofilm structure and morphology. SEM micrograph (Fig. 6.6a) showed that biofilms completely coated the fibers of the carbon cloth anodes and were visually dense. Bacteria obtained from the MES appeared to be predominantly rod shaped and were embedded in extracellular polymeric substances (EPS). These cells were also seen in the CLSM micrographs as shown in Fig. 6.6, which showed the viability staining result of the three points of the same biofilm and they were the layers closest to the anode. High similarity between the three duplicates existed. The green fluorescing shown were the viable cells and the red fluorescing were the dead cells. It could be seen that cells closest to the anode were primarily green, indicating that the preponderance of cells on the surface of anode were viable and metabolically active. The result was consistent with the researches done by Nevin et al. (2008). The horizontally oriented dark areas could also be observed in Fig. 6.6, which were presumed to be voids that allow fluid flow.

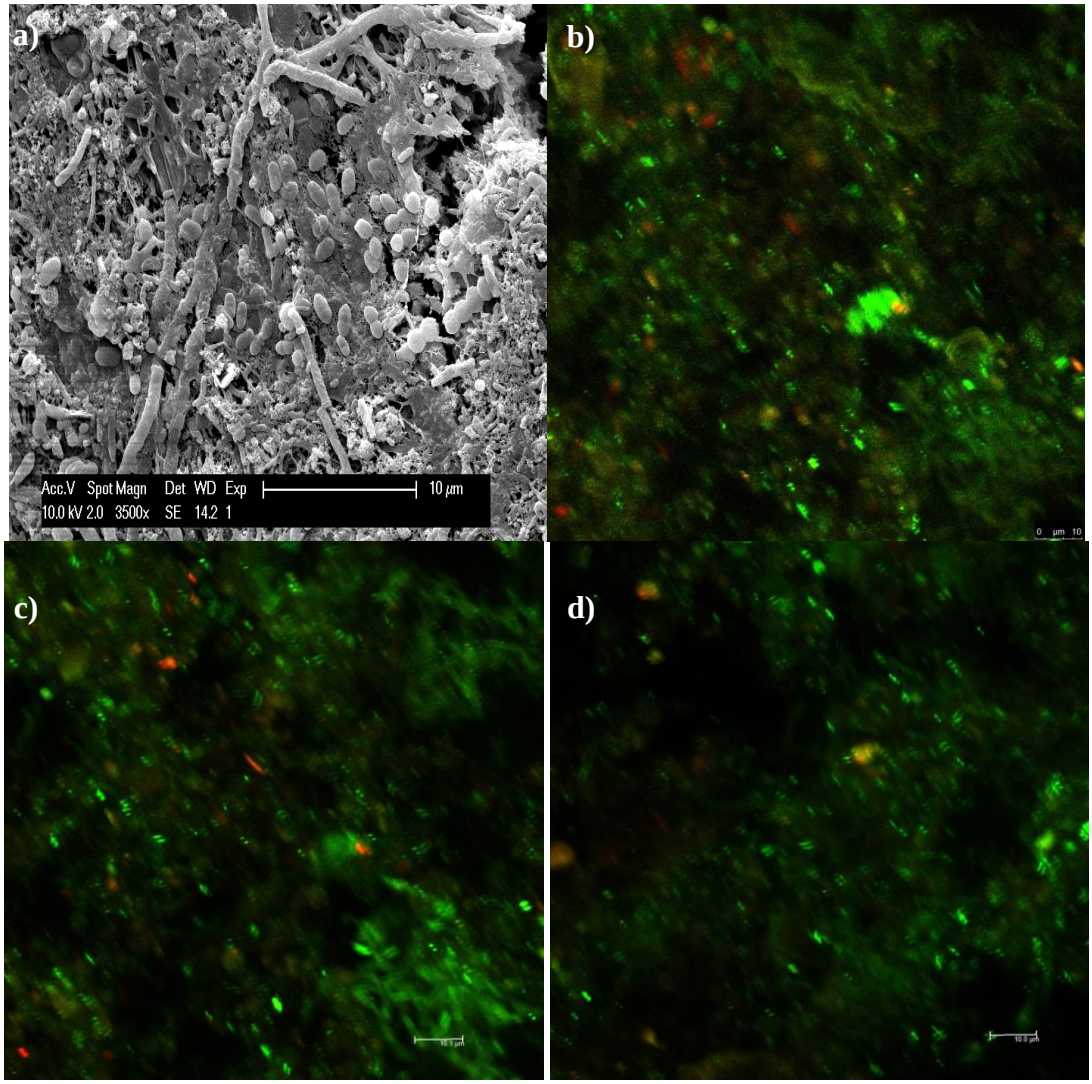

Figure 6.6. Imaging of the anodic biofilm; (a) SEM of the anodic biofilm; (b) (c) (d) CLSM image of the three different points of the same biofilm. Dead cells were stained red with propidium iodide, while live cells were stained green with SYTO9 by using the *Bac*Light LIVE/DEAD viability stain. The micrographs were taken with the CLSM. Solid white line bar indicates the length measurement of 10 µm.

The quantification of the viability of the cells through the CLSM image was done with COMSTAT software (Heydorn et al., 2000) and the results are shown in Fig. 6.7. The majority of the cells (86 to 94%) were live and good repeatability was seen among three different points of the same MESs.

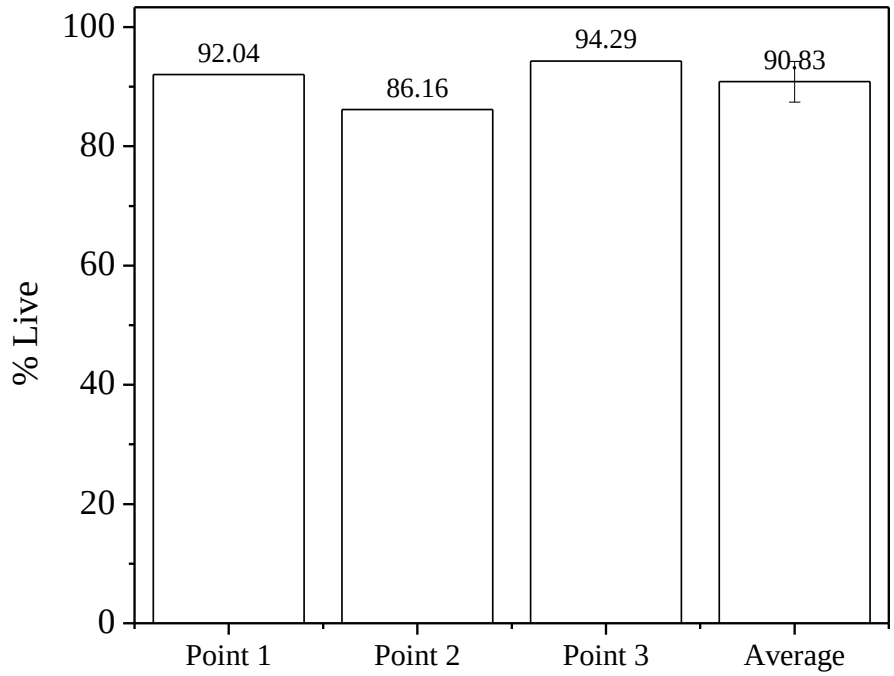

Figure 6.7. COMSTAT calculation of the live ratio of the three different points of a same biofilm from the CLSM image (Fig. 6.6). Average live ratio of the three points was also shown.

DGGE and sequencing were used to investigate the dominant species of the anodic microbial community of the anodic biofilm and Fig. 6.8 showed the DGGE result of the two points of the biofilm from the MES with channels and two obvious bands were shown in the DGGE which were cut for the sequencing. The sequencing analysis of the bacterial communities showed that the dominant species of anodic microbial community of the MFC (Table 6.1) were *Geobacter pickeringii* and *Geobacter uraniireducens.* Microorganisms in the family *Geobacteraceae* has been reported in many researches that they can oxidize organic compounds with electrodes serving as the sole electron acceptor and transfer electrons directly to the electrode surface, harvesting electricity from aquatic sediments and other sources of waste organic matter (Bond and Lovley, 2003; Gregory et al., 2004). This DGGE pattern was used as control in the following studies.

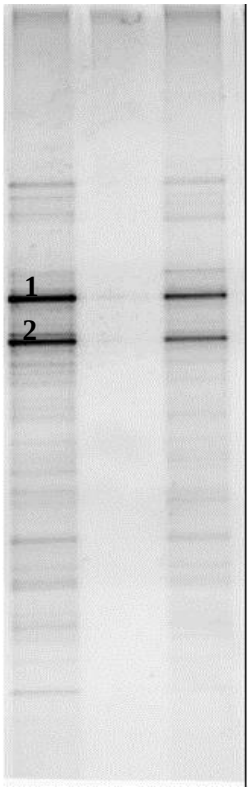

Figure 6.8. DGGE pattern of the microbial community of MFC. The bands representing a sequenced clone are numbered from 1 to 2. The names of the organisms corresponding to the numbered bands can be found in Table 6.1.

Table 6.1 Overview of the microorganisms corresponding with the sequenced bands on the DGGE represented in Fig. 6.8. The bands which were cut out and sequenced are numbered from 1 to 2.

Band number	Organism	% similarity
1	*Geobacter pickeringii*	99
2	*Geobacter uraniireducens*	93

It could be concluded that the rod shaped cells on the anode, which were 90% alive, were dominated by *Geobacteraceae*. All of the results could be connected together and this suggested that it was possible to use the CLSM to examine the viability of the cells that were involved in the current generation.

The big advantage of the CLSM was that it could be used to analyze the distribution of the live/dead ratio within the whole biofilm range (Fig. 6.9). The two fluorescent

stains (SYTO 9 dye and propidium iodide) revealed that live bacteria were distributed throughout the biofilm area and depth. The exterior of the biofilms had a substantial percentage of red cells whereas cells closest to the anode were primarily green, indicating that the live population was preferentially located in direct contact with the anode surface, and that the dead cells were present primarily in the upper biofilm layers.

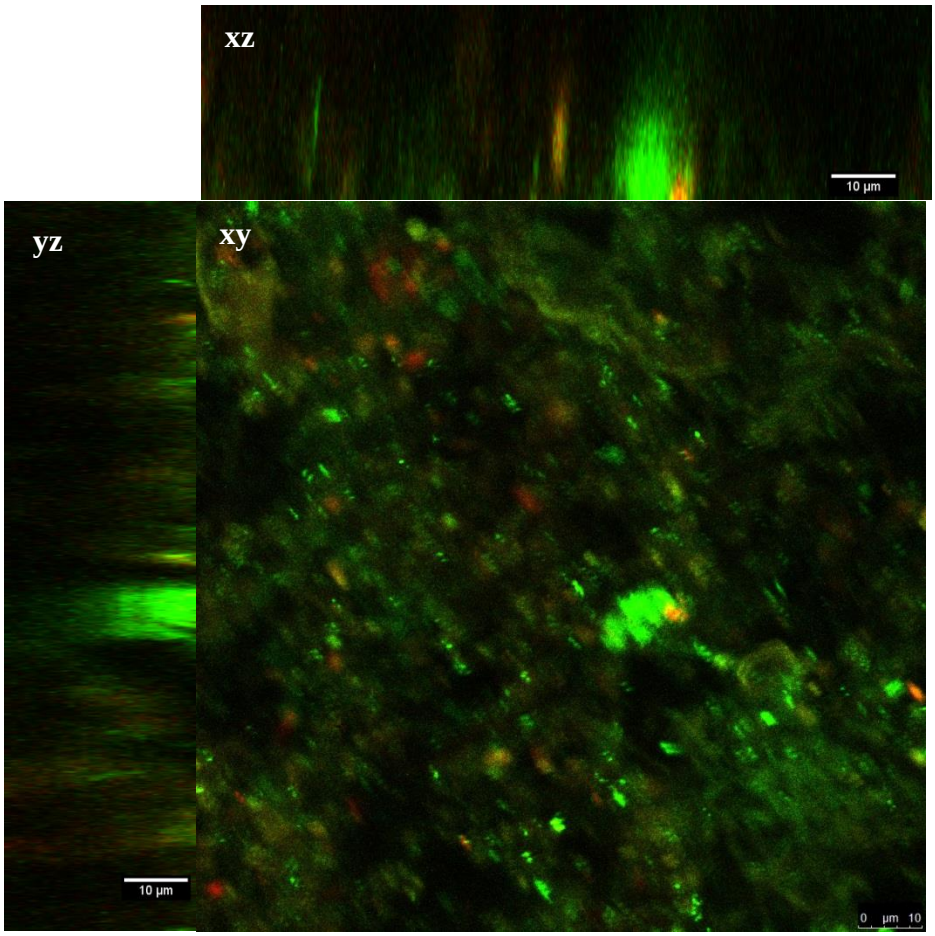

Figure 6.9. Confocal laser scanning microscopy of anode biofilm. Large panel single slice through biofilms xy top view, top (xz) and left (yz) panels perpendicular slices. With the substratum to the right and bottom. Dead cells were stained red with propidium iodide, while live cells were stained green with SYTO9 by using the *Bac*Light LIVE/DEAD viability stain. The micrographs were taken with the CLSM. Solid white line bar indicates the length measurement of 10 µm.

COMSTAT evaluation of the biofilms verified the qualitative examination of the live/dead distribution within the biofilms (Fig. 6.10). The highest live ratio (80%) was

observed at the surface of the electrode (0 μm as shown in Fig. 6.10) of the whole biofilm. With the increasing distance from the anode surface, the live ratio started to decrease slowly and turned to be stable at 75% percentages for some distance (5 to 15 μm). The outer layers of the biofilm had decreased percentages of live cells (50% for the outer-most layer). The result was consistent with some of the studies, for example Read et al. (2010) also revealed a notable increase of the non-viable cells away from the anode. Marcus et al. (2007) concluded that the electroactive microbial biofilm only persist up to tens of micrometers away from the anode and inhabit the inner layer of the biofilm.

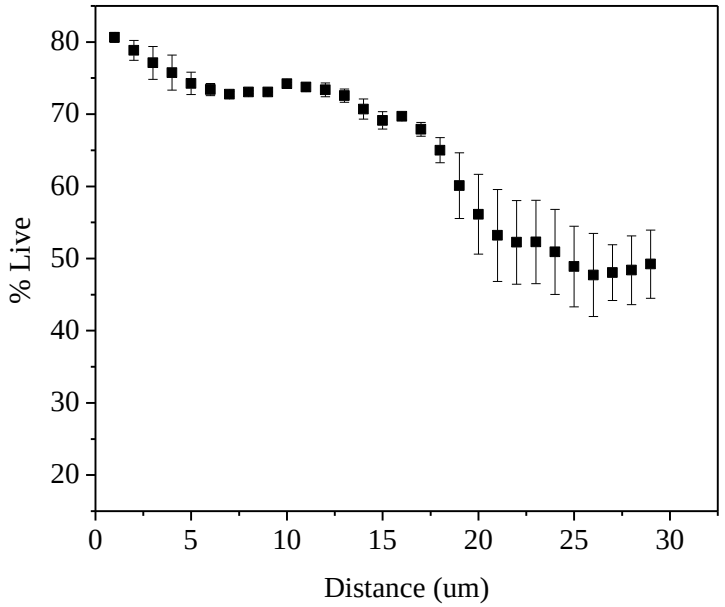

Figure 6.10. Quantification of live and dead cells as determined by using COMSTAT to estimate the the distribution of the live cells ratio within the whole biofilm range. The substratum layer started at the 0 μm.

6.2.2.2 Cd (II) distribution within the biofilm

To study the Cd(II) penetration and distribution within the biofilm at different exposure time to 10 ppm of Cd(II), the biofilm were stained with the green-

fluorescent Leadmium reagent and Cd(II) distributions in the biofilm were examined under CLSM as shown in Fig. 6.11. Cd(II) is in fluorescent green.

It could be seen that during the exposure to Cd(II) regardless of the exposure time, Cd(II) was observed in the interior of the biofilm. Once the recovery started, the signal from the penetration of Cd(II) into the biofilm was significantly reduced during the first hour and after 2 h, it was almost completely washed out of the interior of the biofilm.

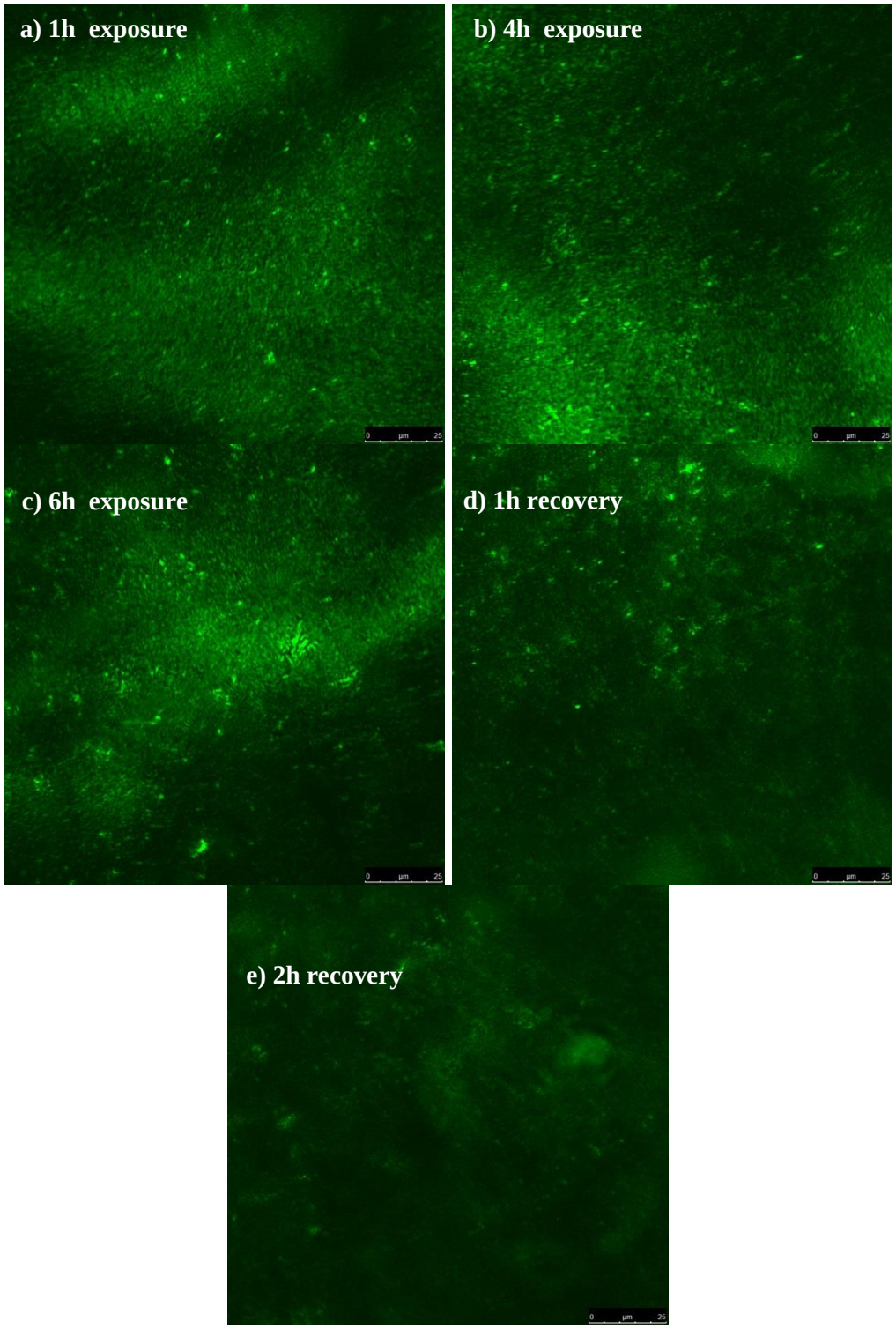

Figure 6.11. CLSM image of the Cd(II) distributions on the anodic surface (a) at at time 1st h (S-1) (b), 4th h (S-4), (c) 6th h (S-6) exposure of 10 ppm Cd(II), and (d) at time 1st h (S-7), (e) 2nd h (S-8) recovery. Cd(II) was stained green with The Measure-iT Assay kit. Solid white line bar indicates the length measurement of 25 µm.

6.2.2.3 Viability under exposure to toxicants

The biofilm samples taken at different exposure time to 10 ppm of Cd(II) were analyzed by two-component fluorescent stain BacLight and examined under CLSM to investigate the cell viability. A visual comparison of the interior layer of the anodic biofilm and the vertical profile of the biofilm (yz section) were presented in Fig. 6.12. Quantitative comparisons achieved by COMSTAT (Heydorn et al., 2000) were given in Fig. 6.13. In all the sampling cases in the presence of 10 ppm of Cd(II), the viability of the interior anodic biofilm was kept around 85%, as which was the case without of Cd(II). This showed that the short-term exposure to Cd(II) did not affect the interior cell viability. This finding was consistent with Teitzel and Parsek (2003) in which after 12 h of Cu(II) or Zn(II) treatment, the cells buried in the depths of the biofilm were still primarily alive. With the fact that the electroactive microbial biofilm only persist up to tens of micrometers away from the anode and inhabit the inner layer of the biofilm (Marcus et al., 2007), it could be concluded that the decrease of the current was not related with the viability of the cells that were engaged in the current generation since the viability was not affected by the Cd(II).

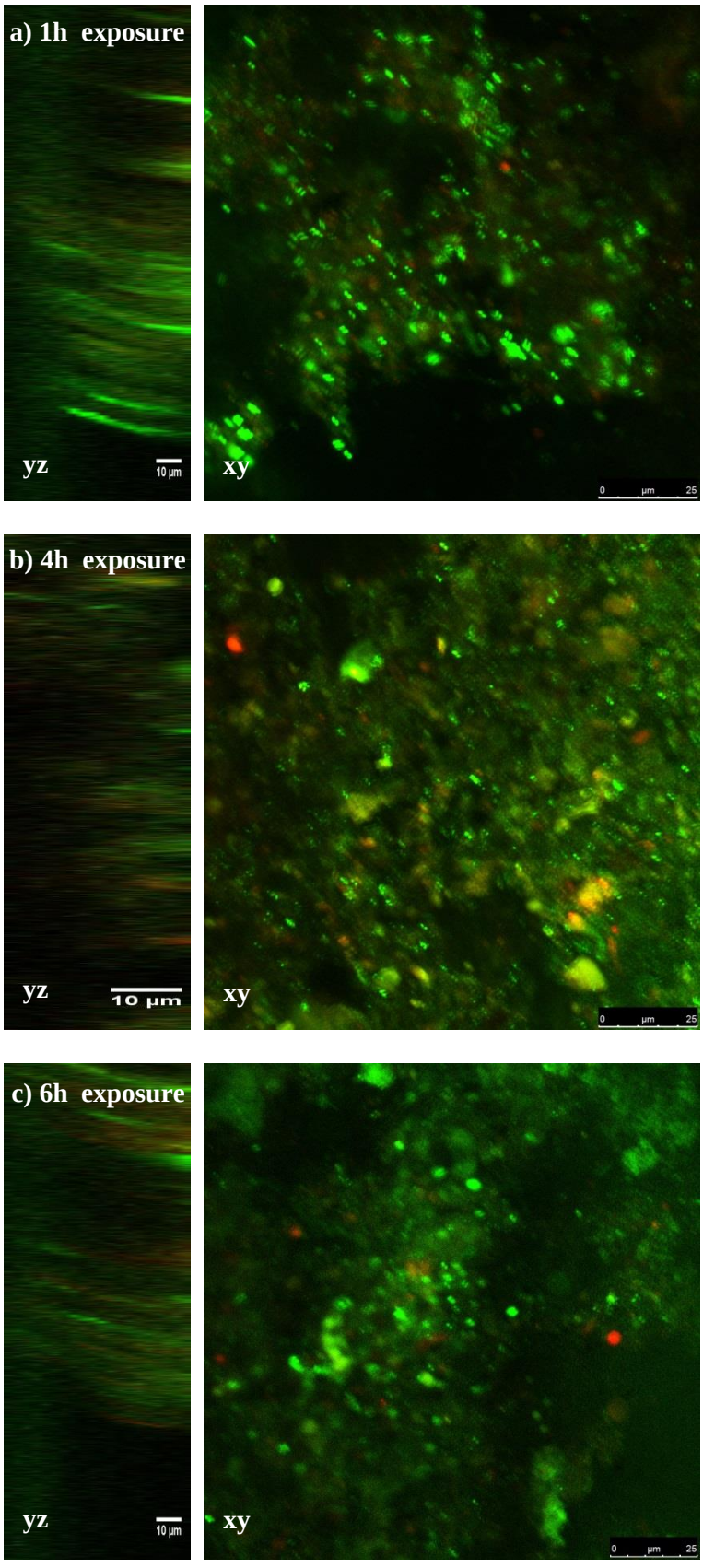
a) 1h exposure
yz
10 µm
xy
0 µm 25
b) 4h exposure
yz
10 µm
xy
0 µm 25
c) 6h exposure
yz
10 µm
xy
0 µm 25

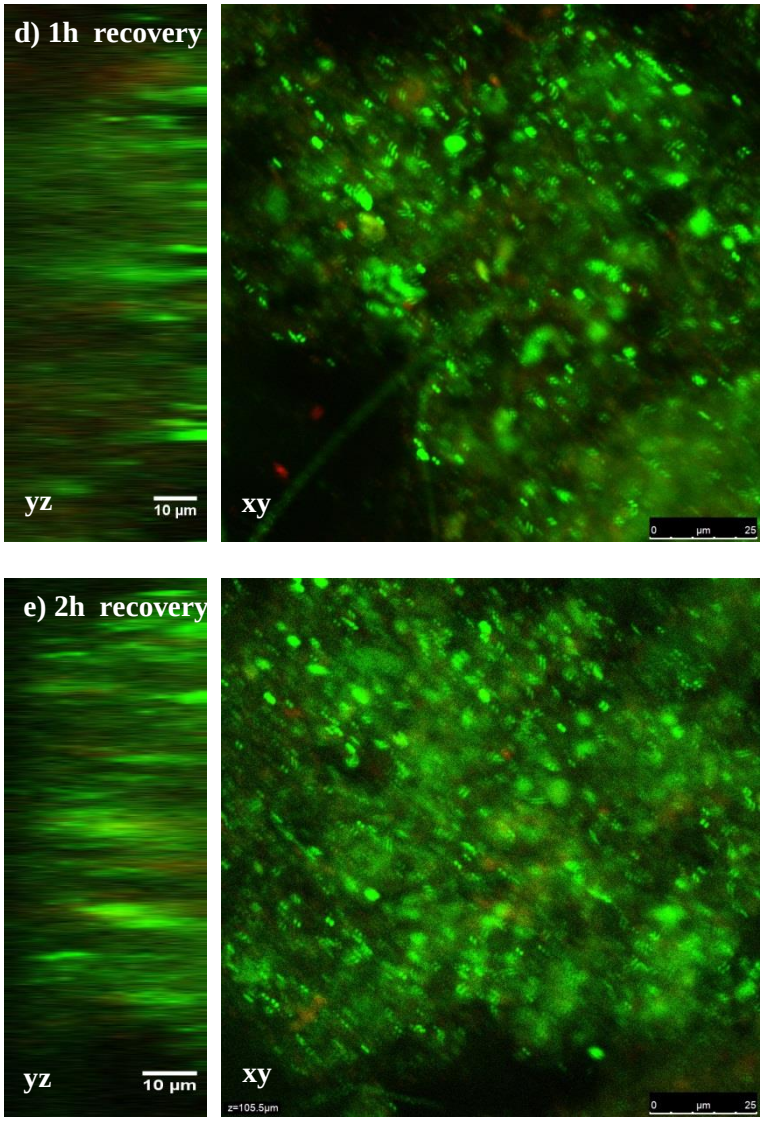

Figure 6.12. Confocal image stacks illustrating the biofilm of the MESs taken at time 1st h (S-1) (a), 4th h (S-4) (b), 6th h (S-6) (c) exposure of 10 ppm Cd(II), and at time 1st h (S-7) (d), 2nd h (S-8) (e) recovery.

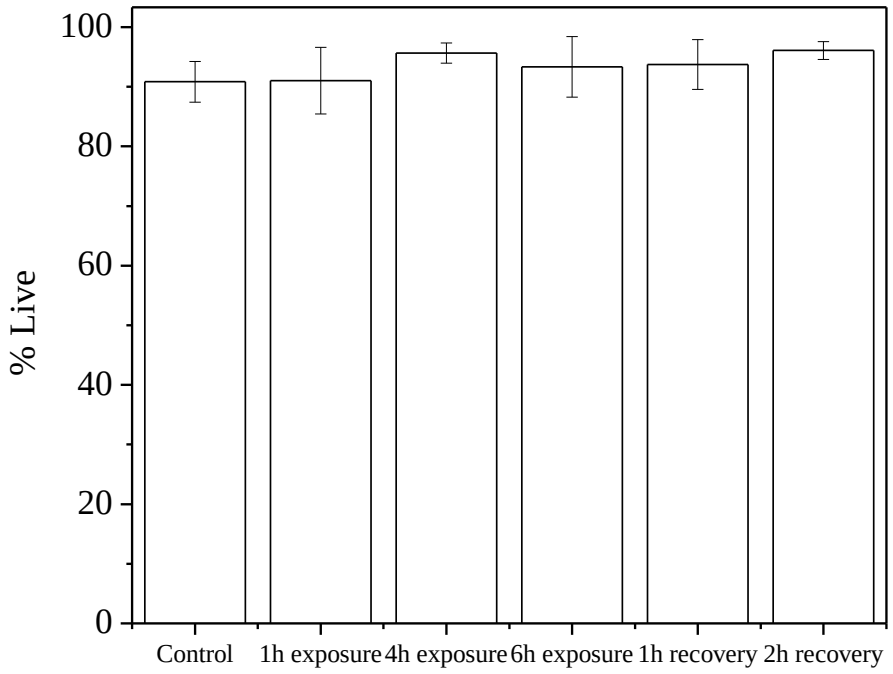

Figure 6.13. Quantification of live and dead cells on the surface of the anode as determined by using COMSTAT to analyze the CLSM images in Fig. 6.12.

6.2.2.4 Microbial Community Studies

DGGE patterns of the individual MESs at different exposure time to 10 ppm of Cd(II) and recovery point were used to investigate the microbial community change (Fig. 6.14). The dominant strains were found the same between the three duplicates, which were sampled at different locations of the same biofilm (top, middle and bottom), showing that the bacteria species were uniform among the whole biofilm. The two bands (*Geobacter pickeringii* and *Geobacter uraniireducens*), dominated in the control MESs as shown in Fig. 6.8, appeared in almost all of them (Fig. 6.14), proving that short term exposure to the toxicant did not change the dominance of the *Geobacteraceae*, also indicating that the drop of the current was not due to the change of the bacteria species.

Other obvious bands also existed in the DGGE profiles of some samples marked by the green numbers, which were further excised and sequenced, and the results are summarized in Table 6.2.

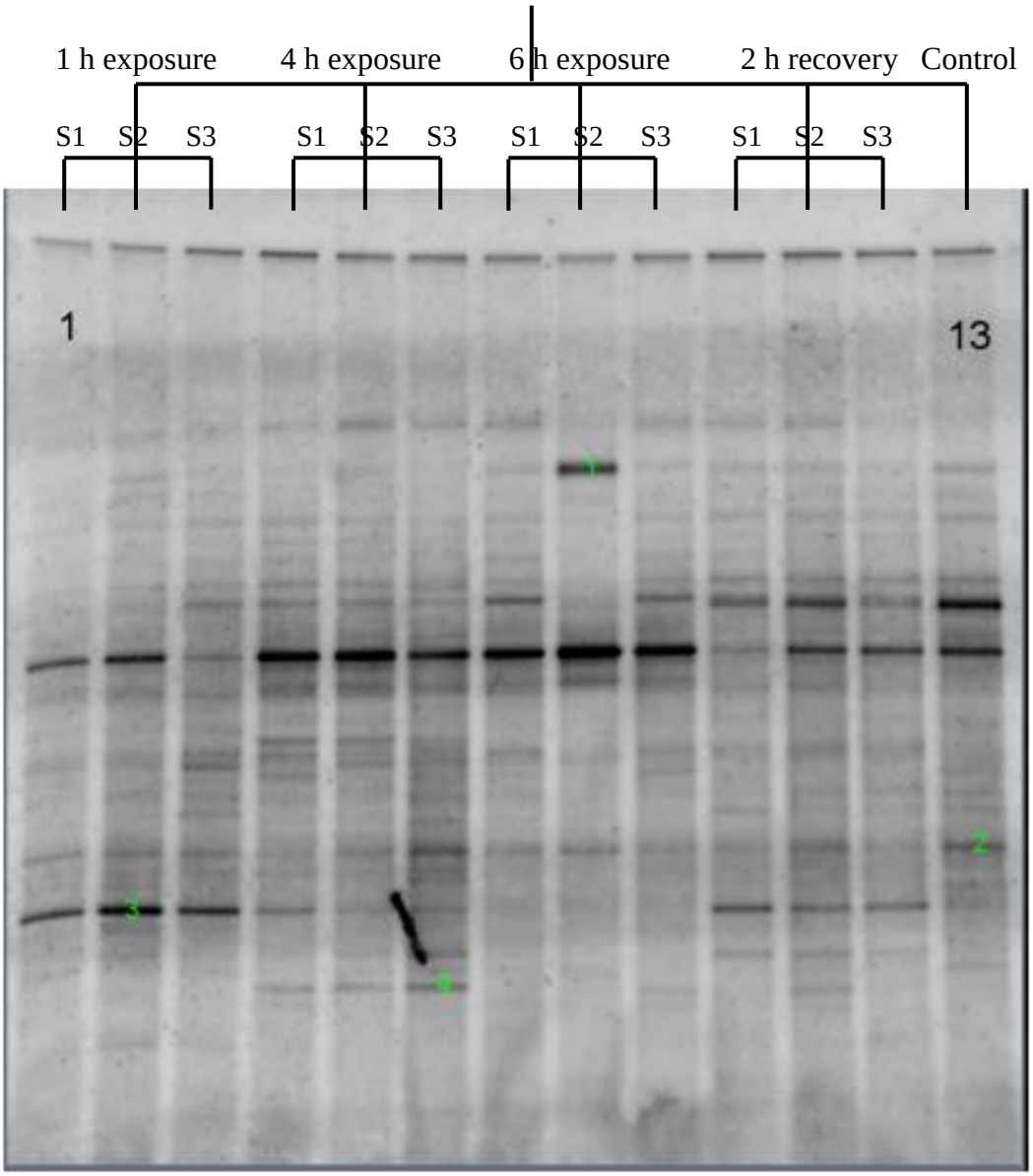

Figure 6.14. DGGE pattern of the microbial community of MESs at time 1st h, 4th h, 6th h exposure of 10 ppm Cd(II); and at time 2nd h recovery. For each condition, three different points of the same biofilm were analyzed. The DGGE profile from the control MES was also included. The bands, which were cut out and sequenced, were numbered from 1 to 4 in green. The names of the microorganisms corresponding to the numbered bands can be found in the following Table 6.2.

Table 6.2 Overview of the microorganisms corresponding with the sequenced bands on the DGGE represented in Fig. 6.14. The bands which were cut out and sequenced are numbered from 1 to 4.

Band number	Organism	% similarity
1	*Paludibacter propionicigenes*	92%
2	*Desulforhabdus amnigena*	92%
3	*Syntrophorhabdus aromaticivorans*	97%
4	*Syntrophorhabdus aromaticivorans*	95%

The DGGE and sequencing analysis of the bacterial communities in the MESs before and after 2 years of operation showed that the dominant strains of the MESs after 2 years of operation was almost the same as that before. No significant shifts in the band pattern were observed with time (Fig. 6.15), which explained the advantage of the long-term stability of the MESs.

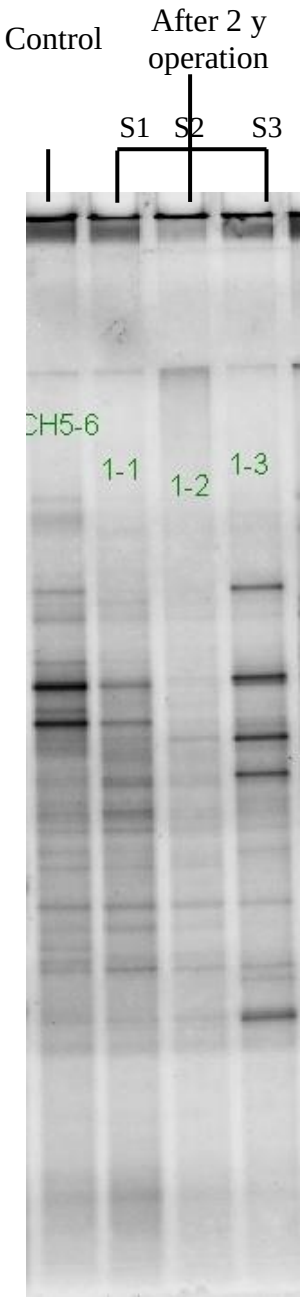

Figure 6.15. DGGE pattern of the microbial community of MESs before (control) and after 2 years operation (three samples were taken as duplicates).

6.2.3 Heavy Metal Concentration

Studies have shown that the available fraction of heavy metals mainly decided the mobility, bioavailability and toxicity of heavy metals (Rauret, 1998). Therefore, the quantification of different chemical fractions of heavy metals in the wastewater and biofilm is necessary for information on metal toxicity. In the present study, the partition of five heavy metals (Cd(II), Pb(II), Cu(II), Zn(II) and Ni(II)) between the dissolved and the particulate phase (precipitation and adsorption) was examined. The mass balances of individual metals were calculated to study the fate of those metals entering the MESs.

6.2.3.1 Distribution of the metals between the dissolved and the particulate phase of wastewater

The distribution of a given metal between the soluble and solid phases are affected by the following mechanisms as suggested by Kodukula et al. (1994): (i) complexation of metal with ligands in the soluble phase; (ii) inorganic metal salt precipitation; and (iii) sorption of metal onto surface sites of the sludge particles. Biological uptake could also be a mechanism; however, the process is rather slow and insignificant compared with the other mechanism influencing metals distribution and thus it is not considered here. The measurement of complexation is difficult and metals in the form of hydrated ions, labile organic and weak inorganic ligands such as chloride, sulfate, carbonate etc., might also contribute to toxicity by dissociating into free form, thus complexation is not discussed here. The distribution of metals between the aqueous and the solid phase (precipitation and sorption) of wastewater was investigated.

The following two mass balance equations were modified from Chang et al. (2006) to investigate the relative roles of biosorption and precipitation of the metals. Equation 6.1 differentiated the total metal mass in wastewater into its species including both biosorption and precipitation

$$MT = MS_1 + MB + MP \quad (6.1)$$

where MT is the total mass of metals, MS_1 is the mass of metals in solution which could be experimentally analyzed, MB is the mass of biosorbed metals, and MP is the mass of precipitated metals. Control samples containing only the filtrate from the wastewater were conducted to evaluate the precipitation effects. The mass balance in the control samples where only precipitation occurred is as follows:

$$MT = MS_2 + MP \quad (6.2)$$

where MS_2 is mass of metals in solution in control samples. Combining Eqns. 6.1 and 6.2, the biosorbed fraction of metals could be obtained from the following equation:

$$MB = MS_2 - MS_1 \quad (6.3)$$

According to the above method, the distribution of the five heavy metals (Cu(II), Ni(II), Zn(II), Cd(II) and Pb(II)) at an initial metal concentration of 10 ppm between the dissolved and the particulate phase of wastewater was calculated and presented in Fig. 6.16. The phase distribution of individual metals exhibited large difference among various metals. Ni(II) was found primarily in the dissolved phase (60%) as expected due to the high mobility of this metal (Karvelas et al., 2003; Sörme and Lagerkvist, 2002). Cd(II) was also found strongly associated with the dissolved phase (45%). But precipitation and adsorption effect contributed differently to the particulate phase for Ni(II) and Cd(II). In the case of Ni(II), precipitation effects (20%) contributed the same as the adsorption effect (20%). While in the case of

Cd(II), no precipitation was observed and adsorption effect (55%) was the main cause. On the contrary, Pb(II) exhibited strongest association with particles and was hardly left in the soluble state (<1%). Large percentage of it (>90%) were precipitated and the left were adsorbed. Cu(II) and Zn(II) exhibited moderate association with particles (7-12% dissolved) compared to Pb(II), yet stronger interaction compared with Ni(II) and Cd(II).

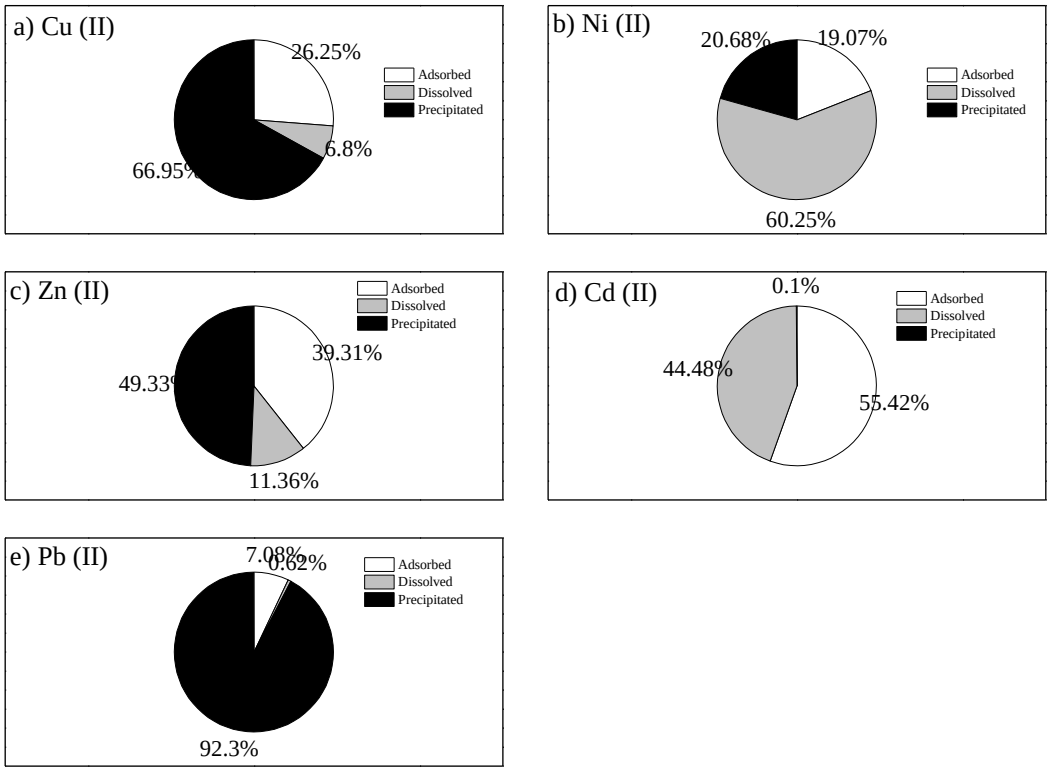

Figure 6.16. Metal distribution in the wastewater for a total metal concentration of 10 ppm (a) Cu(II), (b) Ni(II), (c) Zn(II), (d) Cd(II) and (e) Pb(II). (TSS = 140 ppm; pH= 7.2).

The phase distribution appeared to be metal-specific, suggesting that metals are present in different chemical forms with different water solubility in wastewater. The result was consistent with some of the researches, in which the same order of the solubilities of heavy metals were observed: Pb(II) < Cu(II) < Cd(II) (Brown and Lester, 1979), whereas Jenkins et al. (1981) found the order to be

Cu(II) < Pb(II) < Cd(II) < Zn(II). Conflicting evidence in the literature regarding the relative roles of precipitation and sorption mechanisms in metals distribution seems to be common. The solubility products of heavy metals reported in the literature vary markedly in a complex system such as that of the wastewater and direct application of those theoretical solubility products may not be appropriate. Thus more detailed study on the precipitation and adsorption was necessary, which are discussed in next section.

Precipitation effect

The precipitation effect of metals was assessed by monitoring the metal concentration in the filtrate from the wastewater. The filtrate of the wastewater was obtained by filtering the domestic wastewater with a 0.45-μm membrane filter. Linear relationship could be seen in all the four metal cases (Cd(II), Cu(II), Zn(II) and Ni(II)) (Fig. 6.17). Cd(II) added in initial stages remained completely in solution and no precipitate was observed. In the case of Ni(II), the soluble metal concentration was lower than in the case with Cd(II), and for the case of Zn(II) and Cu(II), it was even lower. Thus the solubility of the metals inside the wastewater followed the following order: Cd(II) > Ni(II) > Zn(II) ~ Cu(II).

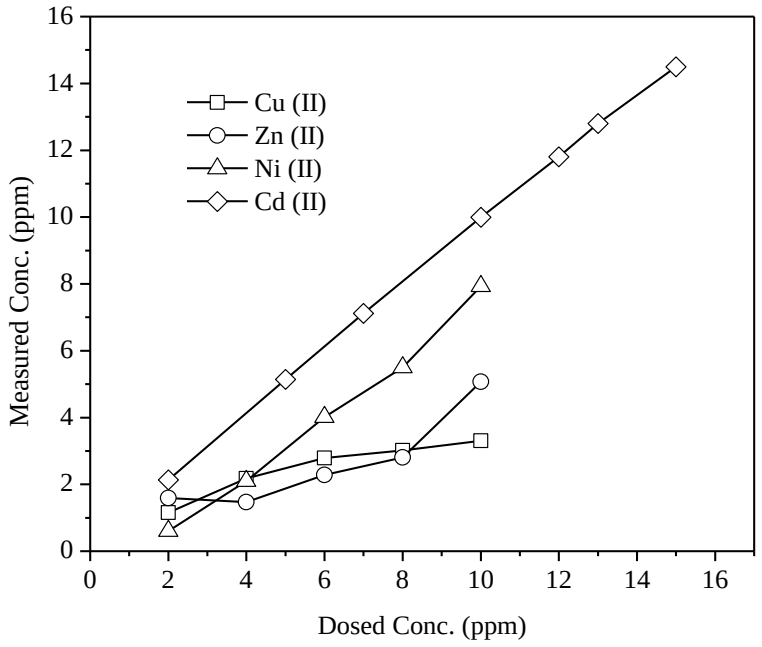

Figure 6.17. Metal concentration in wastewater with filtration of Cu(II) (□), Zn(II) (○), Ni(II) (△), Cd(II) (◇).

Adsorption effect

Fig. 6.18 studied the sorption of the metals on the polymers and particles in the wastewater. With solids concentration of TSS = 140 ppm in the wastewater, as the metal cations were added, they were partially adsorbed on the suspended solids, resulting in lower soluble metal concentrations (Fig. 6.18), and thus yielding a lower slope than in the case without solids (Fig. 6.17). The soluble concentrations of Ni(II) and Cd(II) were larger than the other three at the same added total metal concentrations. It could be noted here that the relationship between the soluble and total metal concentrations was linear, suggesting that saturation of surface sites did not appear to have occurred during the experiments.

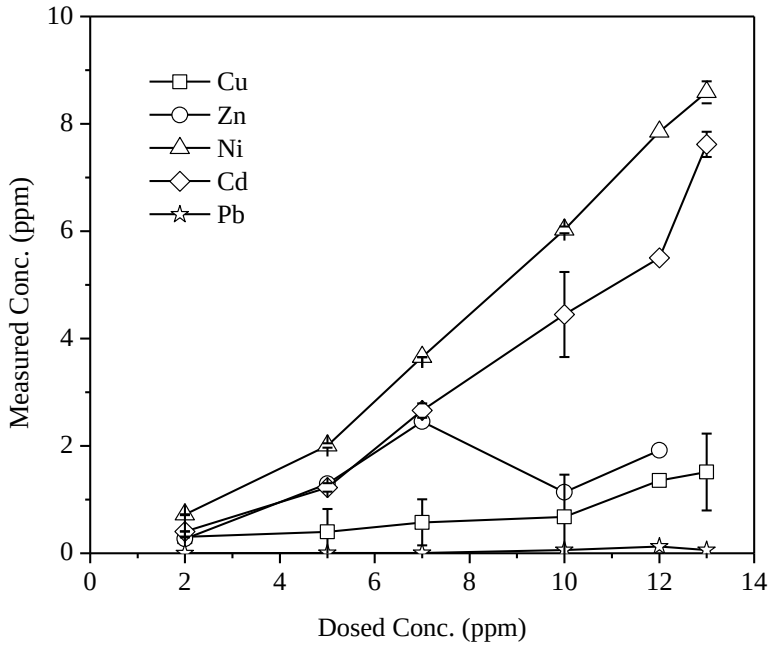

Figure 6.18. Metal concentration in wastewater without filtration of Cu(II) (□), Zn(II) (○), Ni(II) (△), Cd(II) (◇) and Pb(II) (☆). TSS = 140 ppm and pH = 7.2.

Except for Pb(II) that showed the least toxicity to the MESs due to its low solubility, the sorption and precipitation equilibrium of the metals seemed to have no direct relation with the response of the MESs to metals such as Cu(II), Ni(II), Cd(II) and Zn(II). One possible reason was that the metals exerted different toxicity to the bacteria even at same concentrations (Bagby and Sherrard, 1981). Another reason was that it is the "bioavailability" that decided the metal toxicity, yet what is meant by "bioavailability" is usually ill-defined and is rarely quantified, particularly in microbial investigations (Giller et al., 1998).

6.2.3.2 Heavy metals in the influent and effluent

Heavy metal contents in the influent and effluent wastewater of the MESs were compared to study the fate of heavy metals (Cd(II), Cu(II), Zn(II) and Ni(II)) entering the MESs. Also, the heavy metal contents in the anodic biofilm at different exposure

time to 10 ppm of Cd(II) were compared. Fig. 6.19 showed the measured concentration of the metals in the influent entering the MESs right after dosing at different concentrations. It could be seen that the measured concentration was lower than the dosed concentration since adsorption and precipitation occurred during the process. However, the concentration measured was higher than the equilibrium concentration (Fig. 6.18) since it only took 2 min for the metals to contact with the wastewater before measurement. Linear relationship between the measured soluble metal concentration and dosed concentration was observed for all the tested metals within the dosed concentration ranges. Most of the Ni(II) and Cd(II) were left in the soluble form, which were a bit higher than the soluble form of Zn(II) and Cu(II).

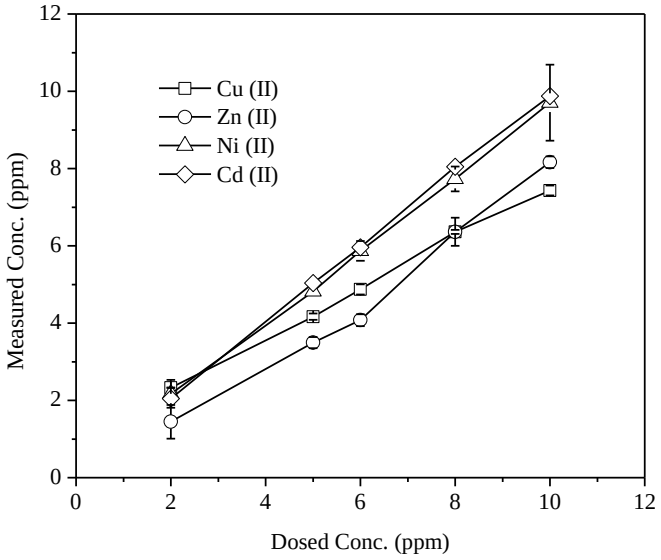

Figure 6.19. Soluble metal concentrations of Cu(II) (□), Zn(II) (○), Ni(II) (△) and Cd(II) (◇) in the influent entering the MESs after dosing.

The achieved least-square linear regressions are summarized in Table 6.3. The slope of the Cd(II) and Ni(II) was both high (0.94~0.98), which showed that most of the Cd(II) and Ni(II) dosed inside the MESs were kept in the soluble state. The linearity suggested that a partition coefficient could be used to describe the partition of heavy

metals between the bulk solution and the total concentration. The concentrations of heavy metals in the solution could then be calculated from the partition coefficient.

Table 6.3 The achieved least-square linear regressions between the measured soluble metal concentration and dosed concentration from Fig. 6.19.

Metal	Cd	Ni	Cu	Zn
Regression	y = 0.9831x +	y = 0.9437x +	y = 0.6508x +	y = 0.8527x -
curve	0.0969	0.208	0.9956	0.5787
R^2	0.9997	0.9993	0.9974	0.9849

Fig. 6.20 showed the measured effluent concentration of the different metals during the exposure time. The concentrations in the effluent were all smaller than the influent data, showing that the loss of the heavy metals occurred inside the MESs.

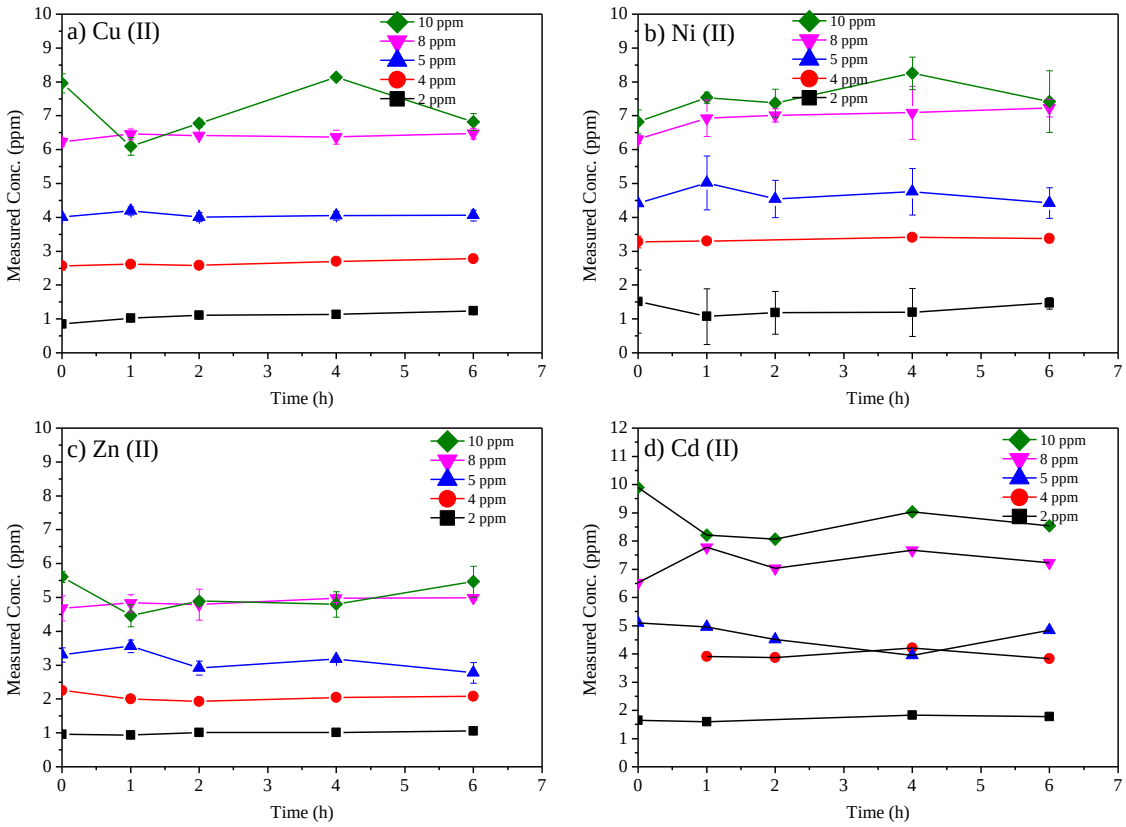

Figure. 6.20. Measured metal concentration in the effluent of the MESs of (a) Cu(II), (b) Ni(II), (c) Zn(II) and (d) Cd(II) at dosed concentrations of 2 (■), 4(●), 5 (▲), 8(▼), and 10 (◆)ppm.

Comparing the content of heavy metals in the influent and the effluent showed heavy metal accumulation by the biofilm of the MESs. Cd(II) was taken as an example to investigate the sorption of metals by the biofilm at different exposure time of 1, 4, 6 h and after 2 h recovery. Fig. 6.21 showed the amount of metal adsorbed by the biofilm. It could be seen that after 2 h of recovery, part of the Cd(II) was washed out of the biofilm and some was left inside the biofilm.

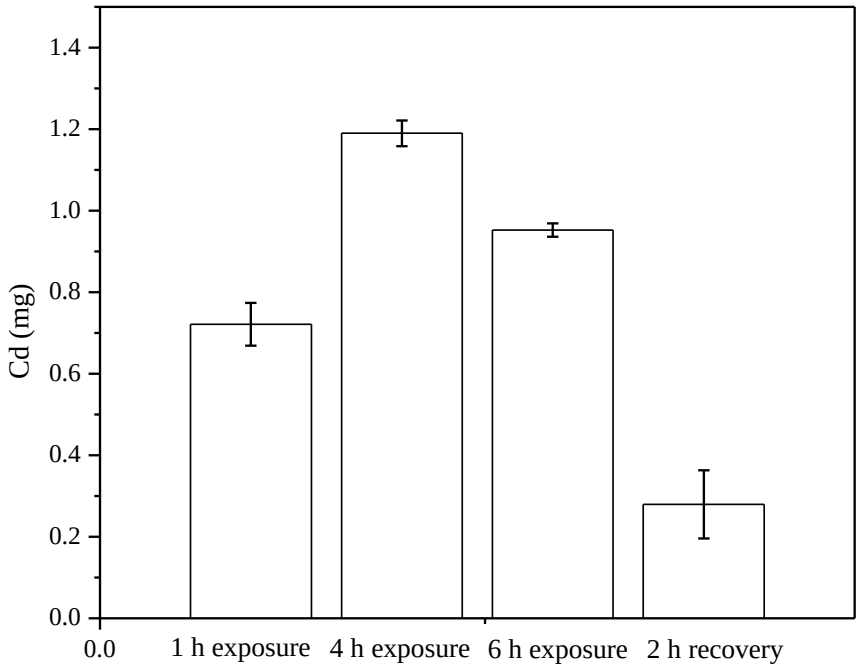

Figure 6.21. Total Cd(II) in the anodic biofilm of MESs at time 1st h, 4th h, 6th h exposure of 10 ppm Cd(II); and at time 2nd h recovery.

6.3 Conclusions

The heavy metal effect on both the electrochemical and microbiological properties of the anodic biofilm was investigated in this Chapter with a view to understand the intrinsic mechanisms of current decrease due to the heavy metals. It was found that neither the viability of bacteria in the anodic biofilm nor the microbial communities was changed due to the short term exposure to the toxicants. It was the inhibition of

the electrochemical activity that led to the decrease of the sensor current, which was proven by the electrochemical analysis. This explained the fast recovery and long-term stability of the MES. The actual pathways of toxic action by which heavy metals inhibit the enzymes and the bacteria were not investigated in our study.

Except for Pb(II) which showed the least toxicity to the MESs due to its low solubility, the sorption and precipitation equilibrium of the metals seemed to have no direct relation with the response of the MESs to heavy metals such as Cu(II), Ni(II), Cd(II) and Zn(II). Linear relationship between the measured soluble metal concentration and the dosed concentration was observed for all the tested metals within the dosed concentration ranges. This suggested that a partition coefficient could be used to describe the partition of heavy metals between the bulk solution and the total concentration, which give further information of the wastewater screened.

CHAPTER 7 Conclusions and Future Work

7.1 Conclusions

The research undertaken within this thesis presented a MES that is an ideal method for detection of influent wastewater toxicity. The MES had the characteristics of quick response, preventative, simple to perform, inexpensive, on-line and relevant to the ASP.

Optimization of both the MES design and biofilm characteristics were investigated to develop an optimal MES that had high and stable baseline, fast response to the toxic event and good recovery ability.

The optimal MES design was a single-chamber design, where the anode and cathode were separated by a Selemion proton exchange membrane and channels were drilled inside to make the flow follows a serpentine path through the system. Under an external resistance of 5 Ω, the maximum power averaged 0.33 ± 0.031 mW with domestic wastewater. Besides, the optimized MES showed high sensitivity and fast recovery when exposed to the acidic toxic event. When the HRT was decreased from 22 to 3.5 min, the sensitivity increased substantially due to the increase of the rate of mass transport. Low external resistance was recommended to be applied to the MESs to generate a looser electroactive biofilm with more void spaces on the anode surface, which would facilitate the mass transport and increase the MES sensitivity to toxicants.

The behavior of the electrochemically-active biofilm was a key parameter of the MES. Biofilm density, porosity and EPS content of the biofilm affected the sensitivity of MES to heavy metals. Flow rate and nitrogen sparging were seen to be two operational parameters that could be easily used to control the characteristics of the biofilm developed on the anode of MESs. It was suggested that MES enriched under low flow rate with intermittent nitrogen sparging could produce an anodic biofilm that was less dense, more porous, contained less EPS and ultimately, displayed higher sensitivity to toxicity.

After the optimization of the 'hardware', biofilm and operational conditions of the MESs, the MES was successfully used here as a real-time online biosensor to detect the presence of various toxicants or extreme pH, nutrient concentration conditions in real wastewater, triggering the alarm within one hour or shorter to allow immediate preventive action and further analysis to be taken. The MES allowed the monitoring of the activity of the anodic biofilm in the presence of various metals with different concentrations by giving specific current responses modeled by linear dose-response and exponential decay regression. Toxic compounds that were tested included common individual heavy metal ions (Cu(II), Zn(II), Pb(II), Cd(II) and Ni(II)), binary mixtures of heavy metals, cyanide and organic chemicals that represented two different chemical structures halogen substituted alkanes an-d aromatics. Heavy metals and cyanide at concentrations of 2 to10 ppm were toxic to the anodic biofilm as they were to microorganisms in the ASP, and the exposure of the anodic biofilm of the MES to those toxicants resulted in current generation repression, the signal of which was dependent on both the toxicant and concentration. Exponential decay regression was used to fit the current decrease profile versus time and dose-response

curve was achieved through regression. The calibration curve was linear over the metal concentration range tested and the MES was very sensitive, with detection limit of 1 to 2 ppm for all the metals except Pb(II). The sensitivity of the MES to different metal ions were 9.5% inhibition/ppm for Zn(II), 11.3% inhibition/ppm for Ni(II), 7.2% inhibition/ppm for Cd(II), 7.6% inhibition/ppm for Cu(II) and 4.0% inhibition/ppm for Pb(II). The IC_{50} (toxicant concentration eliciting a 50% inhibitory effect) was determined to be 6 ppm for Zn(II), 4.9 ppm for Ni(II), 6.5 ppm for Cd (II) and 5.3 ppm for Cu(II), which are relevant to the toxicity information to ASP. It was found that sensitivity, response time, IC_{50} and detection limit were the key parameters to decide and predict the MES response profile curve and dose-response curve. Under appropriate conditions, brief toxicity information could also be predicted through the specific response profiles. Specific information different from response to metals could also be acquired for sensing cyanide. However, MES was found not suitable for detecting organic toxicants. Extreme change of normal wastewater characteristics were also considered as a kind of toxic event and the response to the pH, nitrate, ionic strength and COD were studied.

Continuous inoculating the MESs with small concentration of Ni(II) did not make the sensor acclimatized to the toxicant, showing the stable sensitivity to the toxicants and potential of long-term stability of the MES. The resistance to common variation of the wastewater characteristics, fast and sensitive response to the toxicants, long-term operational stability (over 2 years), and relativity to the ASP made the MES suitable to be served as an early warning system to protect the downstream biological treatment process.

The heavy metal effect on both the electrochemical and microbiological properties of the anodic biofilm was investigated with a view to understand the intrinsic mechanisms of current decrease due to the heavy metals. It was found that neither the viability of bacteria in the anodic biofilm nor the microbial communities was changed due to the short-term exposure to the toxicants. It was the inhibition of the electrochemical activity that led to the decrease of the MES current, which was proven by the electrochemical analysis. This explained the fast recovery and long stability of the biosensor. The actual pathways of toxic action by which heavy metals inhibit the enzymes and the bacteria were not investigated in our study.

Except for Pb(II), which showed the least toxicity to the MESs due to its low solubility, the sorption and precipitation equilibrium of the metals seemed to have no direct relation with the response of the MESs to heavy metals such as Cu(II), Ni(II), Cd(II) and Zn(II). Linear relationship between the measured soluble metal concentration and the dosed concentration was observed for all the tested metals within the dosed concentration ranges. This suggested that a partition coefficient could be used to describe the partition of heavy metals between the bulk solution and the total concentration, which give further information of the wastewater screened.

7.2 Future work

7.2.1 Transport of toxicants within biofilm

The major limitation to the use of biofilm as sensing material is the diffusion of compounds within the biofilm, resulting in a slow response as compared to some

other kinds of sensors such as the one utilizing the suspended microorganisms. Transport and distribution of Cd(II) in the biofilm has been studied with CLSM combined with appropriate fluorescent probes. However, the role of EPS, which is another important structural component in the biofilm, in Cd(II) sorption and distribution was not studied. Further cooperation with microbiologists and chemists, to study the microbial species and Cd(II) behaviors in the biofilm, respectively, are also recommended.

MESs was found to generate different sensitivity patterns to various kinds of toxicants such as positively charged metal ions, negatively charged cyanide ion and neutral organic compounds. The diffusion of those compounds within the biofilm was the key to the different responses. In-depth investigation of the diffusion and interaction of these compounds within the biofilm would give more information on the interpretation of the current output signal.

Another limitation is the low specificity as compared to biosensors containing pure enzymes. However, the modeling of the response curves according to their transport mechanisms, which are specific to different kinds of toxicants, showed potential to further optimize this method in order to achieve more information through the output signal.

7.2.2 Sensor response to multi-toxicants

In practice, wastewater composed of multi-toxicants could enter the WRP and affect the ASP. Binary mixtures of heavy metals were studied in this study and showed

antagonistic effects. It was suggested to further investigate the multi-toxicants effect on MES response, including combinations of various kinds of toxicants. The toxicity information obtained thus will be more complete.

7.2.3 Broader screening of organics

The MESs was found not suitable for detecting the organics since its high detection limit and IC_{50} made it unrealistic in field application. However, it was interesting to find an increase of the generated current due to the degradation of aromatic hydrocarbons by MESs, shedding light on the idea of monitoring those pollutants by analyzing the increased current generated. Furthur research, including a broader screening of organic compounds is necessary.

7.2.4 In-depth toxicity mechanism study

The heavy metal effects on both the electrochemical and microbiological properties of the anodic biofilm were investigated in this study. However, the effects of other toxicants such as nitrate and acidic toxicity were not covered, which could have different intrinsic mechanisms of current decrease. For example, nitrate could serve as an alternative electron acceptor in the anode chamber and thus lead to the current decrease. To better relate the sensor signal with the toxicity information of various toxicants, a more in-depth understanding of the effects of toxicants on electricity generation and the intrinsic reasons behind them are of utmost importance.

REFERENCES

Aelterman, P., Rabaey, K., Pham, H.T., Boon, N. and Verstraete, W. (2006) Continuous electricity generation at high voltages and currents using stacked microbial fuel cells. Environmental Science & Technology 40(10), 3388-3394.

Aelterman, P., Versichele, M., Marzorati, M., Boon, N. and Verstraete, W. (2008) Loading rate and external resistance control the electricity generation of microbial fuel cells with different three-dimensional anodes. Bioresource Technology 99(18), 8895-8902.

Allen, J.B. and Larry, R.F. (2001) Electrochemical methods: fundamentals and applications. Department of Chemistry and Biochemistry University of Texas at Austin, John Wiley & Sons, Inc.

Altas, L. (2009) Inhibitory effect of heavy metals on methane-producing anaerobic granular sludge. Journal of Hazardous Materials 162(2-3), 1551-1556.

Angenent, L.T., Karim, K., Al-Dahhan, M.H. and Domiguez-Espinosa, R. (2004) Production of bioenergy and biochemicals from industrial and agricultural wastewater. TRENDS in Biotechnology 22(9), 477-485.

Bagby, M.M. and Sherrard, J.H. (1981) Combined Effects of Cadmium and Nickel on the Activated Sludge Process. Journal (Water Pollution Control Federation) 53(11), 1609-1619.

Batt, A.L., Kostich, M.S. and Lazorchak, J.M. (2008) Analysis of ecologically relevant pharmaceuticals in wastewater and surface water using selective solid-phase extraction and UPLC-MS/MS. Analytical Chemistry 80(13), 5021-5030.

Battistoni, P., Fava, G. and Ruello, M.L. (1993) HEAVY-METAL SHOCK LOAD IN ACTIVATED-SLUDGE UPTAKE AND TOXIC EFFECTS. Water Research 27(5), 821-827.

Benmoussa, H., Martin, G., Richard, Y. and Leprince, A. (1986) INHIBITION OF NITRIFICATION BY HEAVY-METAL CATIONS. Water Research 20(11), 1333-1339.

Bennetto, H. (1990) Electricity generation by microorganisms. Biotechnology Education 1(4), 163-168.

Bond, D.R. and Lovley, D.R. (2003) Electricity production by Geobacter sulfurreducens attached to electrodes. Applied and Environmental Microbiology 69(3), 1548-1555.

Bond, D.R., Holmes, D.E., Tender, L.M. and Lovley, D.R. (2002) Electrode-reducing microorganisms that harvest energy from marine sediments. Science 295(5554), 483-485.

Boon, N., Top, E.M., Verstraete, W. and Siciliano, S.D. (2003) Bioaugmentation as a tool to protect the structure and function of an activated-sludge microbial community

against a 3-chloroaniline shock load. Applied and Environmental Microbiology 69(3), 1511-1520.

Bott, C.B. and Love, N.G. (2002) Investigating a mechanistic cause for activated-sludge deflocculation in response to shock loads of toxic electrophilic chemicals. Water Environment Research 74(3), 306-315.

Brown, M.J. and Lester, J. (1979) Metal removal in activated sludge: the role of bacterial extracellular polymers. Water Research 13(9), 817-837.

Bullen, R.A., Arnot, T., Lakeman, J. and Walsh, F. (2006) Biofuel cells and their development. Biosensors and Bioelectronics 21(11), 2015-2045.

Cabrero, A., Fernandez, S., Mirada, F. and Garcia, J. (1998) Effects of copper and zinc on the activated sludge bacteria growth kinetics. Water Research 32(5), 1355-1362.

Cao, X., Huang, X., Liang, P., Xiao, K., Zhou, Y., Zhang, X. and Logan, B.E. (2009) A new method for water desalination using microbial desalination cells. Environmental Science & Technology 43(18), 7148-7152.

Carnicero, D., D áz, E., Escolano, O., Rubinos, D., Ballesteros, O., Barral, M., Amils, R. and Garc á Frutos, F. (2009) Preliminary Study of Neutralization and Inhibition of Chemolitotrophic Bacteria in an Acid Mine Drainage from Rio Tinto Site. Advanced Materials Research 71, 677-680.

Çe çen, F., Semerci, N. and Geyik, A.G. (2010) Inhibitory effects of Cu, Zn, Ni and Co on nitrification and relevance of speciation. Journal of Chemical Technology & Biotechnology 85(4), 520-528.

Celmer, D., Oleszkiewicz, J. and Cicek, N. (2008) Impact of shear force on the biofilm structure and performance of a membrane biofilm reactor for tertiary hydrogen-driven denitrification of municipal wastewater. Water Research 42(12), 3057-3065.

Chae, K.J., Choi, M., Ajayi, F.F., Park, W., Chang, I.S. and Kim, I.S. (2007) Mass Transport through a Proton Exchange Membrane (Nafion) in Microbial Fuel Cells†. Energy & Fuels 22(1), 169-176.

Chang, I.S., Moon, H., Jang, J.K. and Kim, B.H. (2005) Improvement of a microbial fuel cell performance as a BOD sensor using respiratory inhibitors. Biosensors & Bioelectronics 20(9), 1856-1859.

Chang, W., Hsu, G., Chiang, S. and Su, M. (2006) Heavy metal removal from aqueous solution by wasted biomass from a combined AS-biofilm process. Bioresource Technology 97(13), 1503-1508.

Cheng, D., Chow, W.L. and He, J. (2009) A Dehalococcoides-containing co-culture that dechlorinates tetrachloroethene to trans-1, 2-dichloroethene. The ISME journal 4(1), 88-97.

Cheng, S., Liu, H. and Logan, B.E. (2006) Increased performance of single-chamber microbial fuel cells using an improved cathode structure. Electrochemistry Communications 8(3), 489-494.

Chow, W.L., Cheng, D., Wang, S. and He, J. (2010) Identification and transcriptional analysis of trans-DCE-producing reductive dehalogenases in Dehalococcoides species. The ISME journal 4(8), 1020-1030.

Clauwaert, P., Aelterman, P., Pham, T.H., De Schamphelaire, L., Carballa, M., Rabaey, K. and Verstraete, W. (2008) Minimizing losses in bio-electrochemical systems: the road to applications. Applied Microbiology and Biotechnology 79(6), 901-913.

Clauwaert, P., Rabaey, K., Aelterman, P., De Schamphelaire, L., Pham, T.H., Boeckx, P., Boon, N. and Verstraete, W. (2007) Biological denitrification in microbial fuel cells. Environmental Science & Technology 41(9), 3354-3360.

Coufort, C., Derlon, N., Ochoa-Chaves, J., Liné, A. and Paul, E. (2007) Cohesion and detachment in biofilm systems for different electron acceptor and donors, pp. 421-428.

Cusick, R.D. and Logan, B.E. (2012) Phosphate recovery as struvite within a single chamber microbial electrolysis cell. Bioresource Technology 107, 110-115.

Dalzell, D.J.B., Alte, S., Aspichueta, E., de la Sota, A., Etxebarria, J., Gutierrez, M., Hoffmann, C.C., Sales, D., Obst, U. and Christofi, N. (2002) A comparison of five rapid direct toxicity assessment methods to determine toxicity of pollutants to activated sludge. Chemosphere 47(5), 535-545.

Dávila, D., Esquivel, J.P., Sabaté, N. and Mas, J. (2011) Silicon-based microfabricated microbial fuel cell toxicity sensor. Biosensors and Bioelectronics 26(5), 2426-2430.

Di Lorenzo, M., Curtis, T.P., Head, I.M. and Scott, K. (2009) A single-chamber microbial fuel cell as a biosensor for wastewaters. Water Research 43(13), 3145-3154.

Di Lorenzo, M., Curtis, T.P., Head, I.M., Velasquez-Orta, S.B. and Scott, K. (2009a) A single chamber packed bed microbial fuel cell biosensor for measuring organic content of wastewater. Water Science and Technology 60(11), 2879-2887.

Dickson, J.S. and Koohmaraie, M. (1989) Cell surface charge characteristics and their relationship to bacterial attachment to meat surfaces. Appl Environ Microbiol 55(4), 832-836.

Dilek, F.B. and Yetis, U. (1992) EFFECTS OF HEAVY-METALS ON ACTIVATED-SLUDGE PROCESS. Water Science and Technology 26(3-4), 801-813.

Dubois, M., Gilles, K.A., Hamilton, J.K., Rebers, P.t. and Smith, F. (1956) Colorimetric method for determination of sugars and related substances. Analytical chemistry 28(3), 350-356.

Elnabarawy, M., Robideau, R. and Beach, S. (1988) Comparison of three rapid toxicity test procedures: Microtox,® polytox,® and activated sludge respiration inhibition. Toxicity assessment 3(4), 361-370.

Fan, Y., Hu, H. and Liu, H. (2007) Sustainable power generation in microbial fuel cells using bicarbonate buffer and proton transfer mechanisms. Environmental Science & Technology 41(23), 8154-8158.

Fan, Y., Sharbrough, E. and Liu, H. (2008) Quantification of the internal resistance distribution of microbial fuel cells. Environmental Science & Technology 42(21), 8101-8107.

Fang, H.H.P., Xu, L.C. and Chan, K.Y. (2002) Effects of toxic metals and chemicals on biofilm and biocorrosion. Water Research 36(19), 4709-4716.

Finkelstein, D.A., Tender, L.M. and Zeikus, J.G. (2006) Effect of electrode potential on electrode-reducing microbiota. Environmental science & technology 40(22), 6990-6995.

Fitzgerald, L.A., Petersen, E.R., Gross, B.J., Soto, C.M., Ringeisen, B.R., El-Naggar, M.Y. and Biffinger, J.C. (2012) Aggrandizing power output from Shewanella oneidensis MR-1 microbial fuel cells using calcium chloride. Biosensors and Bioelectronics 31(1), 492-498.

Frolund, B., Griebe, T., Nielsen, P.H., 1995. Enzymatic-activity in the activated sludge floc matrix. Applied Microbiology and Biotechnology 43(4), 755-761.

Fricke, K., Harnisch, F. and Schröder, U. (2008) On the use of cyclic voltammetry for the study of anodic electron transfer in microbial fuel cells. Energy & Environmental Science 1(1), 144-147.

Gälli, R., Munz, C. and Scholtz, R. (1994) Evaluation and application of aquatic toxicity tests: use of the Microtox test for the prediction of toxicity based upon concentrations of contaminants in soil. Hydrobiologia 273(3), 179-189.

Ghangrekar, M.M. and Shinde, V.B. (2007) Performance of membrane-less microbial fuel cell treating wastewater and effect of electrode distance and area on electricity production. Bioresource Technology 98(15), 2879-2885.

Gikas, P. (2007) Kinetic responses of activated sludge to individual and joint nickel (Ni(II)) and cobalt (Co(II)): An isobolographic approach. Journal of Hazardous Materials 143(1-2), 246-256.

Gikas, P. (2008) Single and combined effects of nickel (Ni(II)) and cobalt (Co(II)) ions on activated sludge and on other aerobic microorganisms: A review. Journal of Hazardous Materials 159(2-3), 187-203.

Gil, G.C., Chang, I.S., Kim, B.H., Kim, M., Jang, J.K., Park, H.S. and Kim, H.J. (2003) Operational parameters affecting the performance of a mediator-less microbial fuel cell. Biosensors & Bioelectronics 18(4), 327-334.

Giller, K.E., Witter, E. and Mcgrath, S.P. (1998) Toxicity of heavy metals to microorganisms and microbial processes in agricultural soils: a review. Soil Biology and Biochemistry 30(10), 1389-1414.

Grady, C.P.L., Daigger, G.T. and Lim, H.C. (1999) Biological Wastewater Treatment, Marcel Dekker.

Gregory, K.B., Bond, D.R. and Lovley, D.R. (2004) Graphite electrodes as electron donors for anaerobic respiration. Environmental Microbiology 6(6), 596-604.

Gu, M.B. and Choi, S.H. (2001) Monitoring and classification of toxicity using recombinant bioluminescent bacteria. Water Science and Technology 43(2), 147-154.

Halling-Sørensen, B. (2001) Inhibition of aerobic growth and nitrification of bacteria in sewage sludge by antibacterial agents. Archives of environmental contamination and toxicology 40(4), 451-460.

Harrison, J.J., Ceri, H. and Turner, R.J. (2007) Multimetal resistance and tolerance in microbial biofilms. Nature Reviews Microbiology 5(12), 928-938.

He, Z. and Angenent, L.T. (2006) Application of bacterial biocathodes in microbial fuel cells. Electroanalysis 18(19-20), 2009-2015.

He, Z. and Mansfeld, F. (2009) Exploring the use of electrochemical impedance spectroscopy (EIS) in microbial fuel cell studies. Energy & Environmental Science 2(2), 215-219.

He, Z., Huang, Y., Manohar, A.K. and Mansfeld, F. (2008) Effect of electrolyte pH on the rate of the anodic and cathodic reactions in an air-cathode microbial fuel cell. Bioelectrochemistry 74(1), 78-82.

He, Z., Minteer, S.D. and Angenent, L.T. (2005) Electricity generation from artificial wastewater using an upflow microbial fuel cell. Environmental Science & Technology 39(14), 5262-5267.

Henriques, I.D. and Love, N.G. (2007) The role of extracellular polymeric substances in the toxicity response of activated sludge bacteria to chemical toxins. Water Research 41(18), 4177-4185.

Heydorn, A., Nielsen, A.T., Hentzer, M., Sternberg, C., Givskov, M., Ersbøll, B.K. and Molin, S. (2000) Quantification of biofilm structures by the novel computer program COMSTAT. Microbiology 146(10), 2395-2407.

Hu, Z., Jin, J., Abruña, H.D., Houston, P.L., Hay, A.G., Ghiorse, W.C., Shuler, M.L., Hidalgo, G. and Lion, L.W. (2007) Spatial distributions of copper in microbial biofilms by scanning electrochemical microscopy. Environmental Science and Technology 41(3), 936-941.

Jacobson, K.S., Drew, D.M. and He, Z. (2011) Efficient salt removal in a continuously operated upflow microbial desalination cell with an air cathode. Bioresource Technology 102(1), 376-380.

Jadhav, G. and Ghangrekar, M. (2009) Performance of microbial fuel cell subjected to variation in pH, temperature, external load and substrate concentration. Bioresource Technology 100(2), 717-723.

Jenkins, R.L., Scheybeler, B.J., Smith, M.L., Baird, R., Lo, M.P. and Haug, R.T. (1981) Metals removal and recovery from municipal sludge. Journal (Water Pollution Control Federation), 25-32.

Kang, K.H., Jang, J.K., Pham, T.H., Moon, H., Chang, I.S. and Kim, B.H. (2003) A microbial fuel cell with improved cathode reaction as a low biochemical oxygen demand sensor. Biotechnology Letters 25(16), 1357-1361.

Karvelas, M., Katsoyiannis, A. and Samara, C. (2003) Occurrence and fate of heavy metals in the wastewater treatment process. Chemosphere 53(10), 1201-1210.

Katuri, K.P., Kavanagh, P., Rengaraj, S. and Leech, D. (2010) Geobacter sulfurreducens biofilms developed under different growth conditions on glassy carbon electrodes: insights using cyclic voltammetry. Chemical Communications 46(26), 4758-4760.

Kim, B., Park, H., Kim, H., Kim, G., Chang, I., Lee, J. and Phung, N. (2004) Enrichment of microbial community generating electricity using a fuel-cell-type electrochemical cell. Applied microbiology and biotechnology 63(6), 672-681.

Kim, B.H., Chang, I.S. and Moon, H. (2006a) Microbial fuel cell-type biochemical oxygen demand sensor. studies 3, 4.

Kim, G.T., Webster, G., Wimpenny, J.W.T., Kim, B.H., Kim, H.J. and Weightman, A.J. (2006b) Bacterial community structure, compartmentalization and activity in a microbial fuel cell. Journal of Applied Microbiology 101(3), 698-710.

Kim, B.H., Chang, I.S., Gil, G.C., Park, H.S. and Kim, H.J. (2003) Novel BOD (biological oxygen demand) sensor using mediator-less microbial fuel cell. Biotechnology Letters 25(7), 541-545.

Kim, B.-H., Kim, H.-J., Hyun, M.-S. and Park, D.-H. (1999a) Direct electrode reaction of Fe (III)-reducing bacterium, Shewanella putrefaciens. Journal of microbiology and biotechnology 9(2), 127-131.

Kim, H., Hyun, M., Chang, I. and Kim, B.H. (1999b) A microbial fuel cell type lactate biosensor using a metal-reducing bacterium, Shewanella putrefaciens. J. Microbiol. Biotechnol 9(3), 365-367.

Kim, H.J., Park, H.S., Hyun, M.S., Chang, I.S., Kim, M. and Kim, B.H. (2002) A mediator-less microbial fuel cell using a metal reducing bacterium, Shewanella putrefaciense. Enzyme and Microbial Technology 30(2), 145-152.

Kim, M., Hyun, M.S., Gadd, G.M. and Kim, H.J. (2007) A novel biomonitoring system using microbial fuel cells. Journal of Environmental Monitoring 9(12), 1323-1328.

Kodukula, P.S., Patterson, J.W. and Surampalli, R.Y. (1994) Sorption and precipitation of metals in activated sludge. Biotechnology and Bioengineering 43(9), 874-880.

Kwok, W.K., Picioreanu, C., Ong, S.L., Van Loosdrecht, M.C.M., Ng, W.J. and Heijnen, J.J. (1998) Influence of biomass production and detachment forces on biofilm structures in a biofilm airlift suspension reactor. Biotechnology and Bioengineering 58(4), 400-407.

Lazarova, V. and Manem, J. (1995) Biofilm characterization and activity analysis in water and wastewater treatment. Water Research 29(10), 2227-2245.

Lefebvre, O., Uzabiaga, A., Chang, I.S., Kim, B.-H. and Ng, H.Y. (2011a) Microbial fuel cells for energy self-sufficient domestic wastewater treatment—a review and discussion from energetic consideration. Applied microbiology and biotechnology 89(2), 259-270.

Lefebvre, O., Shen, Y., Tan, Z., Uzabiaga, A., Chang, I.S. and Ng, H.Y. (2011b) A comparison of membranes and enrichment strategies for microbial fuel cells. Bioresource Technology 102(10), 6291-6294.

Lies, D.P., Hernandez, M.E., Kappler, A., Mielke, R.E., Gralnick, J.A. and Newman, D.K. (2005) Shewanella oneidensis MR-1 uses overlapping pathways for iron reduction at a distance and by direct contact under conditions relevant for biofilms. Applied and Environmental Microbiology 71(8), 4414-4426.

Lin, Y.-M., Yang, X.-F. and Liu, Y. (2003) Kinetic responses of activated sludge microorganisms to individual and joint copper and zinc. Journal of Environmental Science and Health, Part A 38(2), 353-360.

Liu, H. and Logan, B.E. (2004) Electricity generation using an air-cathode single chamber microbial fuel cell in the presence and absence of a proton exchange membrane. Environmental Science & Technology 38(14), 4040-4046.

Liu, H., Cheng, S.A. and Logan, B.E. (2005a) Power generation in fed-batch microbial fuel cells as a function of ionic strength, temperature, and reactor configuration. Environmental Science & Technology 39(14), 5488-5493.

Liu, H., Cheng, S.A. and Logan, B.E. (2005b) Production of electricity from acetate or butyrate using a single-chamber microbial fuel cell. Environmental Science & Technology 39(2), 658-662.

Liu, H., Ramnarayanan, R. and Logan, B.E. (2004) Production of electricity during wastewater treatment using a single chamber microbial fuel cell. Environmental Science & Technology 38(7), 2281-2285.

Liu, J. and Mattiasson, B. (2002) Microbial BOD sensors for wastewater analysis. Water Research 36(15), 3786-3802.

Liu, J., Bjornsson, L. and Mattiasson, B. (2000) Immobilised activated sludge based biosensor for biochemical oxygen demand measurement. Biosensors & Bioelectronics 14(12), 883-893.

Liu, Y. and Tay, J.-H. (2002) The essential role of hydrodynamic shear force in the formation of biofilm and granular sludge. Water Research 36(7), 1653-1665.

Liu, Y., Harnisch, F., Fricke, K., Sietmann, R. and Schröder, U. (2008) Improvement of the anodic bioelectrocatalytic activity of mixed culture biofilms by a simple consecutive electrochemical selection procedure. Biosensors and Bioelectronics 24(4), 1006-1011.

Logan, B.E. (2009) Exoelectrogenic bacteria that power microbial fuel cells. Nature Reviews Microbiology 7(5), 375-381.

Logan, B.E., Hamelers, B., Rozendal, R.A., Schrorder, U., Keller, J., Freguia, S., Aelterman, P., Verstraete, W. and Rabaey, K. (2006) Microbial fuel cells: Methodology and technology. Environmental Science & Technology 40(17), 5181-5192.

Lovley, D.R. (2006) Bug juice: harvesting electricity with microorganisms. Nature Reviews Microbiology 4(7), 497-508.

Lovley, D.R. (2008) The microbe electric: conversion of organic matter to electricity. Current Opinion in Biotechnology 19(6), 564-571.

Lovley, D.R. and Lonergan, D.J. (1990) Anaerobic oxidation of toluene, phenol, and p-cresol by the dissimilatory iron-reducing organism, GS-15. Applied and Environmental Microbiology 56(6), 1858-1864.

Lovley, D.R., Baedecker, M.J., Lonergan, D.J., Cozzarelli, I.M., Phillips, E.J. and Siegel, D.I. (1989) Oxidation of aromatic contaminants coupled to microbial iron reduction. Nature 339(6222), 297-300.

Lucarelli, F., Kicela, A., Palchetti, I., Marrazza, G. and Mascini, M. (2002b) Electrochemical DNA biosensor for analysis of wastewater samples. Bioelectrochemistry 58(1), 113-118.

Lucarelli, F., Palchetti, I., Marrazza, G. and Mascini, M. (2002a) Electrochemical DNA biosensor as a screening tool for the detection of toxicants in water and wastewater samples. Talanta 56(5), 949-957.

Luo, H., Liu, G., Zhang, R. and Jin, S. (2009) Phenol degradation in microbial fuel cells. Chemical Engineering Journal 147(2), 259-264.

Madoni, P., Davoli, D. and Guglielmi, L. (1999) Response of sOUR and AUR to heavy metal contamination in activated sludge. Water Research 33(10), 2459-2464.

Madoni, P., Davoli, D., Gorbi, G. and Vescovi, L. (1996) Toxic effect of heavy metals on the activated sludge protozoan community. Water Research 30(1), 135-141.

Marcus, A.K., Torres, C.I. and Rittmann, B.E. (2007) Conduction-based modeling of the biofilm anode of a microbial fuel cell. Biotechnology and Bioengineering 98(6), 1171-1182.

Marsili, E., Rollefson, J.B., Baron, D.B., Hozalski, R.M. and Bond, D.R. (2008) Microbial biofilm voltammetry: direct electrochemical characterization of catalytic electrode-attached biofilms. Applied and Environmental Microbiology 74(23), 7329-7337.

McDermott, G.N., Moore, W.A., Post, M.A. and Ettinger, M.B. (1963) EFFECTS OF COPPER ON AEROBIC BIOLOGICAL SEWAGE TREATMENT. Journal Water Pollution Control Federation 35(2), 227-241.

Mehanna, M., Saito, T., Yan, J., Hickner, M., Cao, X., Huang, X. and Logan, B.E. (2010) Using microbial desalination cells to reduce water salinity prior to reverse osmosis. Energy & Environmental Science 3(8), 1114-1120.

Mench, M.M., Wang, C.-Y. and Thynell, S.T. (2001) An introduction to fuel cells and related transport phenomena. International Journal of Transport Phenomena 3, 151-176.

Ménil, F., Susbielles, M., Debéda, H., Lucat, C. and Tardy, P. (2005) Evidence of a correlation between the non-linearity of chemical sensors and the asymmetry of their response and recovery curves. Sensors and Actuators B: Chemical 106(1), 407-423.

Min, B. and Logan, B.E. (2004) Continuous electricity generation from domestic wastewater and organic substrates in a flat plate microbial fuel cell. Environmental Science & Technology 38(21), 5809-5814.

Min, B., Kim, J., Oh, S., Regan, J.M. and Logan, B.E. (2005) Electricity generation from swine wastewater using microbial fuel cells. Water Research 39(20), 4961-4968.

Mohan, S.V., Raghavulu, S.V., Srikanth, S. and Sarma, P.N. (2007) Bioelectricity production by mediatorless microbial fuel cell under acidophilic condition using wastewater as substrate: Influence of substrate loading rate. Current Science 92(12), 1720-1726.

Moon, H., Chang, I.S., Jang, J.K., Kim, K.S., Lee, J., Lovitt, R.W. and Kim, B.H. (2005) On-line monitoring of low biochemical oxygen demand through continuous operation of a mediator-less microbial fuel cell. Journal of Microbiology and Biotechnology 15(1), 192-196.

Moore, W.A., McDermott, G.N., Post, M.A., Mandia, J.W. and Ettinger, M.B. (1961) EFFECTS OF CHROMIUM ON THE ACTIVATED SLUDGE PROCESS. Journal Water Pollution Control Federation 33(1), 54-72.

Morris, J.M. and Jin, S. (2009) Influence of NO< sub> 3</sub> and SO< sub> 4</sub> on power generation from microbial fuel cells. Chemical Engineering Journal 153(1), 127-130.

Motulsky, H. (2004) Fitting models to biological data using linear and nonlinear regression: a practical guide to curve fitting, OUP USA.

Nakanishi, K., Ikebukuro, K. and Karube, I. (1996) Determination of cyanide using a microbial sensor. Applied Biochemistry and Biotechnology 60(2), 97-106.

Neufeld, R.D. and Hermann, E.R. (1975) HEAVY-METAL REMOVAL BY ACCLIMATED ACTIVATED-SLUDGE. Journal Water Pollution Control Federation 47(2), 310-329.

Nevin, K.P. and Lovley, D.R. (2000) Lack of production of electron-shuttling compounds or solubilization of Fe (III) during reduction of insoluble Fe (III) oxide by Geobacter metallireducens. Applied and Environmental Microbiology 66(5), 2248-2251.

Nevin, K.P. and Lovley, D.R. (2002) Mechanisms for Fe (III) oxide reduction in sedimentary environments. Geomicrobiology Journal 19(2), 141-159.

Nevin, K.P., Richter, H., Covalla, S., Johnson, J., Woodard, T., Orloff, A., Jia, H., Zhang, M. and Lovley, D. (2008) Power output and columbic efficiencies from biofilms of Geobacter sulfurreducens comparable to mixed community microbial fuel cells. Environmental microbiology 10(10), 2505-2514.

Nicholson, R.S. (1965) Theory and Application of Cyclic Voltammetry for Measurement of Electrode Reaction Kinetics. Analytical Chemistry 37(11), 1351-1355.

Nies, D.H. (1999) Microbial heavy-metal resistance. Applied microbiology and biotechnology 51(6), 730-750.

Oh, S.E. and Logan, B.E. (2006) Proton exchange membrane and electrode surface areas as factors that affect power generation in microbial fuel cells. Applied Microbiology and Biotechnology 70(2), 162-169.

O'Hayre, R.P., Cha, S.-W., Colella, W. and Prinz, F.B. (2006) Fuel cell fundamentals, John Wiley & Sons New York.

Ong, S.A., Toorisaka, E., Hirata, M. and Hano, T. (2004) Effects of nickel(II) addition on the activity of activated sludge microorganisms and activated sludge process. Journal of Hazardous Materials 113(1-3), 111-121.

Pamukoglu, M.Y. and Kargi, F. (2007) Mathematical modeling of copper(II) ion inhibition on COD removal in an activated sludge unit. Journal of Hazardous Materials 146(1–2), 372-377.

Park, D.H. and Zeikus, J.G. (2003) Improved fuel cell and electrode designs for producing electricity from microbial degradation. Biotechnology and Bioengineering 81(3), 348-355.

Patil, S., Harnisch, F. and Schroder, U. (2010) Toxicity Response of Electroactive Microbial Biofilms-A Decisive Feature for Potential Biosensor and Power Source Applications. Chemphyschem 11(13), 2834-2837.

Pea, M., Mara, D. and Sanchez, A. (2000) Dispersion studies in anaerobic ponds: implications for design and operation. Water Science & Technology 42(10), 273-282.

Pham, H.T., Boon, N., Aelterman, P., Clauwaert, P., De Schamphelaire, L., van Oostveldt, P., Verbeken, K., Rabaey, K. and Verstraete, W. (2008) High shear

enrichment improves the performance of the anodophilic microbial consortium in a microbial fuel cell. Microbial Biotechnology 1(6), 487-496.

Pham, T.H., Aelterman, P. and Verstraete, W. (2009) Bioanode performance in bioelectrochemical systems: recent improvements and prospects. Trends in Biotechnology 27(3), 168-178.

Potter, M.C. (1911) Electrical effects accompanying the decomposition of organic compounds. Proceedings of the Royal Society of London Series B-Containing Papers of a Biological Character 84(571), 260-276.

Rabaey, K. and Verstraete, W. (2005) Microbial fuel cells: novel biotechnology for energy generation. TRENDS in Biotechnology 23(6), 291-298.

Rabaey, K., Boon, N., Siciliano, S.D., Verhaege, M. and Verstraete, W. (2004a) Biofuel cells select for microbial consortia that self-mediate electron transfer. Applied and Environmental Microbiology 70(9), 5373-5382.

Rabaey, K., Boon, N., Denef, V., Verhaege, M., Höfte, M. and Verstraete, W. (2004b) Bacteria produce and use redox mediators for electron transfer in microbial fuel cells.

Rabaey, K., Lissens, G., Siciliano, S.D. and Verstraete, W. (2003) A microbial fuel cell capable of converting glucose to electricity at high rate and efficiency. Biotechnology Letters 25(18), 1531-1535.

Rabaey, K., Rodriguez, J., Blackall, L.L., Keller, J., Gross, P., Batstone, D., Verstraete, W. and Nealson, K.H. (2007) Microbial ecology meets electrochemistry: electricity-driven and driving communities. Isme Journal 1(1), 9-18.

Ramírez, E., Granero, A., Zón, M. and Fernández, H. (2011) Development of an Amperometric Biosensor Based on Peroxidases from Brassica napus for the Determination of Ochratoxin a Content in Peanut Samples. J Biosens Bioelectron S 3, 2.

Rauret, G. (1998) Extraction procedures for the determination of heavy metals in contaminated soil and sediment. Talanta 46(3), 449-455.

Read, S.T., Dutta, P., Bond, P.L., Keller, J. and Rabaey, K. (2010) Initial development and structure of biofilms on microbial fuel cell anodes. BMC microbiology 10(1), 98.

Reddy, M.V., Srikanth, S., Mohan, S.V. and Sarma, P.N. (2010) Phosphatase and dehydrogenase activities in anodic chamber of single chamber microbial fuel cell (MFC) at variable substrate loading conditions. Bioelectrochemistry 77(2), 125-132.

Registry, A.f.T.S.a.D. (July 2006) ToxFAQs for Cyanide.

Reguera, G., McCarthy, K.D., Mehta, T., Nicoll, J.S., Tuominen, M.T. and Lovley, D.R. (2005) Extracellular electron transfer via microbial nanowires. Nature 435(7045), 1098-1101.

Reguera, G., Nevin, K.P., Nicoll, J.S., Covalla, S.F., Woodard, T.L. and Lovley, D.R. (2006) Biofilm and nanowire production leads to increased current in Geobacter

sulfurreducens fuel cells. Applied and Environmental Microbiology 72(11), 7345-7348.

Reimers, C., Girguis, P., Stecher, H., Tender, L., Ryckelynck, N. and Whaling, P. (2006) Microbial fuel cell energy from an ocean cold seep. Geobiology 4(2), 123-136.

Ren, S. (2001) Development of a Continuous Bioluminescent Bacteria-based System for POTW Influent Wastewater Toxicity Monitoring, University of Tennessee, Knoxville.

Ren, S. (2004) Assessing wastewater toxicity to activated sludge: recent research and developments. Environment International 30(8), 1151-1164.

Ren, S. and Frymier, P.D. (2002) Estimating the toxicities of organic chemicals to bioluminescent bacteria and activated sludge. Water Research 36(17), 4406-4414.

Ren, S. and Frymier, P.D. (2003) Comparative study of two bioassays for applications in influent wastewater toxicity monitoring. Journal of Environmental Engineering 129(3), 216-221.

Ren, S. and Frymier, P.D. (2005) Toxicity of metals and organic chemicals evaluated with bioluminescence assays. Chemosphere 58(5), 543-550.

Ribo, J. and Rogers, F. (1990) Toxicity of mixtures of aquatic contaminants using the luminescent bacteria bioassay. Toxicity assessment 5(2), 135-152.

Riedel, K., Kunze, G. and König, A. (2002) History and Trends in Bioprocessing and Biotransformation, pp. 81-118, Springer.

Ringeisen, B.R., Henderson, E., Wu, P.K., Pietron, J., Ray, R., Little, B., Biffinger, J.C. and Jones-Meehan, J.M. (2006) High power density from a miniature microbial fuel cell using Shewanella oneidensis DSP10. Environmental science & technology 40(8), 2629-2634.

Ringeisen, B.R., Ray, R. and Little, B. (2007) A miniature microbial fuel cell operating with an aerobic anode chamber. Journal of Power Sources 165(2), 591-597.

Rismani-Yazdi, H., Carver, S.M., Christy, A.D. and Tuovinen, O.H. (2008) Cathodic limitations in microbial fuel cells: An overview. Journal of Power Sources 180(2), 683-694.

Rittmann, B.E., Torres, C.I. and Marcus, A.K. (2008) Emerging environmental technologies, pp. 1-28, Springer.

Rochex, A., Godon, J.J., Bernet, N. and Escudié, R. (2008) Role of shear stress on composition, diversity and dynamics of biofilm bacterial communities. Water Research 42(20), 4915-4922.

Rosso, K.M., Zachara, J.M., Fredrickson, J.K., Gorby, Y.A. and Smith, S.C. (2003) Nonlocal bacterial electron transfer to hematite surfaces. Geochimica et Cosmochimica Acta 67(5), 1081-1087.

Rozendal, R.A., Hamelers, H.V.M. and Buisman, C.J.N. (2006) Effects of membrane cation transport on pH and microbial fuel cell performance. Environmental Science & Technology 40(17), 5206-5211.

Scheller, F.W., Wollenberger, U., Warsinke, A. and Lisdat, F. (2001) Research and development in biosensors. Current Opinion in Biotechnology 12(1), 35-40.

Schröder, U. (2007) Anodic electron transfer mechanisms in microbial fuel cells and their energy efficiency. Physical Chemistry Chemical Physics 9(21), 2619-2629.

Schwartz-Mittelmann, A. and Galil, N.I. (2000) Biological mechanisms involved in bioflocculation disturbances caused by phenol. Water Science and Technology 42(1-2), 105-110.

Sörme, L. and Lagerkvist, R. (2002) Sources of heavy metals in urban wastewater in Stockholm. Science of the Total Environment 298(1), 131-145.

Spanjers, H. and Vanrolleghem, P. (1995) Respirometry as a tool for rapid characterization of wastewater and activated sludge. Water Science and Technology 31(2), 105-114.

Späth, R., Flemming, H.-C. and Wuertz, S. (1998) Sorption properties of biofilms. Water Science and Technology 37(4), 207-210.

Stein, N.E., Hamelers, H.V.M. and Buisman, C.N.J. (2010) Stabilizing the baseline current of a microbial fuel cell-based biosensor through overpotential control under non-toxic conditions. Bioelectrochemistry 78(1), 87-91.

Stein, N.E., Keesman, K.J., Hamelers, H.V.M. and van Straten, G. (2011) Kinetic models for detection of toxicity in a microbial fuel cell based biosensor. Biosensors and Bioelectronics 26(7), 3115-3120.

Stein, N.E., Hamelers, H.V.M. and Buisman, C.N.J. (2012) Influence of membrane type, current and potential on the response to chemical toxicants of a microbial fuel cell based biosensor. Sensors and Actuators B: Chemical 163(1), 1-7.

Steinberg, S.M., Poziomek, E.J., Engelmann, W.H. and Rogers, K.R. (1995) A review of environmental applications of bioluminescence measurements. Chemosphere 30(11), 2155-2197.

Stoodley, P., Cargo, R., Rupp, C.J., Wilson, S. and Klapper, I. (2002) Biofilm material properties as related to shear-induced deformation and detachment phenomena. Journal of Industrial Microbiology and Biotechnology 29(6), 361-367.

Stoodley, P., Sauer, K., Davies, D.G. and Costerton, J.W. (2010) Biofilms as complex differentiated communities. Annu Rev Microbiol 56, 187-209.

Sukkasem, C., Xu, S., Park, S., Boonsawang, P. and Liu, H. (2008) Effect of nitrate on the performance of single chamber air cathode microbial fuel cells. Water Research 42(19), 4743-4750.

Sund, C.J., McMasters, S., Crittenden, S.R., Harrell, L.E. and Sumner, J.J. (2007) Effect of electron mediators on current generation and fermentation in a microbial fuel cell. Applied microbiology and biotechnology 76(3), 561-568.

Teitzel, G.M. and Parsek, M.R. (2003) Heavy metal resistance of biofilm and planktonic Pseudomonas aeruginosa. Applied and Environmental Microbiology 69(4), 2313-2320.

Tender, L.M., Reimers, C.E., Stecher, H.A., Holmes, D.E., Bond, D.R., Lowy, D.A., Pilobello, K., Fertig, S.J. and Lovley, D.R. (2002) Harnessing microbially generated power on the seafloor. nature biotechnology 20(8), 821-825.

ter Heijne, A., Hamelers, H.V., Saakes, M. and Buisman, C.J. (2008) Performance of non-porous graphite and titanium-based anodes in microbial fuel cells. Electrochimica Acta 53(18), 5697-5703.

Thévenot, D.R., Toth, K., Durst, R.A. and Wilson, G.S. (2001) Electrochemical biosensors: recommended definitions and classification. Biosensors and Bioelectronics 16(1–2), 121-131.

Torrens, K.D. (2000) Activated sludge and cyanide: a deadly combination? Pollution Engineering 32(3), 23-24.

Torres, C.s.I., Krajmalnik-Brown, R., Parameswaran, P., Marcus, A.K., Wanger, G., Gorby, Y.A. and Rittmann, B.E. (2009) Selecting anode-respiring bacteria based on anode potential: phylogenetic, electrochemical, and microscopic characterization. Environmental Science & Technology 43(24), 9519-9524.

Tront, J.M., Fortner, J.D., Plotze, M., Hughes, J.B. and Puzrin, A.M. (2008) Microbial fuel cell biosensor for in situ assessment of microbial activity. Biosensors & Bioelectronics 24(4), 586-590.

Watanabe, K. (2008) Recent Developments in Microbial Fuel Cell Technologies for Sustainable Bioenergy. Journal of Bioscience and Bioengineering 106(6), 528-536.

Wen, Q., Wu, Y., Cao, D.X., Zhao, L.X. and Sun, Q. (2009) Electricity generation and modeling of microbial fuel cell from continuous beer brewery wastewater. Bioresource Technology 100(18), 4171-4175.

Wong, K.Y., Zhang, M.Q., Li, X.M. and Lo, W.H. (1997) A luminescence-based scanning respirometer for heavy metal toxicity monitoring. Biosensors & Bioelectronics 12(2), 125-133.

Xing, D., Cheng, S., Logan, B.E. and Regan, J.M. (2010) Isolation of the exoelectrogenic denitrifying bacterium Comamonas denitrificans based on dilution to extinction. Applied microbiology and biotechnology 85(5), 1575-1587.

Yetis, U. and Gokcay, C.F. (1989) EFFECT OF NICKEL(II) ON ACTIVATED-SLUDGE. Water Research 23(8), 1003-1007.

Yuan, Y., Chen, Q., Zhou, S., Zhuang, L. and Hu, P. (2012) Improved electricity production from sewage sludge under alkaline conditions in an insert-type air-cathode microbial fuel cell. Journal of Chemical Technology & Biotechnology 87(1), 80-86.

Zarnovsky, L., Derco, J., Kuffa, R. and Drtil, M. (1994) THE INFLUENCE OF CADMIUM ON ACTIVATED-SLUDGE ACTIVITY. Water Science and Technology 30(11), 235-242.

Zhang, L., Zhu, X., Li, J., Liao, Q. and Ye, D.D. (2011) Biofilm formation and electricity generation of a microbial fuel cell started up under different external resistances. Journal of Power Sources 196(15), 6029-6035.

Zhang, L.G., Yin, J. and Liu, L. (2009) Characterization of metabolic activities of waste-activated sludge from the SBR process. Journal of Environmental Science and Health, Part A 44(8), 752-757.

Zhang, T., Gannon, S.M., Nevin, K.P., Franks, A.E. and Lovley, D.R. (2010) Stimulating the anaerobic degradation of aromatic hydrocarbons in contaminated sediments by providing an electrode as the electron acceptor. Environmental Microbiology 12(4), 1011-1020.

Zhao, F., Harnisch, F., Schröder, U., Scholz, F., Bogdanoff, P. and Herrmann, I. (2006) Challenges and constraints of using oxygen cathodes in microbial fuel cells. Environmental Science & Technology 40(17), 5193-5199.